RegClim

Regional Climate Development Under Global Warming

General Technical Report No. 6

Presentations from Workshop
6 – 7 May 2002 at Kjeller, Norway

Edited by Trond Iversen and Chris Lunder

Norwegian Meteorological Institute
Institute for Maritime Research
Department of Geophysics
Geophysics Department
Nansen Environment and Remote Sensing Centre
Norwegian Institute for Air Research

Contents

Page

Full names and addresses of participating institutions

NMI : Norwegian Meteorological Institute
P.O. Box 43 Blindern
N-0313 OSLO
NORWAY

Gfi-UiB : Geophysical Institute
University of Bergen
Allégt. 70
N-5007 BERGEN
NORWAY

IfG-UiO : Department of Geophysics
University of Oslo
P.O. Box 1022 Blindern
N-0315 OSLO
NORWAY

IMR : Institute of Marine Research
P.O. Box 1870 Nordnes
N-5024 BERGEN
NORWAY

NERSC : Nansen Environmental and Remote Sensing Center
Edv. Griegsvei 3A
N-5037 SOLHEIMSVIKEN
NORWAY

NILU : Norwegian Institute for Air Research
P.O. Box 100
N-2027 KJELLER
NORWAY

For questions regarding the project, please contact:

Chris Lunder
Norwegian Institute for Air Research
P.O. Box 100
N-2027 KJELLER, NORWAY
Phone: +47 63 89 82 09
Fax: +47 63 89 80 50
e-mail: chris.lunder@nilu.no

Names and e-mail addresses of central personnel

Project management group:	**E-mail address:**
Leaders:	
Professor Trond Iversen, IfG-UiO	trond.iversen@geofysikk.uio.no
Professor Sigbjørn Grønås, Gfi-UiB	sigjorn@gfi.uib.no
Dr. Eivind A. Martinsen, DNMI	eivind.ansgar.martinsen@dnmi.no
Scientific secretary:	
Chris Lunder, NILU	chris.lunder@nilu.no
Principal investigators:	
PT 1 Professor Thor Erik Nordeng, DNMI	t.e.nordeng@dnmi.no
PT 2 Professor Lars Petter Røed, DNMI	larspetter.roed@dnmi.no
PT 3 Eirik Førland, DNMI	e.forland@dnmi.no
PT 4 Dr. Nils Gunnar Kvamstø, Gfi-UiB	nilsg@gfi.uib.no
PT 5 Dr. Helge Drange, NERSC	helge.drange@nrsc.no
PT 6 Dr. Jón Egill Kristjánsson, IfG-UiO	j.e.kristjansson@geofysikk.uio.no
PT 7 Professor Ivar Isaksen, IfG-UiO	ivar.isaksen@geofysikk.uio.no
Contact person at IMR:	
Dr. Bjørn Ådlandsvik, IMR	bjorn@imr.no

Preface

Trond Iversen
Project Leader of RegClim

The 2002 spring seminar of RegClim took place 6-7 May 2002 at Olavsgaard Hotel, Kjeller, Norway. In addition to RegClim scientists, invited guests from Norway (NOClim, and Cicero), from the NordEnsClim co-operation (Danish Climate Centre and the Rossby Centre), and three other international experts, were present. As usual this gave a good chance for RegClim scientists to present preliminary results to a well competent audience, as well as being presented interesting results and viewpoints from international research.

Prof. Ulrich Cubasch from MPI, Hamburg (now Free University of Berlin) presented a climate model simulation of the response of the late Maunder minimum in solar activity believed to have occurred during 1675-1715, towards the end of the "Little Ice Age" believed to have occurred over the Northern Hemisphere. A single response simulation of a reconstructed forcing scenario for greenhouse gases, solar activity and volcano eruptions were made for the late 450 years. Interesting features for the North Atlantic circulations in the atmosphere and the ocean is seen.

Dr. Tim Stockdale presented the work done at ECMWF for seasonal forecasting using a coupled model system. To make forecasts of weather up to 6 months ahead is a demanding challenge for a coupled model system. Such a system should not differ considerably from coupled climate models, except that critical sensitivity to the initial state is important by definition for the forecast problem. As opposed to short- and (partly) medium-range weather prediction, however, the seasonal forecasts must be probabilistic, and model errors influence the forecasts much more relative to initial errors. The relation to climate modelling is important.

Dr. Göran Broström, University of Göteborg, Sweden, presented a profound discussion on how assumptions on diapycnic mixing in the ocean may influence the change in the North Atlantic deep water (NADW) formation as a response to increased fresh-water flux at high latitudes. Based on simplified model calculations, the response may even change sign depending on the diffusive mixing assumption. As shown in the last IPCC-report, different models give very different response in the NADW formation when greenhouse gas forcing increases. Some models almost switch off the NADW, whilst a few give little change. Amongst the latter is the MPI-Hamburg model, and the Bergen Climate Model developed in RegClim. Between these extremes there are many different response patterns, hence this problem remains one of the more uncertain in climate change research.

From the NordEnsClim-group ***Dr Ole B. Christensen*** (DCC) presented some new fine-scale results for Europe. He presented results from the SRES A2 and B2

scenarios and compared with results by simple linear scaling of the A2-scenario to B2 with respect to global temperature change. This method was used in the paper by Christensen et al. (2001) (GRL, 28, 1003-1006), and the results clearly support the method as long as it is interpolation and not extrapolation w.r.t. global temperature. ***Dr. Phil Graham*** (Rossby Centre) gave an update on planned activities at RC and in NordEnsClim. In particular the plans for hydrological projects (Climate, Water and Energy) were mentioned.

The main body of this report summarizes major recent advances in the RegClim project since the Progress Report of December 2001.

A considerable step forward has been made with the ***Bergen Climate Model*** (Arpege coupled to MICOM with Oasis) during the latest year. In addition to sensitivity tests with atmosphere-only and ocean-only model versions, a coupled control run over 300 years has been made, as well as an 80-year CMIP2 simulation in which CO_2 increases 1% per year. The control run shows a stable climate with a fairly well simulation of a regional flow pattern such as the North Atlantic Oscillation (NAO). Flux adjustments are needed. The CMIP2-run show a trend towards a higher NAO index as CO_2 increases, and there is no sign of a weakening of the North Atlantic Ocean currents as a response of increased freshwater forcing. This confirms the results also reported with the ocean-only experiments. So far the experiments with the BCM does not indicate a significant change of the oceanic transport of heat in the North Atlantic Ocean, and discussions points to a number of negative feedbacks that tend to stabilize our region's climate. However, this result is not robust so far. Many other models give different results, even though the MPI-Hamburg model gives the same result as BCM. More ensemble members and scenarios are planned in the forthcoming RegClim Phase III.

Also results from model response calculations of ***anthropogenic aerosols*** have taken a major step forward recently. Atmosphere-only simulations of the direct and indirect aerosol effects were presented using the Oslo-version of the NCAR CCM3.2 model. The calculations are based on a new scheme for the life-cycle of sulphate and black carbon that enables *a posteriori* estimates of particle size and composition. Experiments show a considerably large sensitivity with respect to the model formulation of processes in deep convective clouds. The indirect effects also depend crucially on the assumption behind realised super-saturations and microphysical properties of clouds. Test calculations with chemical transport and radiative transfer models that are more advanced than present climate models can use, were presented. In particular the global radiative forcing of sulphate is seen to be sensitive to grid resolution down to 100 km grid resolution. Also, up to a factor 2 difference in sulphate radiative forcing is seen depending on the vertical distribution of relative humidity.

New results from ***downscaling*** focussed on wind, sea-state and storm surge along the Norwegian coast. Considerable changes in sea-state and storm surge is only seen for the very rare and extreme events. Hence there is a problem of the level of confidence for these extremes, and there is a need for extending the simulations with more ensemble members. Tests have also been made to reveal to what extent the atmospheric downscaling over a relatively large domain, covering substantial

portions of the North Atlantic Ocean, is able to change the large-scale flow pattern due to better resolution in the downscaling model. This analysis was made by flow-regimes analyses. Only changes with low levels of significance are seen. Examples of preparation of impact-related parameters were also presented based on results from empirical downscaling.

Oslo, Norway
November 2002

Trond Iversen
Project Leader of RegClim

Presentations

Modelling the Late Maunder Minimum with a 3-dimensional OAGCM

by

I. Fischer-Bruns[1], U. Cubasch[1], H. von Storch[2], E. Zorita[2], F. Gonzáles-Rouco[3] and J. Luterbacher[4]

[1]Model & Data Group, Max-Planck-Institute for Meteorology, Hamburg, Germany
[2]Institute for Coastal Research, GKSS Research Center, Geesthacht, Germany
[3]Depto. de Astrofísica y Ciencias de la Atmósfera, Universidad Complutense de Madrid, Spain
[4]National Competence Center of Research in Climate, University of Bern, Switzerland

ABSTRACT

A fully coupled OAGCM has been forced with the solar variability, the volcanism and the greenhouse gas concentrations for the last 450 years. The simulation shows almost global cooling during the Late Maunder Minimum (LMM, 1675-1715) with the lowest values in the North Atlantic. This is consistent with the available historic reconstructions. The rate of cooling at the onset of the LMM and the rate of warming at the end of the LMM is in the same range or even larger than what has been experienced since the industrialization. During the first half of the LMM the NAO has a negative phase allowing cold Siberian air to penetrate deeply into Europe. During the second half, the NAO shifts into a positive phase, thus contributing to the warming, which eventually marked the end of the LMM. The North Atlantic experiences a "Great Salinity Anomaly", which leads to an increased ice-coverage in the Denmark Straight.

1. Introduction

So far, fully coupled 3-dimensional OAGCM's have successfully simulated the present day climate, the climate since the beginning of the industrialization, and have been used to calculate future climates (IPCC, 2001). In the study presented here, such a model is used to simulate the climate since 1550. These simulations are performed in response to the discussion about the attribution of the recently observed climate change to anthropogenic factors. In this context it is debated whether the climate change experienced since the beginning of industrialization is unique in its rate and magnitude, and how this change compares to the climate change during the Little Ice Age (LIA). It is also an interesting test for the models, where we can gain more confidence in their ability to simulate a future climate, if we can calculate realistically historic climate events. Furthermore such a simulation can be used to validate historic climate reconstructions, for example from tree rings.

Cubasch et al. (1997) and Cubasch and Voss (2000) performed the first numerical experiments of this kind. They forced an earlier version of the model, which has been used to run climate change simulations with the solar variability since the

17th century. They found a significant response to long periodic large amplitude variations of the solar radiation. These data where further analyzed by Hegerl et al. (1997). They could distinguish between a natural forcing signal and a greenhouse gas signal and could prove that during the recent decades the anthropogenic signal was significantly larger than the natural forcing signal. Tett et al. (1999, 2000) extended this approach running multiple experiments and the inclusion of volcanic forcing. They confirmed the results of Hegerl et al. (1997) and Cubasch et al. (1997) that the natural forced variability is smaller than the anthropogenically forced climate change and does not explain the temperature increase recently observed. Both sets of experiments did, however, not go far back enough in time to be able to simulate the LIA.

Crowley (2000) performed a simulation starting at the year 1000, but using only a 1-dimensional energy balance model. Shindell et al. (2002) performed an equilibrium study with an atmosphere model coupled to a mixed layer ocean for the LMM.

In the present study the natural and anthropogenic forcing described by Crowley (2000) has been used to drive a fully coupled 3-dimensional ocean atmosphere in a transient mode, i.e. the time evolution of the climate before, during and after the LMM is calculated.

The experimental set up and the model used are described in section 2, the results are discussed in section 3. Besides an analysis of the temperature evolution, particular emphasis has been placed on the investigation of the role of the NAO during this time. This is followed by a general discussion in section 4.

2. The model and the experimental set up

The T30 version of the ECHAM4 atmosphere model (Roeckner et al., 1992) coupled to the HOPE ocean model (Wolff et al., 1997; Legutke and Maier-Reimer, 1999; Legutke and Voss, 1999) is used for the simulation. The ocean model has a resolution of 2.8° which increases to 0.5° near the equator in order to be able to simulate ENSO events. Two simulations have been performed: a 1000 year long control simulation, in which the solar and greenhouse gas forcing have been held fixed to present day conditions, and a historic climate change simulation with time dependent forcing. For the latter experiment, the solar forcing (reconstructed from ^{10}Be data), the volcanic forcing and the greenhouse gas forcing have been prescribed using the same data, which Crowley (2000) applied in his experiments. The albedo effect of the volcanoes is implemented as a reduction of the solar forcing. Figure 1 shows the different forcings prescribed during the forced simulation. The simulation starts from present-day forcing conditions and these are slowly changed in 35 model years to the estimated values for year 1500 AD. This time period is not sufficient to obtain a deep ocean circulation at equilibrium with the forcing, but it is long enough to obtain a realistic response in the top layers of the ocean and in the atmosphere. The model achieves a stable state around year 1550 AD.

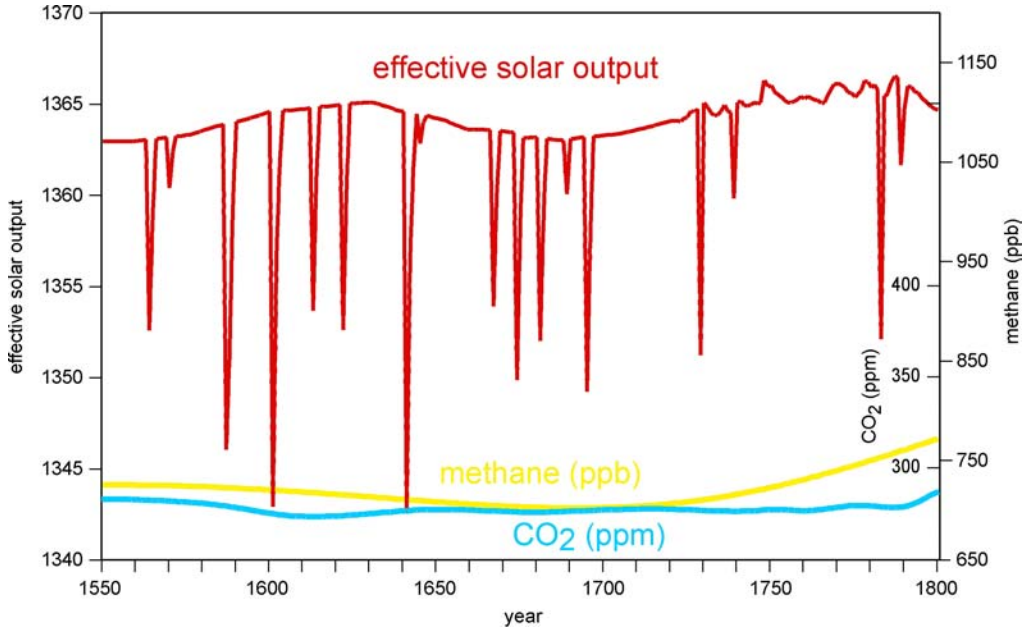

Figure 1: Effective solar output (in W/m^2) and concentrations of CO_2 and methane from 1550 to 1800 used to force the climate model.

3. Results

Temperature Evolution

The mean temperature evolution can be found in Figure 2. In order to make it comparable to the observational data by Mann et al. (1998), for the years up to 1860 only the Northern Hemisphere (NH) has been displayed. The temperature has two distinct minima, one during the LMM, and one during the Dalton Minimum (circa 1780-1829). These minima have a larger amplitude than in the reconstruction by Mann et al. (1998). Their amplitude is more comparable to the recent reconstructions by Esper (2002). It is interesting to note that the warming (cooling) rates are in the same range or even larger than what has been observed during the 20th century.

The global mean temperature change for the LMM period shows a cooling over the whole globe with the lowest temperatures in the NH, and particularly in the North Atlantic region (Figure 3). This is in contrast to the findings by Shindell et al. (2001) and Cubasch et al. (1997), which more or less obtain the global warming pattern with an inverse sign once the solar input is reduced. This shows the importance of the volcanic forcing, which had been neglected in these two studies, as Shindell (pers. com.) has been able to show.

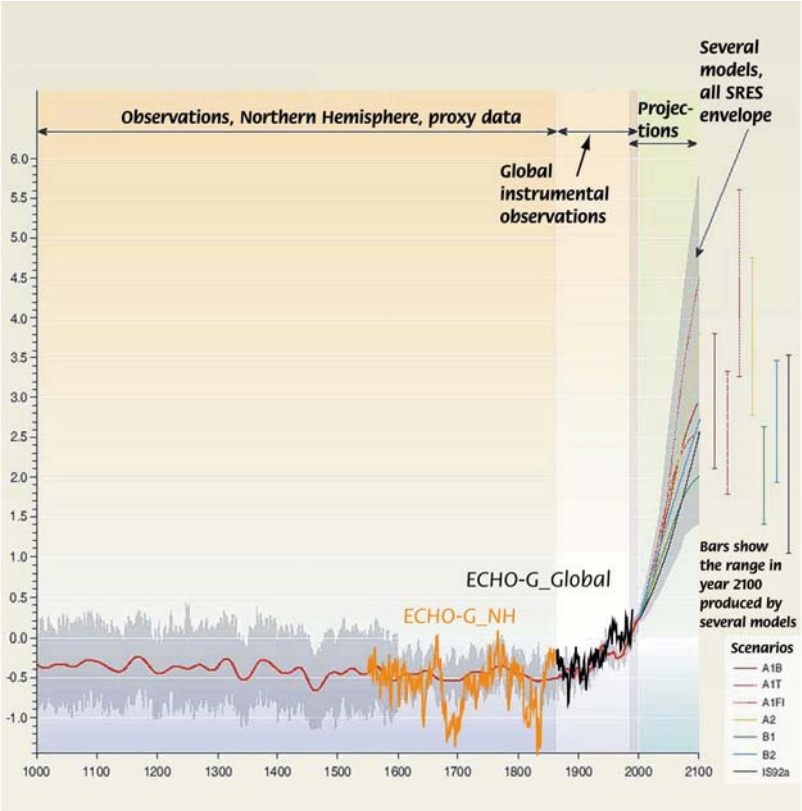

Figure 2: Time series of mean temperature anomalies simulated in the 1550-1860 run for the NH (orange), for the whole globe from 1860 to 1990. These curves have been superimposed on the diagram of the IPCC synthesis report (Albritton et al., 2001) showing the temperature evolution according to Mann et al. (1998) and the projections up to the year 2100.

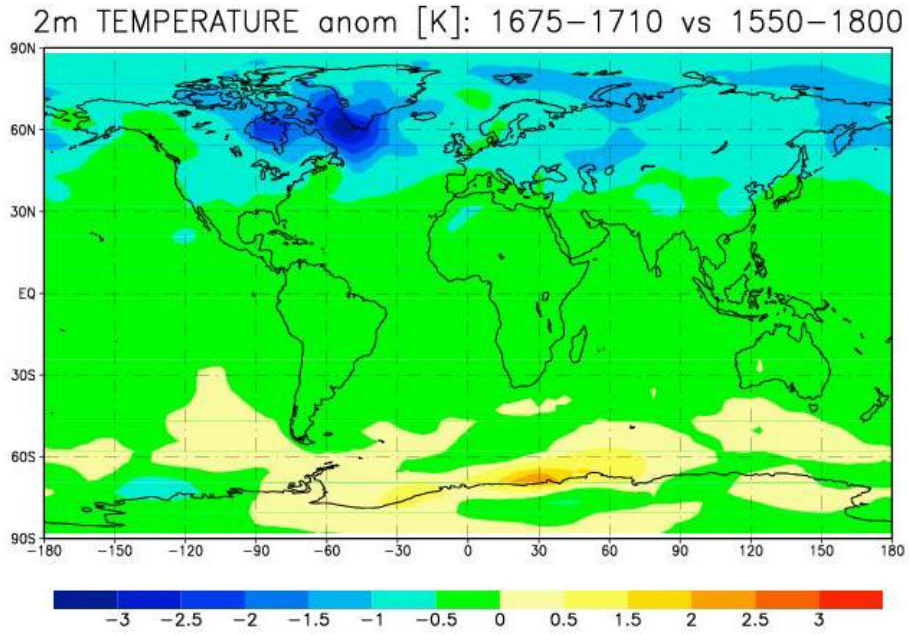

Figure 3: Difference in annual mean near-surface air temperature, simulated during the Late Maunder Minimum event, 1675-1710, and the mean in 1550-1800 AD, in the forced simulation.

The largest cooling can be found in the western North Atlantic, where south of Greenland and close to Iceland a large ice covered area emerges. This ice cover diminishes the heat flow of the ocean into the atmosphere. It bears the signature of a "Great Salinity Anomaly" (GSA) as described by Dickson et al. (1988) and Mysak et al. (1990). Such an anomaly has been found in simulations by Hall and Stouffer (2001), where it has been generated by non-linear dynamics without additional forcing. In the case presented here it is caused by increased precipitation in the years before the LMM. The LMM simulation by Shindell et al. (2001) cannot simulate a GSA since it is a transient feature and demands a fully interactive ocean, because it needs the dynamical interplay of atmosphere, ocean and sea-ice.

North Atlantic Oscillation

The North Atlantic Oscillation (NAO) characterizes atmospheric variability at monthly to decadal time scales. Since the interdecadal variability appears to be most evident during the winter season, an EOF analysis of the mean sea level pressure anomalies for the North Atlantic region based on winter data (DJF) has been performed. The model produces a realistic representation of the winter NAO pattern (Figure 4) in the historic climate change simulation (1550-1990).

The NAO index is defined as the difference between the area averaged and normalized mean sea-level pressure anomalies representing the teleconnectivity centers located northwest of Portugal and over Iceland (Ulbrich and Christoph, 1999, Portis et al., 2001). The principal component time series corresponding to the leading EOF is highly correlated (r=0.92) with the NAO index in the simulation. The simulated NAO index has also been compared with the reconstructed NAO index by Luterbacher et al. (1999, 2002), who used long-term instrumental time series and high-resolution documentary proxy data for his reconstruction. Both time series show considerable variability and differences in phase. They never enter a quasi-permanent low index phase during the LMM associated with weaker mean westerlies over the North Atlantic as suggested by Shindell et al. (2001).

Furthermore, an analysis of the modeled annual global mean temperature in relation to the modeled NAO index for the time period 1550-1800 reveals that during approximately the first half of the LMM (LMM1, 1671-1684) the NAO index is negative, together with a sharp drop in temperature, while it turns positive approximately during in the second half of the LMM (LMM2, 1685-1708) with an increase in temperature (Figure 5). During the first phase of the LMM the advection of continental cold air dominates in central Europe, while in the second phase the NAO contributes with an enhanced advection of warmer Atlantic air masses to the decay of the LMM. This cooling-warming transition can be verified with the temperature reconstruction of van den Dool et al. (1978).

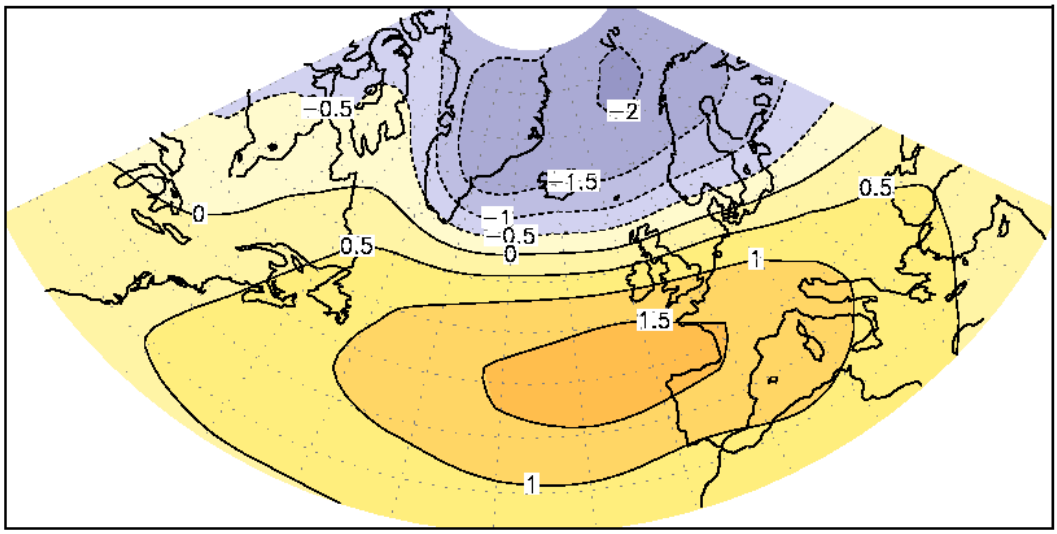

Figure 4: Leading EOF of North Atlantic mean sea level pressure anomalies based on winter means (DJF) of the historic climate change simulation (1550-1990) explaining 38% of the total variance.

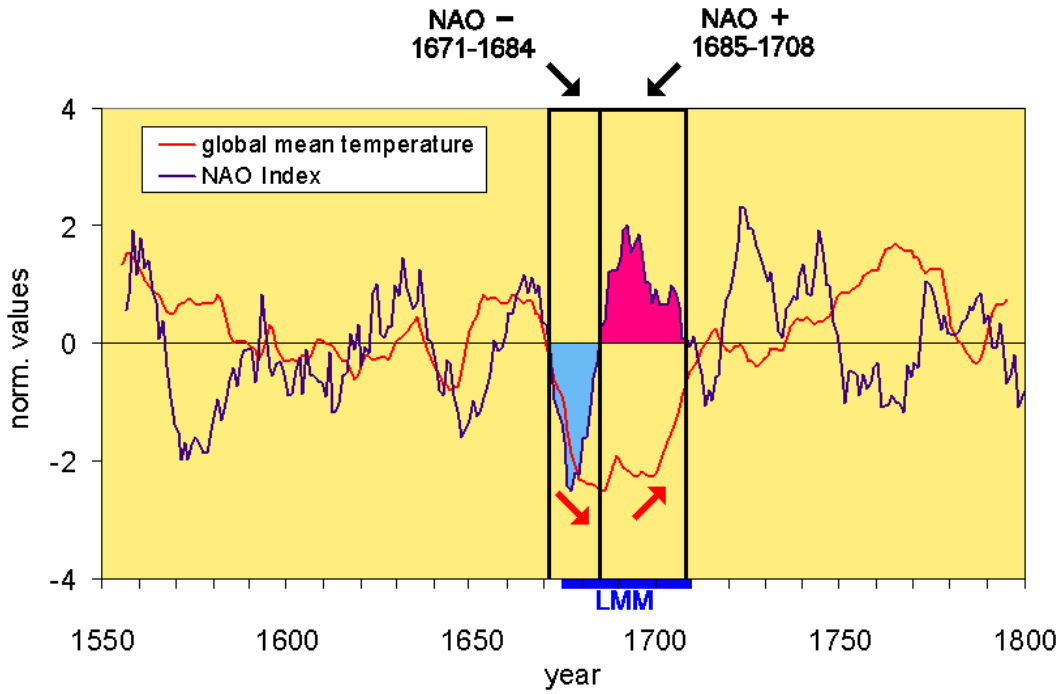

Figure 5: Modelled annual global mean temperature and NAO index (1550-1800, normalized time series, 11 year moving average). In the LMM1 period (1671-1684, cooling phase) the NAO index is negative, in the LMM2 period (1685-1708, warming phase) the NAO index is positive.

The NAO index calculated here is positively correlated with the North Atlantic storm track (defined as the 2.5 to 6 day band pass filtered variance of the 500 hPa geopotential height) with a maximum correlation of 0.6 in the central North Atlantic (cf. Osborn et al., 1999). During the first half of the LMM a significant decrease of storm track activity in the North Atlantic and West European region is

found, while for the second half of the LMM an significant increase of storm track activity over the European continent is simulated.

4. Discussion

The model simulation presented here agrees with the equilibrium mixed layer model simulation of Shindell et al. (2001) by simulating a distinct Maunder Minimum with a global drop of temperature and a particulary large drop of temperature over Europe. Contrary to the simulation by Shindell et al. (2001), it shows a large cooling connected to a GSA in Denmark Strait. Also, its NAO is variable, which agrees well with the observational reconstructions. The more stable NAO in Shindell et al.'s calculation might be caused by their experimental design, but might also be caused by their more elaborate representation of the stratosphere.

It has to be stressed that our result is just one realization. Multiple experiments have to be run to enhance the significance of the findings. The excessive amount of computing resources was so far prohibitive.

Acknowledgement

The model simulations have been performed by GKSS at the DKRZ computing center. Irene Fischer-Bruns has been supported by the SFB 512 sponsored by the DFG. The experiments have been part of the KIHZ-project of the Helmholtz-Society. The authors also wish to express thank to D. Shindell for the useful discussion during the AGU Spring Meeting in Washington (2002), and to T. Crowley for making the data available.

References

Albritton, D.L., T. Barker, I.A. Bashmakov, O. Canziani, R. Christ, *U. Cubasch*, O. Davidson, H. Gitay, D. Griggs, J. Houghton, J. House, Z. Kundzewicz, M. Lal, N. Leary, C. Magadza, J.J. Mccarthy, J.F.B. Mitchell, J.R. Moreira, M. Munasinghe, I. Noble, R. Pachuri, B. Pittock, M. Prather, R.G. Richels, R.B. Robinson, J. Sathaye, S. Schneider, R. Scholes, T. Stocker, N. Sundararaman, R. Swart, T. Taniguchi, and D. Zhou, 2001: Climate Change 2001: Synthesis Report. R. T. Watson ed., Cambridge University Press, 200 pp.

Crowley, T. J., 2000: Causes of climate change over the past 1000 years. *Science,* **289**, 270-277.

Cubasch, U., G.C. Hegerl, R. Voss, J. Waszkewitz and T.C. Crowley, 1997: Simulation with an O-AGCM of the influence of variations of the solar constant on the global climate. *Climate Dynamics*, **13**, 757-767.

Cubasch, U. and R. Voss, 2000: The influence of total solar irradiance on climate. *Space Science Reviews*, **94**, 185-198.

Dickson, R.R., J. Meincke, S.-A. Malmberg, A.J. Lee, 1988: The „Great Salinity Anomaly" in the Northern North Atlantic 1968-1982. *Prog. Oceanog.,* **20**, 103-151.

Esper, J., E.R. Cook, F.H. Schweingruber, 2002: Low-frequency signals in long tree-ring chronologies for reconstructing past temperature variability. *Science,* **295**, 2250-2254.

Hall, A. and R.J. Stouffer, 2001: An abrupt climate event in a coupled ocean-atmosphere simulation without external forcing. *Nature*, **409** (6817), 171-174.

Hegerl, G.C., K. Hasselmann, U. Cubasch, J.F.B. Mitchell, E. Roeckner, R. Voss and J. Waszkewitz, 1997: Multi-fingerprint detection and attribution analysis of greenhouse gas, greenhouse gas-plus-aerosol and solar forced climate change. *Climate Dynamics***, 13**, 613-634.

IPCC, 2001: Projections of future climate change. In: Climate Change 2001: The Scientific Basis. Contribution of Working Group I to the Third Assessment Report of the Intergovernmental Panel on Climate Change [Houghton, J.T., Y. Ding, D.J. Griggs, M. Noguer, P. van der Linden, X. Dai, K. Maskell, C.I. Johnson (eds.)]. Cambridge University Press, ISBN 0521 01495 6.

Legutke, S. and R. Voss, 1999: The Hamburg Atmosphere-Ocean Coupled Circulation Model ECHO-G. Technical Report No. **18**, DKRZ, Hamburg.

Legutke, S. and E. Maier-Raimer, 1999: Climatology of the HOPE-G Global Ocean - Sea Ice General Circulation Model. Technical Report No. **21**, DKRZ, Hamburg.

Luterbacher, J., C. Schmutz, D. Gyalistras, E. Xoplaki, and H. Wanner, 1999: Reconstruction of monthly NAO and EU indices back to AD 1675. *Geophysical Research Letters*, **26**, 2745-2748.

Luterbacher, J., E.Xoplaki, D. Dietrich, P.D. Jones, T.D. Davies, D. Portis, J.F. Gonzalez-Rouco, H. von Storch, D. Gyalistras, C. Casty, and H. Wanner, 2002: Extending North Atlantic Oscillation Reconstructions Back to 1500. *Atmos. Sci. Lett*., **2**, 114-124 (doi:10.1006/asle.2001.0044).

Mann, M.E., R.S. Bradley und M.K. Hughes, 1998: Global scale temperature patterns and climate forcing over the past six centuries. *Nature*, **392**, 779-787.

Mysak, L.A., D.K. Manak, R.F. Marsden, 1990: Sea-ice anomalies observed in the Greenland and Labrador Seas during 1901-1984 and their relation to an interdecadal Arctic climate cycle. *Climate Dynamics* **5**, 111-133.

Osborn T.J., K.R. Briffa, S.F.B. Tett, P.D. Jones and R.M. Trigo, 1999: Evaluation of the North Atlantic Oscillation as simulated by a coupled climate model. *Climate Dynamics,* **15**, 685-702.

Portis, D.H., J.E. Walsh, M. El Hamly, and P.J. Lamb, 2001. Seasonality of the North Atlantic Oscillation. *J. Climate,* **14**, 2069-2078.

Roeckner, E., K. Arpe, L. Bengtsson, S. Brinkop, L. Dümenil, M. Esch, E. Kirk, F. Lunkeit, M. Ponater, B. Rockel, R. Sausen, U. Schlese, S. Schubert und M. Windelband, 1992: Simulation of the present-day climate with the ECHAM model: Impact of model physics and resolution. Report No. **93**, Max-Planck-Institut für Meteorologie, Bundesstr 55, Hamburg.

Shindell, D.T., G-A. Schmidt, M.E. Mann, D. Rind and A. Waple, 2001: Solar forcing of regional climate change during the Maunder minimum. *Science*, **294**, 2149-2154.

Tett, S.F.B., P.A. Stott, M.R. Allen, W.J. Ingram und J.F.B. Mitchell, 1999: Causes of twentieth-century temperature change near the Earth's surface. *Nature*, **399**, 569-572.

Tett, S.F.B., G.S. Jones, P.A. Stott, D.C. Hill, J.F.B. Mitchell, M.R. Allen, W.J. Ingram, T.C. Johns, C.E. Johnson, A. Jones, D.L. Roberts, D.M.H. Sexton and M.J. Woodage, 2000: Estimation of natural and anthropogenic contributions to 20th century. Hadley Centre Tech Note 19, Hadley Centre for Climate Prediction and Response, Meteorological Office, RG12 2SY, UK pp52.

Ulbrich, U., and M. Christoph, 1999: A shift of the NAO and increasing storm track activity over Europe due to anthropogenic greenhouse gas forcing. *Climate Dynamics*, **15**, 551-559.

van den Dool, H.M., H.J. Krijnen and C.J.E. Schuurmans, 1978: Average winter temperatures at De Bilt (The Netherlands): years 1634-1977. *Climatic Change*, **1**, 319-330.

Wolff, J.-O., E. Maier-Raimer and S. Legutke, 1997: The Hamburg Ocean Primitive Equation Model HOPE, Technical Report No. **13**, DKRZ, Hamburg.

Coupled modelling for seasonal forecasts

by

Dr Tim Stockdale

Seasonal Forecast Group, European Centre for Medium-range Weather Forecasts

Numerical seasonal forecasting is the attempt to make predictions of future weather patterns several months in advance, using numerical models of the atmosphere and ocean. The sort of predictions which might be possible are of course probabilistic and not deterministic. The possibility of seasonal forecasting largely depends on the way in which the sea surface temperature influences the behaviour of the atmosphere, and on our ability to predict the evolution of sea surface temperature several months into the future.

The state-of-the-art of numerical seasonal forecasting is still "youthful", which is perhaps an optimistic way of saying that there are many difficulties, and that it will take a lot more development and improvement before we are comfortable that we have reached a "mature" stage, where the performance is basically satisfactory and only small increments in skill can be expected. It is the youthful nature of numerical seasonal forecasting that makes it such an interesting and challenging field to work in, and which gives it a strong position to interact with other areas of climate science.

The major motivation for numerical seasonal forecasting is the very large practical value that successful forecasting systems can give. However, there are also important scientific benefits, in terms of improving and in particular in validating important aspects of climate models. If we are at all interested in what a changed global climate means for local weather patterns and climate, then we need to be very interested in whether the models for seasonal numerical prediction are able to capture the observed relationships of climate variability.

Having given this general introduction, I want to give a brief overview of seasonal forecasting and the approach used at ECMWF. I will then finish by discussing some of the future directions we are likely to move in.

El Nino, and more generally the variability of SST in the equatorial Pacific Ocean, is the biggest single source of predictability for the atmosphere on seasonal to interannual timescales. Seasonal forecasting is a tractable problem because of ENSO. However, there are many other potential factors that may contribute to seasonal predictability, not all of which are well quantified or understood. A list, in roughly decreasing order of importance, is as follows: other tropical ocean SST; all forms of climate change; local land surface conditions; mid-latitude ocean temperatures; remote impacts of snow cover and soil moisture; volcanic eruptions; sea-ice anomalies; stratospheric QBO; dynamic memory of the atmosphere; solar cycle and stratosphere; other unknown or unexpected influences.

The large number of possible contributors to seasonal predictability is one justification for using comprehensive numerical models. Given ECMWF's expertise in atmosphere models and computer resources, it is also a natural approach for us to explore. Empirical and statistical techniques can capture some aspects of seasonal predictability, and these provide a first test for a fully numerical approach. Eventually, we expect that numerical methods will be clearly better than other approaches, but as with NWP it may be quite some time before numerical models supplant other techniques and human expert judgement.

The basic approach is very simple. We use an OI assimilation method to prepare ocean initial conditions. We take atmosphere and land surface initial conditions from the ECMWF operational 10 day forecast system. We couple the ocean and atmosphere together, and run the coupled model for 6 months. In order to account for the indeterminacy of the atmosphere on these timescales, we repeat the calculation 40 times, with perturbations made to the initial conditions which are representative of what we believe are the uncertainties in the initial state. The ocean model used is HOPE (originally from the Max-Planck-Institute for Meteorology in Hamburg) with an equivalent 1 deg resolution in mid-latitudes, and 0.3 deg meridional resolution at the equator. The atmosphere model is the ECMWF IFS, but run at a T95L40 resolution. The system is fully coupled (i.e. no flux correction), but sea ice is specified to follow a prescribed seasonal cycle, since there is no sea ice model contained within the system.

This simple forecast approach gives as an ensemble forecast of the global ocean-atmosphere system, from which we archive a wide range of fields with a high temporal resolution (some fields daily, others 6 hourly). However, the big problem is that the model systematic error is typically as big as the interannual signals we are trying to predict. For example, the drift in Nino 3 SST can exceed 1 deg C in amplitude, which is comparable to the observed interannual standard deviation of this quantity. To deal with this problem, we also run a set of forecasts with the same model, and initialised in the same way, for a set of earlier years with the same calendar start date. For well observed fields such as SST, we can use this set of hindcasts to estimate the mean model drift (or systematic error) as a function of lead time, and subtract this drift from the forecast model output to create a set of predicted absolute values. For fields which are not so well globally observed (and this includes most surface fields such as rainfall and temperature), it is simpler to compare the forecast distribution with the climate distribution (i.e. the set of values obtained by the integrations for previous years), and derive the forecast anomaly.

If the system was linear, this approach would work perfectly. Of course, this is not the case. Nonetheless, this approach appears to work remarkably well. It has been most thoroughly examined for the prediction of equatorial SST anomalies (the variation of which involves a number of non-linear processes), and has been shown to work very effectively. Of course, there will be circumstances when it does not work satisfactorily, for example when a model has a climatological rainband in the wrong position. Overall, though, it is a very feasible method for numerical seasonal forecasting. The errors in forecast SST are substantially smaller than the model drifts, the main ENSO teleconnections are well reproduced, and the influence of other tropical SST anomalies is reasonably

handled. The impact of model errors and non-linearities on European teleconnections, is, however, not easy to assess from the results we presently have available. To give an idea of what is possible in a large ENSO event, Figure 1a shows the ensemble mean 500hPa anomaly from our real-time coupled forecasts of DJF 1997/98, while Figure 1b shows the ensemble mean 500hPa anomaly from a set of integrations made with an atmosphere model and observed SST after the event. Verification (not shown) is very similar to both of these ensemble means, but the real point of this figure is that the real time coupled forecast, complete with its drift in SST, does pretty much just as well as the atmosphere model forced with a perfect SST field.

A few more comments on the generation of the 40 member forecast ensemble. The initial conditions are perturbed in two different ways. Firstly, wind perturbations are added to the forcing fields during the ocean analysis. Ideally we would use 40 different winds to create 40 different analyses, but this is too expensive, so we are restricted to creating 5 different analyses. Uncertainty in the wind can give considerable uncertainty in the sub-surface of the ocean analyses, although where there is lots of data the uncertainty is substantially reduced. By perturbing in initial conditions in this way, we have a system that automatically adjusts the size of the uncertainty as the observing system changes. As well as considering the impact of the wind, SST perturbations are also added. This is done immediately prior to starting the coupled integration, so there is no limit to the number that can be generated. Thus all 40 ensemble members are given a different initial SST. Uncertainties in SST are not small, and previous work has shown that perturbing the SST can have a strong impact on the coupled ocean-atmosphere system in the tropics. Indeed, the SST perturbations are responsible for a considerable spread in the forecast SST values, even at the start of the forecast. The perturbations are based on (fairly conservative) estimates of the true uncertainty in SST. Improving the quality of the SST data would reduce the uncertainty in the forecasts which comes from this source, and would hopefully also improve the accuracy of the forecasts.

Note, however, that although the perturbations used to generate the 40 member ensemble account in an approximate way for the majority of the uncertainty in the initial conditions, they do NOT account for errors and uncertainties in the models themselves. In practice, model error is likely to be responsible for the majority of forecast error on seasonal timescales, and thus the 40 member model ensemble is not a particularly good representation of the true uncertainty in the forecast. We can try to alleviate this by using forecasts from several different models to construct a multi-model ensemble. This can help, in particular by exposing errors which are specific to one particular model, but the sub-space spanned by a handful of models is unlikely to include reality.

This brings us to three main challenges for the future. Firstly, there is no substitute for improved models. For the atmosphere, the key issue appears to be the modelling of tropical convection. We also need better ocean models, especially as regards their handling of equatorial processes. We also need better representation of the high latitudes, in particular regarding sea-ice. This is not likely to have much of a global impact, but is at the very least important locally. A second main challenge is the reliable calibration of our forecast products. This involves more

than simply removing the mean bias or calculating measures of skill; rather we have to create a credible forecast probability density function (pdf). The question can be posed thus: given the model forecast pdf, the past history of forecast pdfs and the past history of observed outcomes, what is the best estimate of the true pdf? The third main challenge is to account properly for decadal and longer term change. This involves proper definition of climate reference periods, proper accounting for sources of low frequency climate change, and creating stable ocean analyses decades into the past.

In conclusion, seasonal forecasting is important because:

1) the forecasts can be very useful
2) in the context of a changing climate, a good seasonal forecast system tells us what the present climate is
3) seasonal forecasting is a very demanding way of testing numerical models of climate.

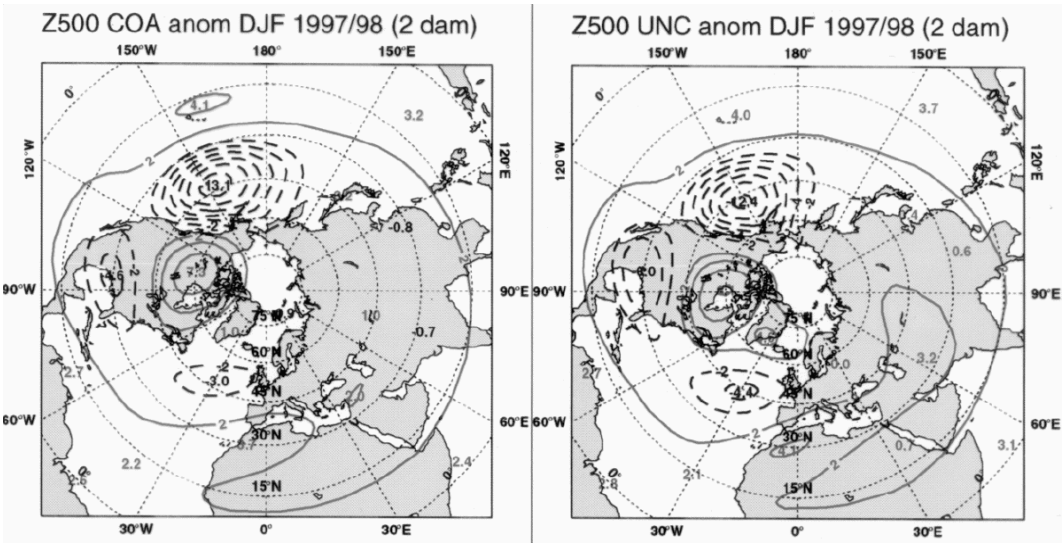

Figure 1a: The ensemble means 500hPa height anomaly from real-time coupled model forecasts for the winter of 1997/98, in units of decametres. The anomaly is with respect to the climate of the coupled model.
1b: The ensemble mean 500hPa height anomaly from atmosphere-only model hindcasts for the winter of 1997/98, made after the event using observed SST. The anomaly is with respect to the climate of the uncoupled model.

Recent Results with Regional Climate Modelling at the DMI

by

Ole Bøssing Christensen

Danish Meteorological Institute, Denmark

Introduction

By now, regional climate modeling has become an established part of the effort to extract useful predictions of global warming from greenhouse gas emission scenarios. Since global climate models (GCMs) have a limited spatial resolution, regional climate models (RCMs) can play a role in the downscaling of large-scale climate change signals from the GCMs.

In this presentation, two specific initiatives with Nordic participation has been investigated: The Nordic Ensemble Climate model intercomparison (NordEnsClim) and the EU project Prediction of Regional scenarios and Uncertainties for Defining EuropeaN Climate change risks and Effects (PRUDENCE)

NordEnsClim

During the last several years, regional climate simulations have been performed intensively in the Nordic countries, especially at the Danish Meteorological Institute, the Norwegian RegClim project, and at the Swedish Rossby Centre. The models applied at these three institutions are similar though not identical. The same applies to the choice of driving GCMs.

Table 1. The four NordEnsClim regional climate change experiments with experimental specications and global scenario temperature change. GHG: Greenhouse gas only experiment. HIRHAM: See Christensen et al. [1998]. RCA: See Rummukainen et al. [2000].

	DMI	DNMI/RegClim	RCA-E	RCA-H
RCM	HIRHAM (18 km)	HIRHAM (55 km)	RCA1 (44 km)	RCA1 (44 km)
GCM	ECHAM4/OPYC	ECHAM4/OPYC	ECHAM4/OPYC	HadCM2
Forcing scenario	GHG	GHG+sulf.+trop. O_3	GHG	GHG
Control period	Pre-industrial (9 y)	1980-1999 (20 y)	1980's (10 y)	Pre-industrial (10 y)
Scenario period	2070's (8 y)	2030-2049 (20 y)	2070's (10 y)	2040's (10 y)
Global warming	3.4°C	0.9°C	2.7°C	2.6°C
Warming 1990-2050	1.7°C	1.1°C	1.7°C	1.7°C
Scaling coefcient (ΔX_{norm})	0.5	1.2	0.6	0.7

In order to take advantage of this collection of rather similar RCM experiments, an intercomparison was performed between 4 runs as sketched in Table 1. Since the global climate change signals of these experiments are quite different, a very simple scaling was applied in order to make the RCM runs more comparable:

Climate change signals of all kinds were simply scaled with the global temperature change and thus scaled to represent the difference between present days and a period around 2050 according to the various GCMs driving the RCM experiments.

This approach proved quite successful, and the treatment of these 4 scaled experiments as a quasi-ensemble rendered several interesting and robust results for the Scandinavian region. Some results agreed upon to a significant extent:

– The temperature increase is roughly 50% larger in winter than in summer

– The diurnal temperature range decreases significantly, particularly in autumn and winter

– Autumn precipitation increases a lot, the present results scatter around 15%

– There is an even more clear increase in the number of heavy precipitation events, here defined as the frequency of days with more than 10mm of precipitation

The work has been published in Christensen et al., GRL 28, 1003-1006 (2001).

Prudence

This European project started in December 2001. There are 21 partners in the project, which includes tasks ranging from atmospheric global climate modeling to applications in agriculture, economics, and social sciences. The particular aim of this project is to quantify the amount of uncertainty that is accumulated in the model cascade usually employed to obtain estimates of the effect of global warming on society. The PRUDENCE consortium collaborates with two other EU projects focusing on climate change: MICE and STARDEX. More information can be obtained through the PRUDENCE web page http://www.dmi.dk/f+u/klima/prudence

Recent HIRHAM experiments

Some recent RCM simulations at the Danish Meteorological Institute are relevant to the PRUDENCE project as well as to the NordEnsClim scaling hypothesis. The HIRHAM RCM has been run for 3x30 years in a control period corresponding to 1961-90, a scenario period according to the SRES emission scenario A2, and finally a scenario period according to SRES scenario B2, both for the period 2071-2100. The integration area covers Europe and parts of the Atlantic and has a resolution of approximately 50km. The GCM providing the boundary conditions is the ECHAM4/OPYC model developed at the Max-Planck Institute for Meteorology in Germany.

Since this set of experiments provides two different climate change signals, though the control climate is shared between the two, and since the model setup resulting in these two signals is quite identical, we are now able to do a quite clean test of the credibility of the scaling method employed in the NordEnsClim work.

Of course, this comparison cannot be treated statistically, but will nevertheless give an indication of the viability of this approach.

In Figures 1-3 the scaling is tested for three different fields, temperature, precipitation, and precipitation falling in events with more than 15 mm per day. Upper panels show the direct climate signal of the B2 experiment between the two periods. Middle panels show an estimate of change in the depicted fields corresponding to the global warming in the B2 experiment between the two periods, but extracted from the A2 experiment and scaled according to global temperature change. Finally, lower panels show the difference between the scaled A2 climate signal and the direct B2 climate signal, i.e., the error of the scaling approach. This error of course includes contributions of natural decadal-scale climate variability from all three 30-year periods.

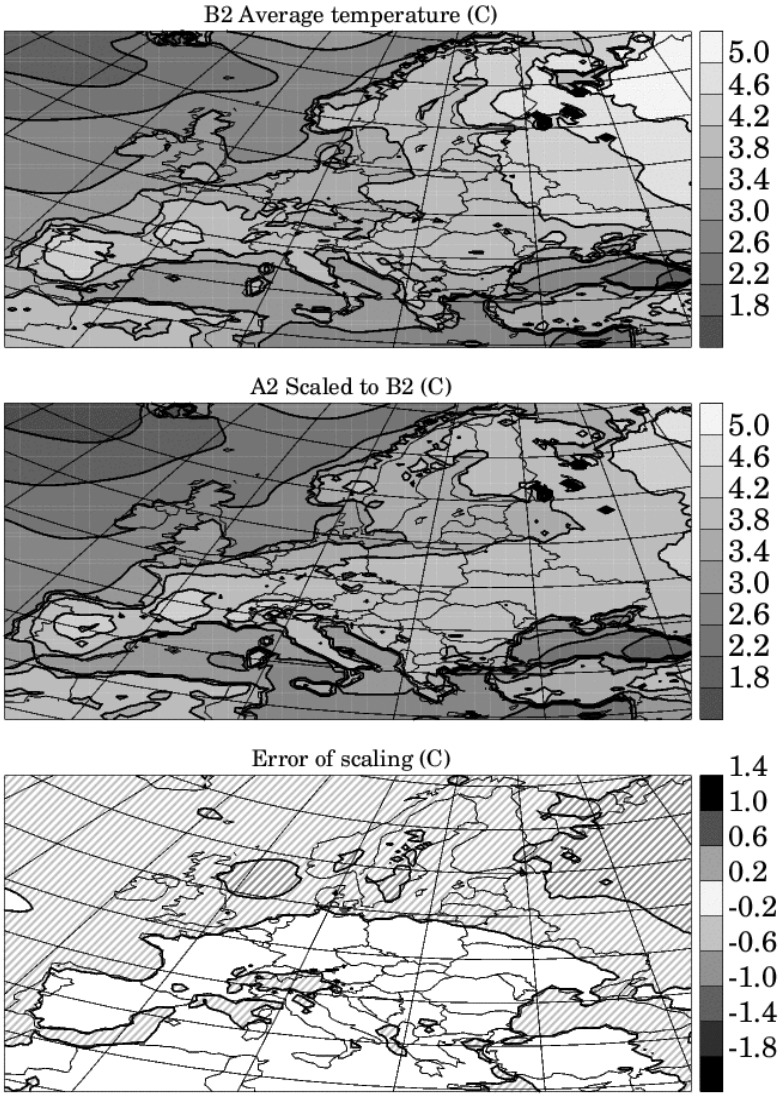

Figure 1: Upper panel: Change in surface air temperature between 30 years 2071-2100 according to SRES scenario B2 and 1961-90. Middle panel: The same difference according to scenario A2, but multiplied by a factor 0.754 corresponding to the ratio of global warming signals between the two experiments.

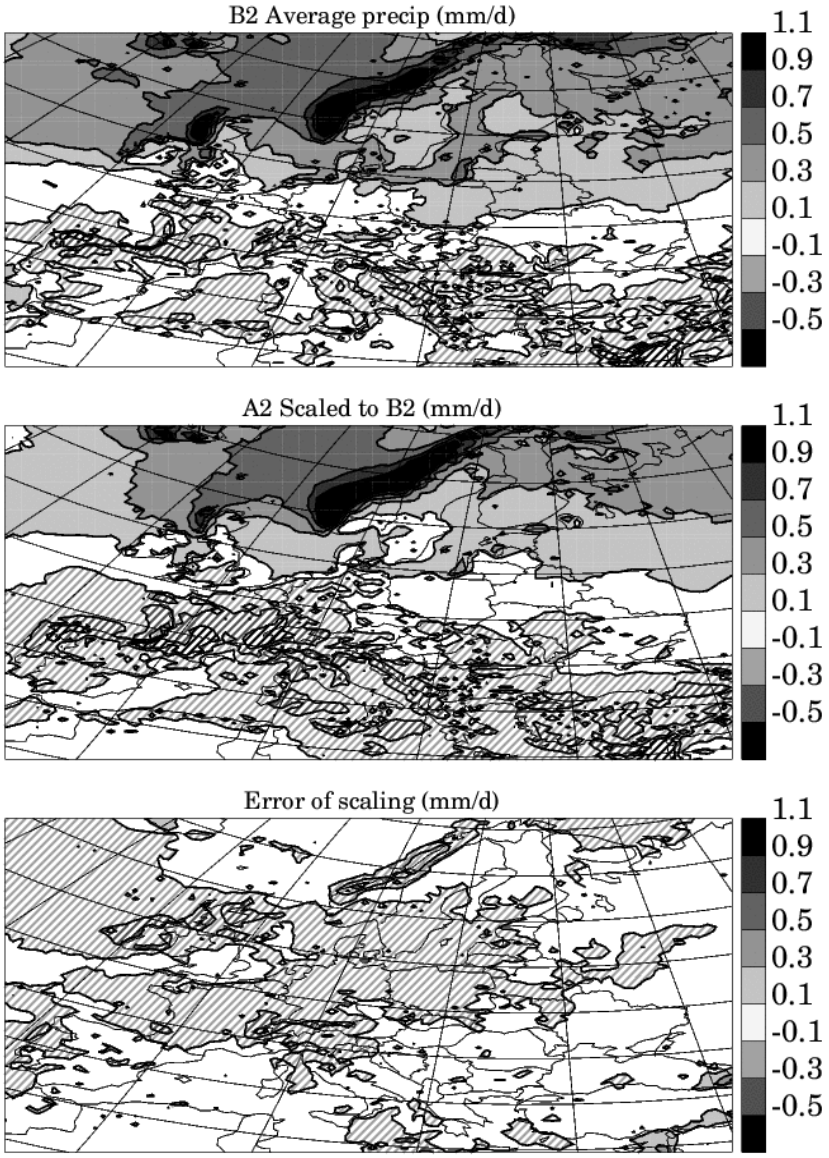

Figure 2: Like Figure 1, but for average precipitation (mm/day).

The scaled precipitation signal (Figure 2) is generally smaller than the B2 signal, apart from the Norwegian coast. This could be due to a more zonal climate in scenario A2 than in B2. A further analysis is needed of this hypothesis. The intense precipitation depicted in Figure 3 shows a behavior similar to the average precipitation.

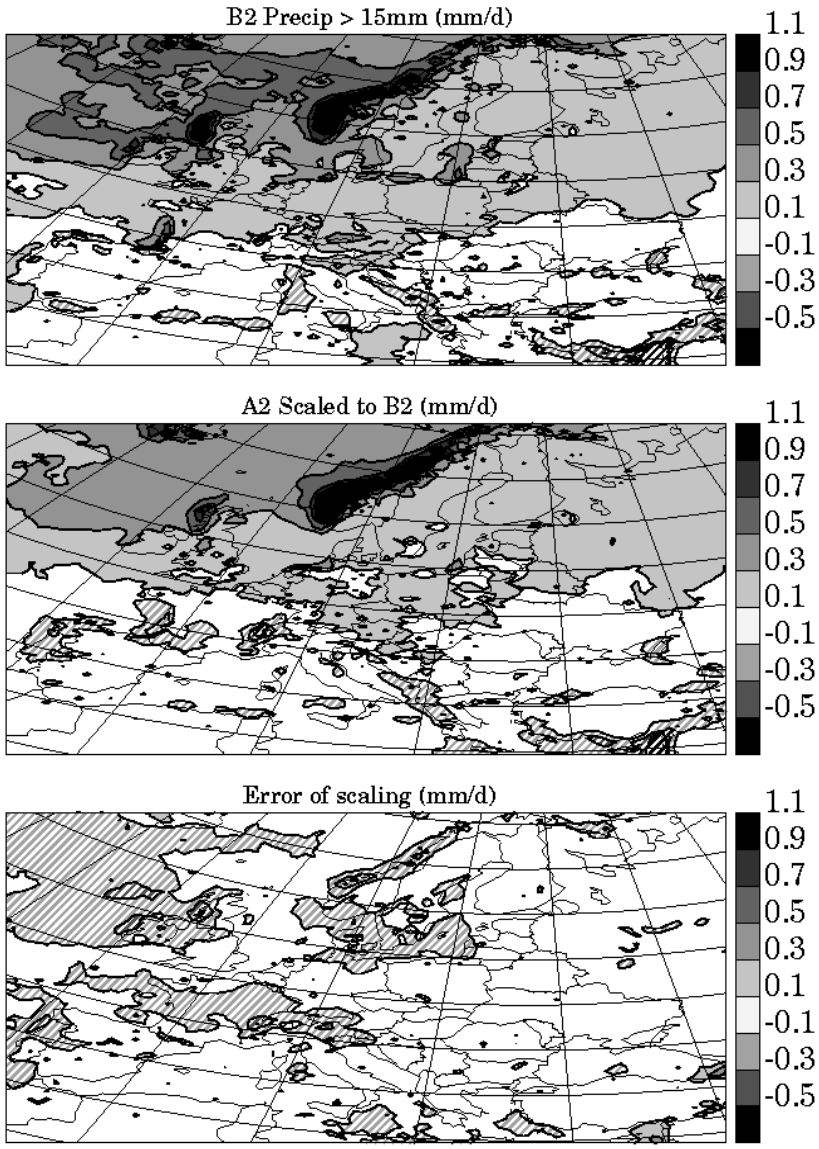

Figure 3: Like Figure 1, but for the precipitation on days with more than 15 mm of precipitation (mm/day).

For all three fields the scaling seems reasonable. The error of scaling is considerably smaller than either of the climate change signals, though some clear variations appear.

Regarding temperature (Figure 1), the scaled warming is smaller than the direct B2 warming, especially over sea. This is probably due to the large heat capacity of the oceans: The heating is not instantaneous and will therefore not vary so much between the two scenarios at a given point in time, as it is indicated by the difference in forcing.

Conclusion

The Nordic countries have started a promising collaboration with the aim to compare regional climate experiments. In the near future the PRUDENCE project

will give access to several more multi-year experiments covering Europe. The investigation of the linearity of regional climate change signals should be able to benefit from these data, and the limitations of this very rough approach could be better determined.

References

Christensen, J.H., J. Räisänen, T. Iversen, D. Bjørge, O.B. Christensen, and M. Rummukainen, 2001: A sythesis of regional climate change simulations -A Scandinavian perspective. *Geophys. Res. Lett*., **28**, 1003-1006.

Christensen, O.B., J.H. Christensen, B. Machenhauer, and M. Botzet, 1998: Very high-resolution regional climate simulations over Scandinavia. Present climate. *J. Climate*, **11**, 3204-3229.

Rummukainen, M., J. Räisänen, B. Bringfelt, A. Ullerstig, A. Ornstedt, U. Willén, U. Hansson, and C. Jones, 2001: A regional climate model for northern Europe - model description and results from the downscaling of two GCM control simulations. *Climate Dynamics*, **17**, 339-359.

Update on SWECLIM activities and Nordic climate cooperation

by

L. Phil Graham

Rossby Centre, SMHI, Swedish Meteorological and Hydrological Institute, Sweden

The Swedish Regional Climate Modelling Programme (SWECLIM) continues its activities at a steady pace. Model development and production of climate scenarios are carried out parallel to each other. The intent of this summary is to both introduce new cooperation activities and to highlight some recent results from the Rossby Centre.

Climate, Water and Energy

A new cooperation project with the title "Climate, Water and Energy" (CWE) was recently started with financing from the Nordic Council of Ministers. This initiative originated from the CHIN group (Chiefs of the Hydrological Institutes in the Nordic Countries) and is being coordinated from the Hydrological Service of the National Energy Authority on Iceland. The aim of the project is to address impacts of climate change on the energy sector. Particular focus will be placed on effects to hydrological systems, which are crucial components to energy production in the Nordic region.

Four key groups have been identified to integrate Nordic research efforts around the CWE theme. These are listed below together with the respective coordinating agencies:

Climate	- Swedish Meteorological and Hydrological Institute (SMHI)
Glaciers	- Icelandic Meteorological Office (IMO)
Hydrological Models	- Swedish Meteorological and Hydrological Institute (SMHI)
Long Time Series	- Norwegian Water Resources and Energy Directorate (NVE)

All of the groups include participants from each of the Nordic countries. The task of the climate group is to collect and compare comprehensive and compatible regional climate scenarios for the Nordic Region. The glaciers group will study the response of glaciers to the regional scenarios. The hydrological modelling group will identify key hydrological processes and strategies to assess climate change impacts on sensitive indices such as flood and drought risks. The long time series group will assess the long-term variability, seasonality and extremes in existing long historical time series of climate and hydrology as well as appropriate proxy series from the Nordic Region.

CWE is divided into two one-year phases spanning 2002-2003. Although the budget for this period is modest, an initial assessment of the sensitivity of the energy sector to climate change should be achieved. The aim is to establish both a scientific base and a working network of researchers dealing with climate, water

and energy issues in the Nordic region. Recommendations for future work and the formulation of in-depth proposals for continued research are an expected important outcome of this project.

REFOCUS

A proposal titled "Regional effects of climate and land use changes for the energy sector" (REFOCUS) has recently been submitted to the Nordic Energy Research Programme. The main aim is to integrate and apply models of the physical climate system and the biosphere to produce practical inputs on climate change effects for the energy sector. This should provide a more detailed basis for regional planning of the future energy mix and for support of decisions on international agreements to reduce emissions, such as the Kyoto commitment. This application builds on existing Nordic regional climate projects together with combined expertise in vegetation, carbon cycle and biomass at universities in the region. A managed coordination of these national resources will open new areas of research that so far have been too complex for individual research teams to deal with.

The interaction of regional climate change and biology has direct relevance to biomass production and greenhouse gas budgets. There is also relevance to hydropower and wind as land cover and vegetation exert control on evapo-transpiration and atmospheric stability. REFOCUS aims to further develop regional climate models and scenarios to better address these issues and meet the needs of the energy sector. Some relevant science questions are as follows:

- Does climate change affect the stability of natural carbon sinks?
  - and thus choice between using forests to store CO_2 or to produce biomass to replace fossil fuels
- What positive and negative effects will climate change have on biomass production?
  - e.g. longer growing season, increased insect damage and summertime dryness
- Will land use change or the response of vegetation to climate change affect evapotranspiration?
  - and thus water resources and hydropower

REFOCUS intends to approach these questions by using vegetation and carbon cycle models to introduce interactive vegetation into regional climate models. As this is done, the description of soil moisture, evapotranspiration and snow will also be improved. Regional climate scenarios produced with interactive vegetation can then be compared to scenarios with static vegetation effects (as most scenarios are done to date) to assess the importance of climate/vegetation links in the Nordic region.

The project will be carried out through research, education and extended visits within the Nordic climate and biomass research communities. Five PhD students are proposed, each in close collaboration with a Nordic climate modelling team. In addition to producing new scientists, the PhD emphasis will provide an important link between national meteorological institutes and respective universities. Dialogue with the energy sector and with government authorities

responsible for forest and land use management will keep climate scientists aware of the practical needs from these users.

The principal proposers for REFOCUS are the Swedish, Danish, Norwegian, Finnish and Icelandic meteorological institutes. The project leader is the director of SWECLIM. The potential collaborating universities include Lund University, Swedish University of Agricultural Sciences, Copenhagen University, Oslo University, University of Joensuu and University of Iceland. The proposed timeframe for the project is the period 2003-2006.

SWECLIM: Model Development

RCA, the atmospheric and land surface component of the Rossby Centre Regional Climate Model has its roots in the HIRLAM operational forecast model versions 2.5 and 2.7 (Källén, 1996). Many changes have been introduced during the past five years of SWECLIM to improve RCA's climate modelling capabilities. RCA2 is the current version of the atmospheric model component being used for climate scenario production. At the same time, work continues on development for the next version of RCA. Many of the model changes have been presented at previous RegClim seminars. The primary changes that have occurred since then include improvements to the moist physics, the land surface, introduction of river routing (lateral transport of runoff) and coupling to the Rossby Centre regional ocean model (RCO). Details of these changes can be found in Bringfelt et al. (2001), Döscher et al. (2001), Graham (2001), Jones and Ullerstig (2002), Undén (2002), and Willén and Jones (2002).

For verification of RCA2 (in uncoupled mode), model simulations using ECMWF ERA-15 as boundary conditions were made. These "perfect boundary conditions" were complemented with more recent years of operational analyses to form a 17-year simulation run from 1984 to 2001. Some results of this simulation are shown in Figures 1 and 2.

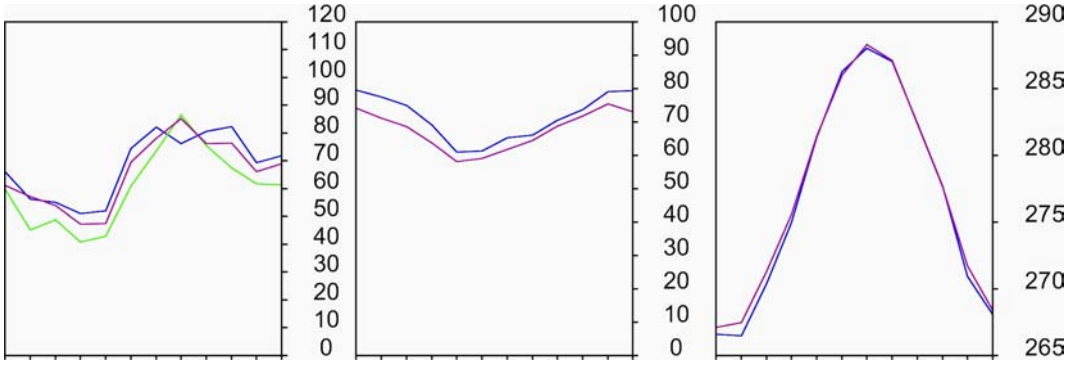

Figure 1: The mean annual cycle of (left) precipitation in mm/month, (middle) total cloud cover in % and (right) screen temperature in K for the Nordic land area, in 1985-1999. Comparisons are made to various observations-based data (see text). The blue curves are for the RCA2-modeled results, the model being forced by ECMWF analyses.

Figure 1 shows the climatological mean annual cycle of precipitation, as a mean for the Nordic land region. Two observational data sets are included for comparison. The blue curve shows the RCA2-modeled result. The green curve

shows the annual cycle according to CRU-data. These data are uncorrected for undercatch. RCA2 overestimates precipitation, relative to the CRU data, by as much as 20% in fall and in winter. However, it is well known that uncorrected precipitation data sets underestimate, in particular, wintertime precipitation. The red curve is for a corrected data set, the GPCP (Global Precipitation Climatology Project) version 2 (Huffman and Bolvin 2001). These data are global and combine both satellite and station estimates. Local corrections have been applied to account for precipitation undercatch and wind effects (Huffman and Bolvin 2001; Rubel and Hantel, 2001). It is concluded that at these spatial scales, RCA2 has a realistic simulation of precipitation.

Figure 1 also shows the mean annual cycle of total cloudiness for the Nordic land region, the observations being from the CRU data. The annual cycle is well simulated by RCA2 with a minimum in the summer period. There is a slight overestimate of total cloud cover, relative to the CRU data. Some of this can be explained by the known negative bias in station-based observations during periods of darkness. Hahn et al (1995) indicate climatological wintertime observations of cloudiness can be up to 2-3% underestimated. Nevertheless, there appears to be a positive bias in the RCA2 cloud field. This will be studied in the further development of the RCA-model. The simulated temperatures seem realistic for northern Europe, although it is noted that the CRU data are problematic for regions of variable orography.

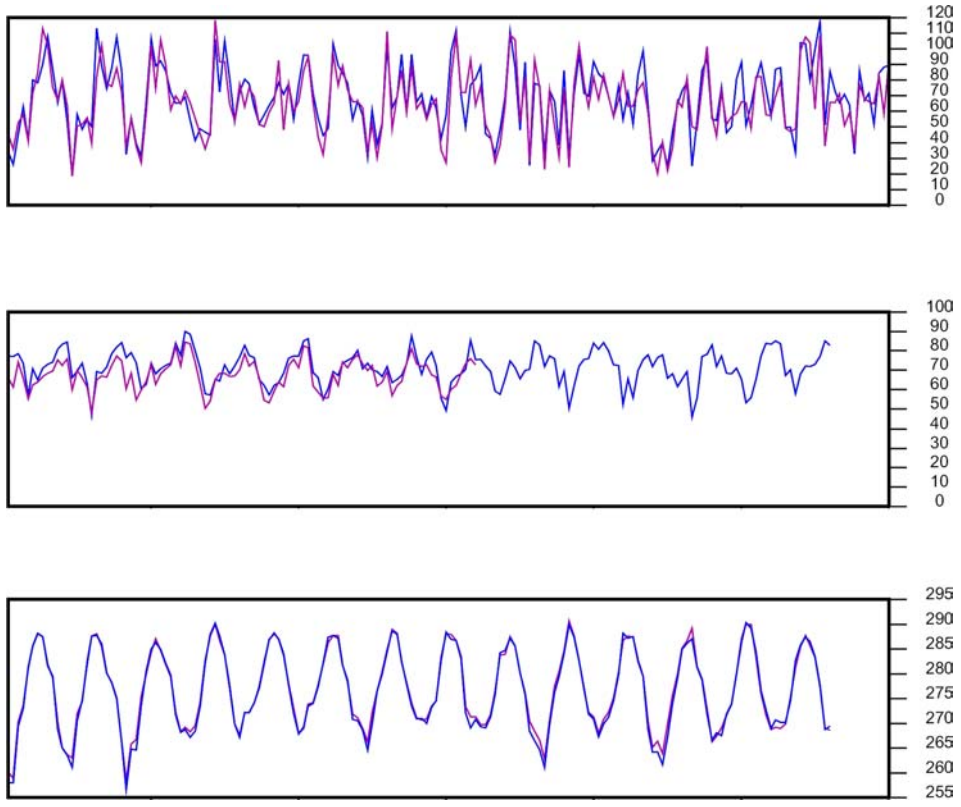

Figure 2: The monthly course of (top) precipitation in mm/month, (middle) total cloud cover in % and (bottom) screen temperature in K for the Nordic land area, in 1985-1999. Comparisons are made to various observations-based data (see text). The blue curves are for the RCA2-modeled results, the model being forced by ECMWF analyses.

Figure 2 illustrates the monthly fields, starting from 1985, upon which the climatological mean annual cycles were based. After 1992 the CRU cloud data becomes unusable due to the lack of actual observations. Cloud observations are therefore only plotted out to the end of 1992. Similarly the temperature data set is only presently available to the end of 1998. The precipitation observations are available for the entire period. The intra-seasonal variability is well represented in all 3 parameters. The strong seasonal variability in the precipitation field is well simulated. With respect to the cloud field it is worth noting that the positive bias in the modelled cloud field occurs mainly in the first three winters, these being relatively cold. This may indicate a problem in representing clouds in cold conditions, although it is felt more likely that the problem lies in the longwave clear sky portion of the radiation code.

SWECLIM: Latest Scenario Results

As mentioned above, Rossby Centre regional atmospheric model (RCA) is now coupled to the Rossby Centre regional ocean model (RCO). The first climate change scenario simulation with the RCAO coupled regional climate model has recently been completed (Räisänen et al., 2002). This is based on the HadCM3 and HADAM3 (Hadley Center) simulations of the SRES-A2 emissions scenario. A 30-year time slice for the control simulation and the scenario simulation were used, in contrast to all previous SWECLIM scenario simulations with 10-year time slices. Preliminary results for changes in temperature and precipitation are shown in Figures 3 and 4, respectively. The figures show both the new results and results from RCA1 with HadCM2 boundary conditions. In general, the average annual RCAO temperature change in the Nordic region is similar to RCA1 and the RCAO precipitation change is lower than RCA1.

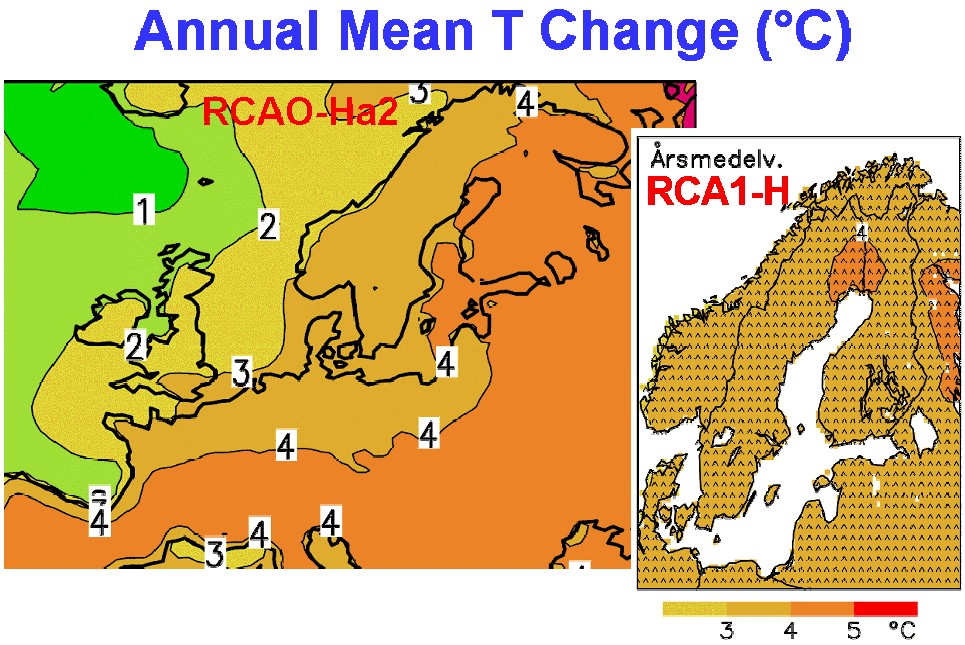

Figure 3: Annual mean change in temperature for RCA2 simulations (left) compared to RCA1 simulations (right).

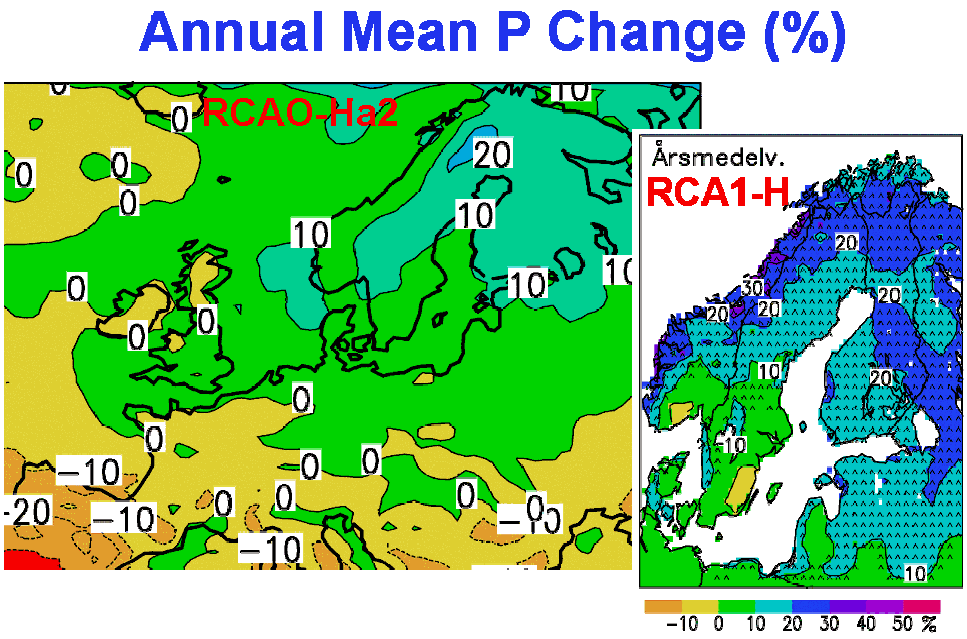

Figure 4: Annual mean change in precipitation for RCA2 simulations (left) compared to RCA1 simulations (right).

Acknowledgements

SWECLIM and the Rossby Centre are funded by MISTRA (Swedish Foundation for Strategic Environmental Research) and SMHI. The Hadley Centre provided global model results. The regional model results presented here are from the combined efforts of the scientists at the Rossby Centre. This work is a part of the Rossby Centre, SMHI, undertaking in the PRUDENCE-project, EU contract no. EVK2-CT2001-00132.

References

Bringfelt, B., Räisänen, J., Gollvik, S., Lindström, G., Graham, L.P. and Ullerstig, A., 2001: *The Land Surface Treatment for the Rossby Centre Regional Atmospheric Climate Model - Version 2 (RCA2)*. SMHI Reports RMK No.98, Swedish Meteorological and Hydrological Institute, Norrköping, 40 pp.

Döscher, R., Willén, U., Jones, C., Rutgersson, A., Hansson, U. and Meier, M., 2001: The state of development of the coupled 3D Atmosphere-Ocean Model RCAO. *SWECLIM Newsletter* **10**, 9-15.

Graham, L.P., 2001: Runoff routing in RCA underway. *SWECLIM Newsletter* **10**, 18-20.

Hahn, C.J., Warren, S.G. and London, J., 1995: The effect of moonlight on observation of cloud cover at night, and application to cloud climatology. *J. Clim.* **8**, 1429-1446.

Huffman, G.J. and Bolvin, D.T., 2001: GPCP version 2 combined precipitation data set documentation. Available from ftp.ncdc.noaa.gov, at pub/data/gpcp/v2/ documentation/v2_doc

Jones, C. and Ullerstig, A., 2002: The representation of precipitation in the RCA2 model. *SWECLIM Newsletter* **12**, (in press).

Källén, E. (ed.), 1996: *HIRLAM documentation manual. System 2.5*. Swedish Meteorlogical and Hydrological Institute, Norrköping. 178 pp. + 55 pp. appendix.

Rubel, F. and Hantel, M., 2001: BALTEX 1/6-degree daily precipitation climatology 1996-1998. *Meteorol. Atmos. Phys.* 77, 155-166.

Räisänen, J., Hansson, U. and Ullerstig, A., 2002: First GCM-driven RCAO runs of recent and future climate. *SWECLIM Newsletter* **12**, (in press).

Undén, P. (ed.), 2002: *HIRLAM-5 Reference System*. HIRLAM Technical Report, Swedish Meteorlogical and Hydrological Institute, Norrköping, Sweden, (in press).

Willén, U. and Jones, C., 2002: Comparison of model and cloud radar derived cloud overlap. *SWECLIM Newsletter* **12**, (in press).

The Norwegian Ocean Climate Project (NOClim)

A brief overview of the project and some recent results of ocean climate variability

by

Harald Loeng

Institute of Marine Research, P.O. Box 1870 Nordnes, N-5024 Bergen, Norway

Abstract

NOClim is the youngest of the national coordinated research projects under the umbrella of KlimaProg. The project leader is Dr. Peter M. Haugan, University of Bergen. The overall objectives of NOClim are to:

- Improve and enhance our understanding of rapid changes in the thermohaline circulation in the Northern seas
- Improve and enhance our understanding of ocean and ice processes related to climate, and mechanisms causing significant variability in the hydreography, circulation and ice cover in the Northern seas
- Maintaining time series for detecting climate change in the Northern seas.

The project has seven tasks focusing on different aspects of climate variability and change. This includes studies on past rapid and dramatic changes, deepwater ventilation both from shelves and in deep sea, frontal processes, signal propagation, analysis of long-term time series, and long-term observations. The relation between the 7 tasks is shown in the figure.

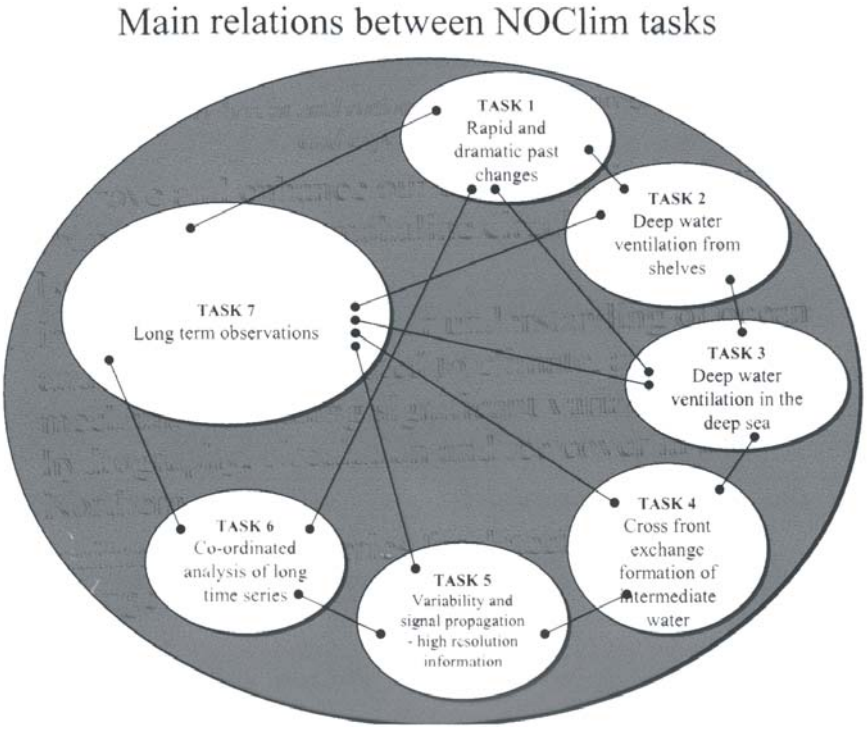

A few results are presented. The analysis of propagation of anomalies in temperature and salinity across the North Atlantic is an important task. One main question is related to a possible connection between North Atlantic and Nordic Seas SST. Another important issue is the nature and physics of the "Great Salinity Anomalies" that are observed in the 1970s, 1980, and 1990s.

Time series based on ocean temperature, sea ice paleo data have been analysed. The results indicated decadal SST variations in central part of the Nordic Seas for the last 2000 years are reconstructed from cores, and oscillations of 14 and 7.7 years period is found. These periods may reflect atmospheric variability, as also found from shorter timeseries from Svinøy section off Stadt, Norway, where the outer current branch seems to be somewhat colder and fresher in years with strong western wind forcing (high NAO-phase). Similar periods are also found in instrumental time series.

Observations in the Greenland Sea have shown deepwater ventilation in anti-cyclonic eddies. The eddies have lifetime of 1 year with a cold core, and they reach down to 2000m depth and have a radius of a few kilometres. A simple conceptual model suggests that instabilities of the gyre rim current generates anomalies amiable to convection. These weakly stratified eddies will mix and stretch when subject to cooling. The accompanying numerical model experiments are consistent with such a scenario. For large scale modelling of deepwater ventilation, control integrations shows a basin scale dipole pattern in mixing depths in agreement with the observations, while the characteristics is degraded due to instantaneous convective adjustment scheme currently used in the model.

Simulated influence of increased greenhouse gas forcing on the North Atlantic Oscillation

by

Asgeir Sorteberg[1], Tore Furevik[2] and Nils Gunnar Kvamstø[2]

[1]Bjerknes Climate Reseach Centre, University of Bergen, Norway.
[2]Geophysical Institute, University of Bergen, Norway.

ABSTRACT

The quality of the coupled Bergen Climate Model (BCM) 300-year control run with respect to the North Atlantic Oscillation (NAO) and the influence of increased CO_2 on the NAO has been investigated.
It is found that the model has a quite realistic representation of the NAO both with respect to spatial and temporal characteristics. Both the variation on interannual and decadal time scales are close to the observations. Compared to the NCEP reanalysis the leading mode of MSLP variability shows a similar pattern, but the BCM has the centers of action further west than the reanalyzed data.
The simulated NAO index has a trend towards more positive values with increased greenhouse forcing and the trend corresponds to a one standard deviation increase in NAO in 100 years and there is a slight easterly shift in the centers of action, which is more in line with the NCEP data.
The decadal scale changes in wintertime precipitation over Scandinavia with increased CO_2 are strongly related to the NAO response on changes in greenhouse gases.

1. Introduction

The North Atlantic Oscillation is a major mode of variability and has received much attention the last decade due to the persistent trend towards the positive phase the last three decades. NAO has a broad specter of variations on inter-monthly to interdecadal timescales. Bjerknes made a distinction between the short-term variability (2-3 years), which he attributed to a passive North Atlantic upper-ocean response to the atmospheric forcing, and longer term variability which he attributed to a two-way coupling between the atmosphere and the ocean involving the strengthening of the oceanic gyres (Bjerknes, 1962;Bjerknes, 1964). More than 70% of the NAO variance can be explained by short-term fluctuations having periods of less than 10 years, however decadal trends are clearly present. The presence of these longer time trends have been given a lot of attention in recent literature and proposed explanations include long-term changes in the North Atlantic Ocean, external influence such as global warming or stratospheric ozone depletion (Eichelberger and Holton, 2002; Hartmann, 2000) and natural stochastic variations (Wunsch, 1999).

The aim of this study is to investigate if increased CO_2 manifest itself by amplifying a natural mode of the climate system like the NAO. This has been explored with the coupled Bergen Climate Model (Furevik et al., 2002).

In order to have some faith in the results it is important that the numerical model is simulating the known features of the NAO pattern in a realistic way. A large part of the paper is therefore devoted to investigation of the realism of the simulated NAO pattern.

2. The simulated NAO signal

Several definitions of the NAO index appear in the literature, ranging from the use of the east west signature in temperature in earlier studies (Hann, 1890; Walker and Bliss, 1932; van Loon and Rogers, 1978) to pressure related indexes as (standardized) pressure differences between different station pairs (Rogers, 1984; Hurrell, 1995; Jones et al., 1997), area-weighted pressure extremes (Santer, 1988) and principal component analysis (Rogers, 1990).

The aim of this section is to evaluate the model's performance so the choice of definition of the index is less important as long as the same definition is used both for the observational and simulated data. We therefore have used the length of the available observational records as the determining factor in the choice of which observational datasets to use. As with the index definition, the definition of the winter season has also varied among different investigator DJF, (van Loon and Rogers, 1978); DJFM, (Hurrell, 1995); NDJFM, (Jones et al., 1997). In this study we use December to March (DJFM) as the winter season.

2.1 The mean state and variability of the NAO

The longest available observational based NAO index is the index from Jones et al., 1997 (1824-2000), which uses the observed pressure time series at Iceland and Gibraltar. For inter-comparison we use the pressure differences between the two stations without any standardization. The reason for this is that a standardization process may hide model errors (small amplitudes compensated by a small standard deviation). Figure 1 and Table 1 both show that the mean pressure difference between the two stations, the variability and the correlation are close to observed values.

Power spectra of the observed and simulated Gibraltar - Iceland NAO (Figure 2) indicate a white spectrum both for the observations and the simulations, but there exist peaks both in the observed and simulated spectrum around 8 and 2.5 years. The significance of these peaks are unclear.

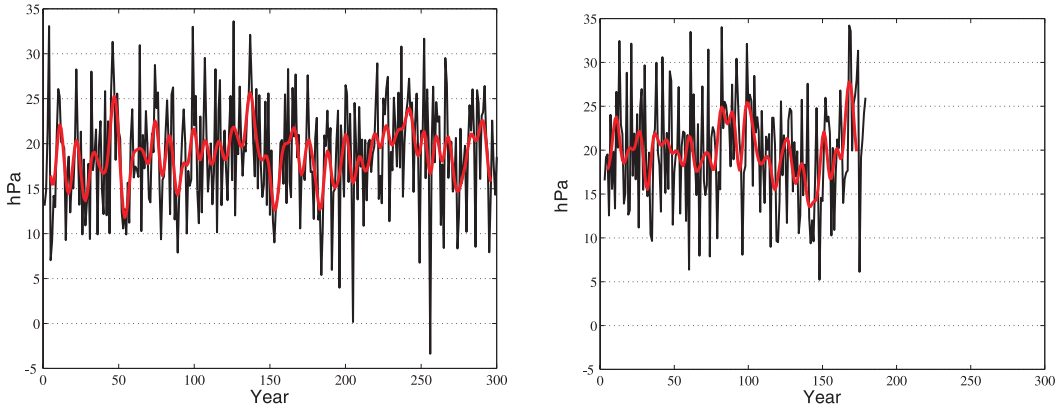

Figure 1: Time series of wintertime (DJFM) NAO taken as the pressure difference between the grid squares covering Gibraltar and Iceland (MSLP (Gibraltar)-MSLP (Iceland)) in the BCM control run (left) and observed (right, Jones (1824-2000)). Smoothed curves are long-term variations using a 9-year low-pass filter

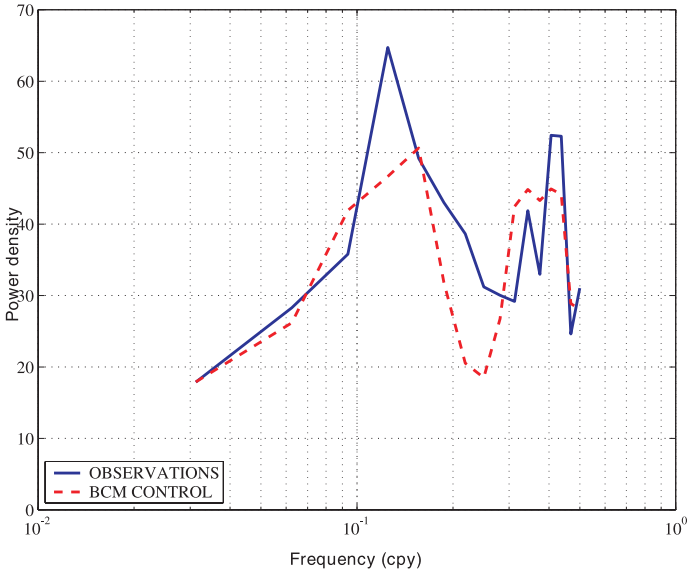

Figure 2: Power spectra of wintertime (DJFM) NAO taken as the pressure difference between the grid squares covering Gibraltar and Iceland (MSLP (Gibraltar)-MSLP (Iceland)) in the BCM control run (dashed) and observed (solid), Jones (1824-2000).

Table 1: Statistics of observed (Jones et al., 1997) (1824-2000) and simulated wintertime (DJFM) NAO. NAO has been taken as the pressure difference between the grid squares covering Gibraltar and Iceland (MSLP (Gibraltar)-MSLP (Iceland)). Unit: hPa.

	Observations	**Control simulation**
Maximum	34.2	33.6
Minimum	5.2	-3.4
Inter Quartile Range	8.9	8.6
Mean	19.9	18.8
Standard deviation	6.3	6.0
Correlation between Gibraltar and Iceland MSLP	-0.62	-0.65

The standard deviations are 6.3 and 6.0 hPa for the observations and the simulation, respectively and the model describes both the interannual and long term variability in the NAO close to the observations.

The interannual variability was calculated as the standard deviation of the year-to-year differences using the method of Bjerknes (1964). This is obtained by simply taking the differences (Δz (y)=z (y)-z (y-1)) between the NAO value one year and the value in the previous year. The difference Δz /2 can be considered a high pass filter, which attenuates the amplitude of the low frequencies and let the 2-year signal go by without any attenuation. Performing this filtering gave an interannual standard deviation of 4.5 hPa in the observations compared to 4.2 hPa in the simulations.

The long term variability (using a 9-year low-pass forward-and-backward filter) was 2.8 hPa in the observations compared to 2.6 hPa in the simulation.

2.2 The occurrence of long term trends in the NAO signal

During the last 3 decades there has been a strong positive trend in NAO and speculations on the reason for this trend have been many. In order to investigate if there exist any long-term trends of similar magnitude due to natural variability in the simulation, 30-year trends have been calculated using a moving 30-year window for the whole simulation period (300 years). Figure 3 shows the probability of occurrence of different 30 years trends in the simulation and comparison with the observations before and after 1950. Both the simulation and the observations before 1950 shows no preference for positive or negative long-term trends, however the observed distribution is skewed towards more frequent occurrences of positive long term trends for the post 1950 observations.

The control run simulates the distribution of different long term trends in NAO close to the observed values if the last 50 years of observations are excluded, but the observed long term trends for the last 50 years are not represented in the control run.

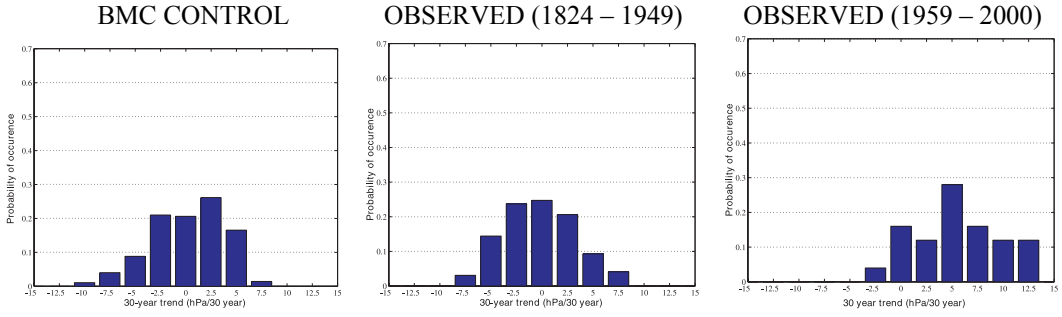

Figure 3: Occurrence of wintertime (DJFM) NAO 30-year trends (using a moving 30 year window) in the BCM control run and the occurrence of observed trends for 1824-1949 (middle) and 1950-2000 (right). Unit: hPa/30 year.

2.3 Spatial pattern

In order to investigate the co-variations of MSLP in different areas over the North Atlantic/European area we have calculated the leading mode of variability using standard PCA analysis. This pattern may be interpreted as the spatial characteristics of NAO (Rogers, 1990) and allow us to investigate spatial differences between the observed and simulated NAO signal. Even though the PCA method is an objective method, the choice of spatial domain must be done subjectively. Here we follow Stephenson and Pavan (1999) and choose the North Atlantic and surrounding land areas (120W-60E and 20-80N). This will minimize any strong signals from tropical signals (ENSO) and reduce the effect of anomalous Arctic sea ice behavior.

Figure 4 shows the leading mode mode of MSLP variability, where anomalously high pressure in the sub-tropics is associated with anomalously low pressure over the Nordic Seas and Arctic Ocean. The BCM show a fairly realistic pattern, but the positive centre of action is shifted to the west compared with the observation. The simulated leading mode account for 43% of the MSLP variation in the region compared to 42% in the NCEP reanalysis.

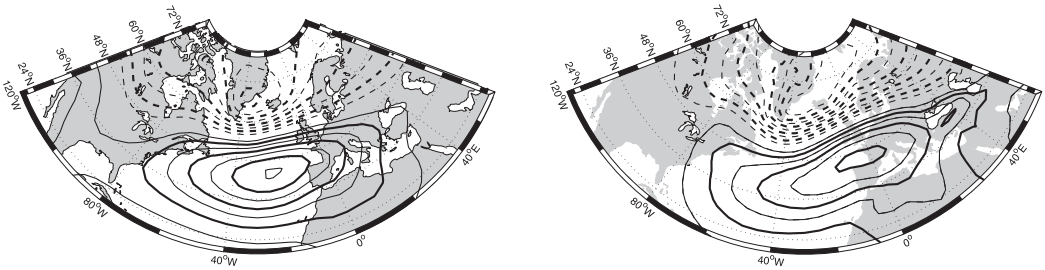

Figure 4: Wintertime (DJFM) MSLP anomalies regressed on the principal component of the leading model of variability (first EOF) over the north Atlantic area (120W-60E and 20-80N) for BCM control integration (left) and NCEP 1950-1995 (right). Contour interval is 0.5hPa.

In early NAO related literature (Walker and Bliss, 1932; van Loon and Rogers, 1978) surface temperature was used to define the NAO. This has the advantage that the centers of action are more geographically fixed due to the land-sea temperature differences and secondly the possibility to use the Jones 1855-1995 temperature record instead of the much shorter reanalyzed NCEP pressure data. Figure 5 shows the leading mode of variability of the standardized 2 m temperatures during the winter (DJFM) months. BCM has a good representation of the observed leading mode of T2m variability with the well known pattern associated with the NAO which is a quadrupole in temperature, with positive phase of the NAO associated with higher than normal temperatures centered over northern Europe and the south-eastern part of the North America, and lower than normal temperatures centered over the Labrador Sea and the north-western Africa. For the winter mean data, the pattern describes 20% of the variance in the BCM and NCEP data (not shown), and 16% in the Jones data set.

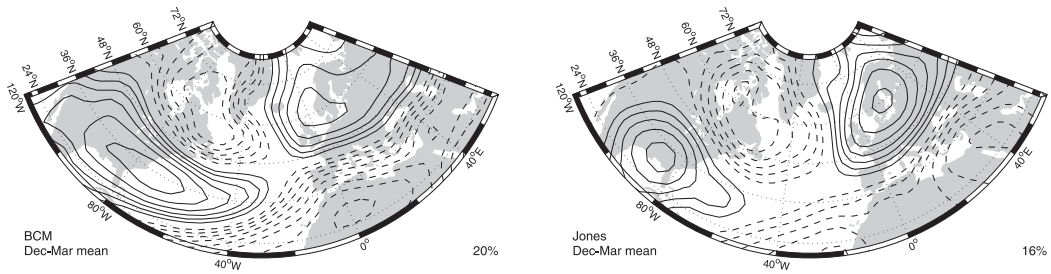

Figure 5: The 2 m temperatures regressed on the leading mode of variability (1. EOF) of the winter (DJFM) mean calculated over the area 120W to 60E, 20N to 80N for BCM (left) and Jones, 1855-1995 (right). Contour interval is 0.1°C, with negative contours dashed.

3. The influence of increased CO_2 on NAO

Several studies have linked the recent decades positive trend in NAO to the change in greenhouse gas forcing and reduction in stratospheric ozone (eg. Eichelberger and Holton, 2002; Hartmann, 2000). Simulated (AOGCM) responses in NAO due to increased CO_2 is rather model dependent. The ability of the BCM to simulate a realistic NAO signal gives some confidence that a perturbation of CO_2 concentration may give a realistic response in the NAO signal.

An 80-year transient 1% per year increase in CO_2 (CMIP2) simulation starting at 1993 concentrations (353 ppm, same as the control integration) has been performed with the BCM. Parameters related to natural variations (solar intensity, volcanic activity etc.) have been kept constant to isolate the effect of increased CO_2.

3.1 Spatial and temporal characteristics

Figure 6 shows the NAO in the BCM 1% CO_2 per year increase simulation. The amplitudes of the signal are slightly weaker in this simulation compared to the control run (standard deviation of 5.5 hPa compared to 6.0 hPa in the control run). This is due to the reduced occurrence of years with small differences between the Gibraltar and Iceland MSLP (negative NAO phase).

The spatial NAO pattern in the increased CO_2 run resembles the control run (Figure 4), but there is a slight easterly shift in the centers of action eastward (compare to Figure 7). This is more in line with the NCEP data, which represent the characteristics of the leading MSLP mode for the last 50 years.

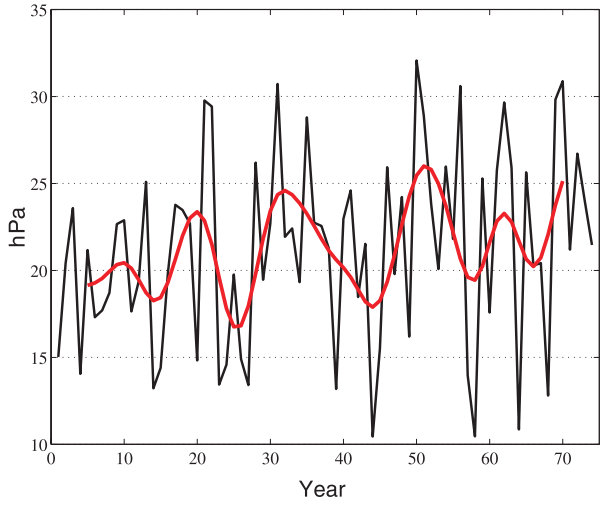

Figure 6: Time series of wintertime (DJFM) NAO taken as the pressure difference between the grid squares covering Gibraltar and Iceland (MSLP(Gibraltar)-MSLP(Iceland)) in the BCM 1% CO_2 per year increase simulation. Smoothed curve is long-term variations using a 9-year low-pass filter.

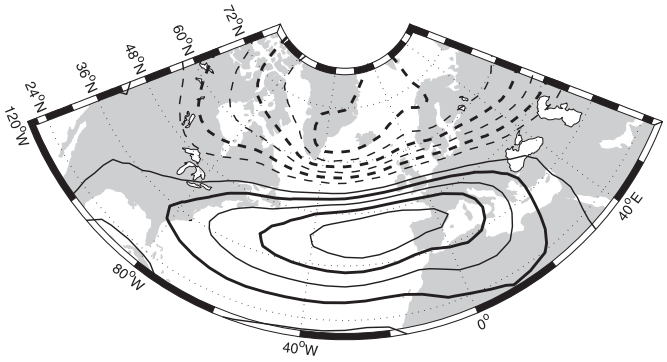

Figure 7: Wintertime (DJFM) MSLP anomalies regressed on the principal component of the leading model of variability (first EOF) over the north Atlantic area (120W-60E and 20-80N) for BCM 1% CO_2 per year increase simulation. Contour interval is 0.5hPa

3.2 Long term trends due to increased CO_2

As noted previously, the control simulation with fixed CO_2 simulated the distribution of 30-years trends close to the trends observed before 1950. In the increased CO_2 simulation there was an increased occurrence of positive long-term trends (Figure 8). The probability of a positive long-term trend increased from around 50% in the fixed CO_2 simulation to 70% in the increased CO_2 simulation. One should note that this shift might be influenced by the short sampling time in the increased CO_2 simulation (80 year).

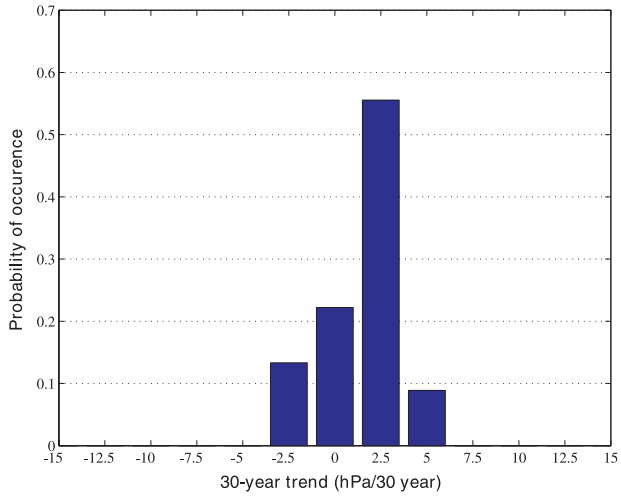

Figure 8: Occurrence of wintertime (DJFM) NAO 30-year trends (using a moving 30 year window) in the BCM 1% CO_2 per year increase simulation. Unit: hPa/30 year.

The simulated increase in occurrences of positive NAO in the increased CO_2 simulation is similar to, but not as strong as the observed trend over the last decades. Figure 9 shows that a 0.06 hPa per year increase in the difference between MSLP at Gibraltar and Iceland was found in the increased CO_2 simulation. This corresponds to a one standard deviation increase in NAO in 100 year.

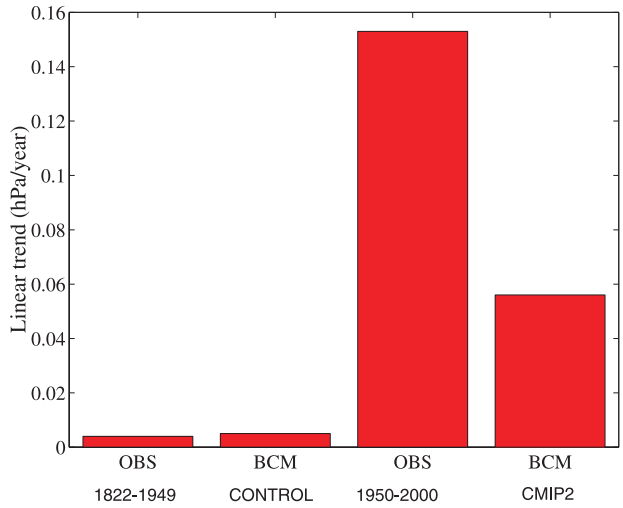

Figure 9: Observational and simulated linear trends. NOTE: The observed 1950-2000 trend is very sensitive to the time window chosen. It should not be directly compared to the trend in the increased CO_2 simulation, since the increased CO_2 simulation represent possible future trends in NAO.

3.3 Other models NAO response on increased CO_2

There is no consensus among different models on how the NAO will respond to a increase in CO_2. Figure 10 shows the trend in NAO for some state of the art models running the same scenario (1% CO_2 increase per year). We see that the both the magnitude and the sign of the trend are different among the models.

It should be noted that the trends may be somewhat sensitive to the way NAO is defined, however the same definition is used for all models.

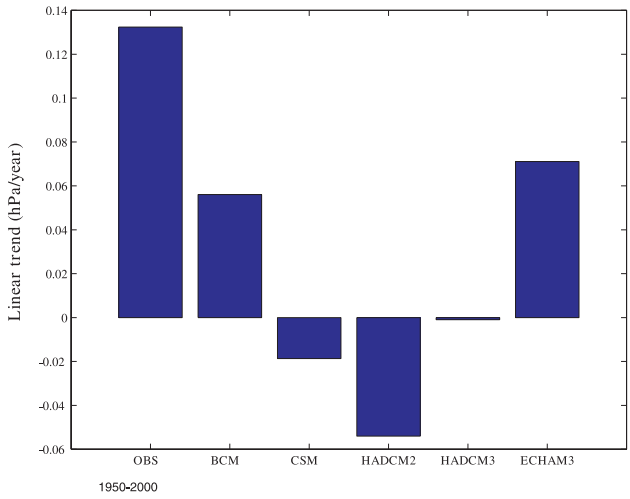

Figure 10: Simulated linear trends in NAO due to increased CO_2 in different coupled climate models.

4. The influence of long term changes in NAO on changes in Scandinavian wintertime precipitation

Figure 11 shows the relationship between changes in the long-term south Scandinavian wintertime (DJFM) precipitation due to increased CO_2 and the changes in NAO between the control and increased CO_2 run. The long term response in precipitation has a strong link to the magnitude of the NAO response. Not surprising the relationship is strongest near the west coast of Norway with a correlation of 0.8 (detrended data sets).

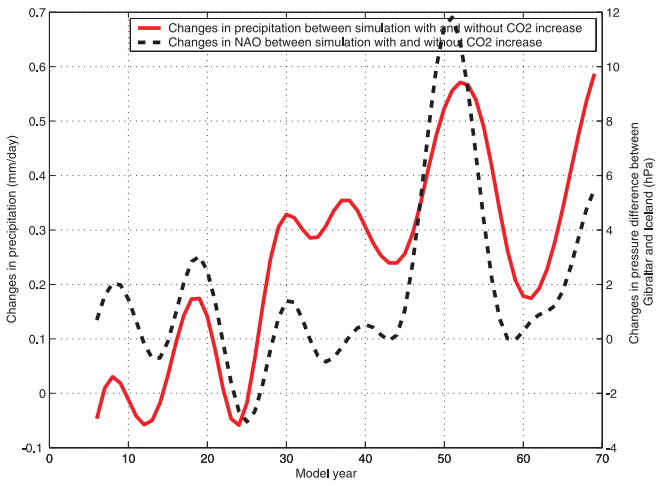

Figure 11: The relationship between changes in the long-term (11-year low-pass filter) south Scandinavian wintertime (DJFM) precipitation due to increased CO_2 (CMIP2-CONTROL) (solid) and the changes in NAO (CMIP2-CONTROL) (dashed). NAO is taken as the pressure difference between the grid squares covering Gibraltar and Iceland (MSLP (Gibraltar)-MSLP (Iceland)). South Scandinavia is defined as the area between 2.5W-20E and 54-64N.

The response of the European wintertime precipitation is quite consistent (Figure 12) with the change in NAO ranging from a increase in northern and central Europe due to a increase in the NAO in BCM to a decrease in north-westerly Europe due to decrease in NAO in the NCAR CSM model.

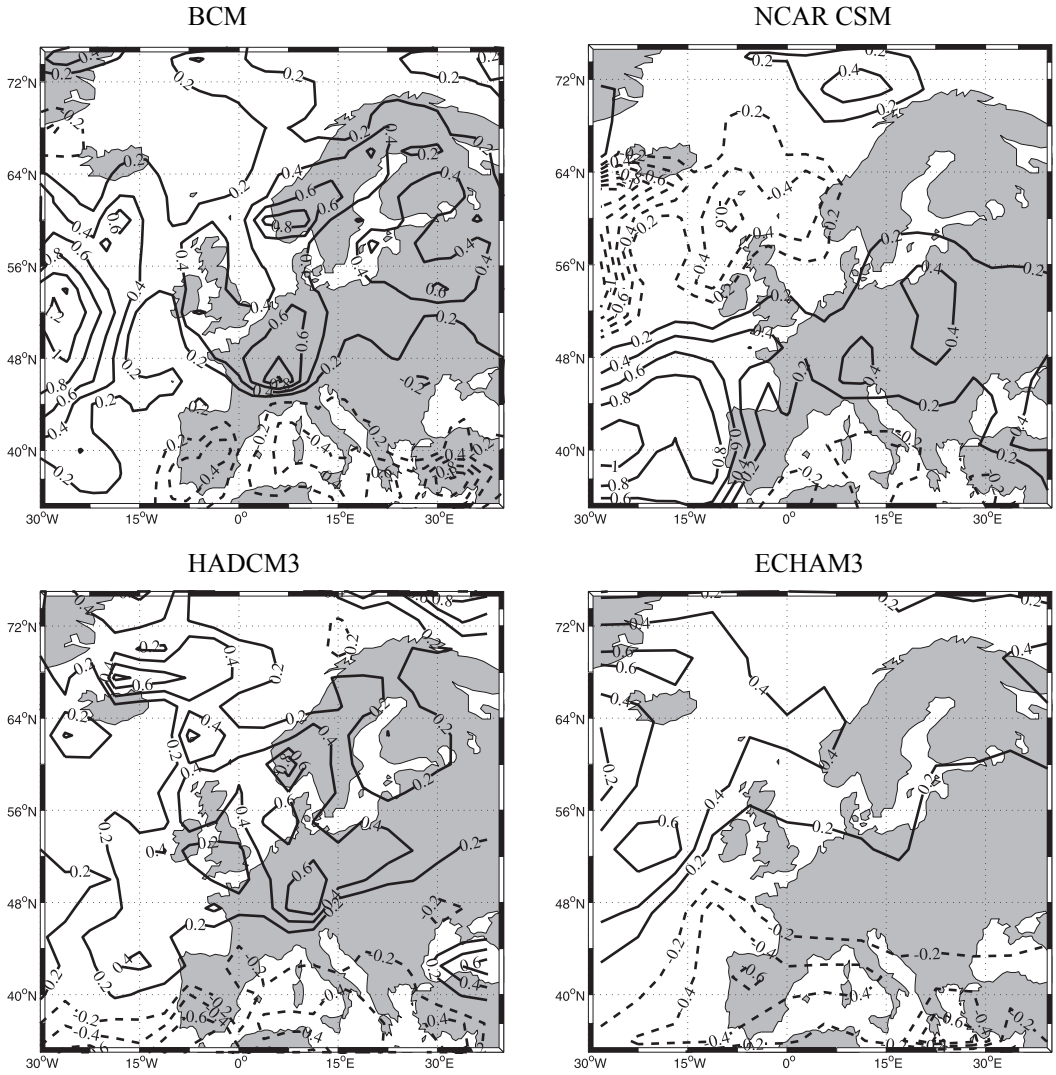

Figure 12: The changes in European wintertime (DJF) precipitation (mm/day) due to doubling of CO_2 (mean from year 60-80, doubling at year 70) compared to the control run for different coupled models.

5. Conclusions

The BCM control simulation (300 years) simulates the NAO fairly well with respect to both the mean and amplitude of the NAO signal close to observations. The variation on interannual and long-term variations are close to the observations. The power spectrum indicates a white spectrum, both for the observations and the simulations. There are no significant peaks in the spectrum, but there exist peaks both in the observed and simulated data around 8 and 2.5 years.

Compared to the NCEP reanalysis the leading model of MSLP variability shows a similar pattern, but with the southerly center of action further west than the reanalyzed data.

A 1% CO_2 per year increase simulation (80 years) has been performed and the NAO pattern closely resembles the control integration. However there is a slight easterly shift in the centers of action, which is more in line with the NCEP data, which represent the characteristics of the leading MSLP mode for the last 50 years.

The increased CO_2 simulation showed a trend towards more positive NAO index corresponding to a one standard deviation increase in the MSLP difference between Gibraltar and Iceland in 100 years (0.06 hPa per year increase) Thus this study supports recent studies suggesting that changes in greenhouse gas forcing may have an impact on natural mode of variabilities such as the NAO.

However, the physical reasons for this is still unclear and may possibly involve SST interactions (Hoerling et al., 2001), changes in the propagation of planetary waves due to changes in the atmospheric temperatures (Eichelberger and Holton, 2002) or feedback mechanisms from reduced sea ice and snow cover.

The response of long-term trends in Scandinavian wintertime precipitation due to increased CO_2 shows that the simulated changes are related to the NAO response on changes in greenhouse gases. This emphasis the role of changes in large scale circulation on the Scandinavian climate.

Refrences

Bjerknes, J., 1962: Synoptic survey of the interaction of sea and atmosphere in the North Atlantic. *Geophys. Norv*., **24(3)**:115-145.

Bjerknes, J., 1964: Atlantic Air-Sea Interaction, *Adv. Geophys*., **10**:1-82.

Eichelberger, S. and Holton, J.R., 2002: A Mechanistic Model of the Northern Annular Mode, Submitted to *J. Geophys. Res*.

Furevik, T., Bentsen, M., Drange, H., Kindem, I. K. T., Kvamst, N. G., and Sorteberg, A., 2002: Description and Validation of the Bergen Climate Model: ARPEGE coupled to MICOM., Submitted to *Climate Dynamics*.

Hann, J., 1890: Zur Witterungsgeschichte von Nord-Grönland Westküste, *Meteorologische Zeitschrift*, **7**:9109-110.

Hartmann, D., 2000: Can ozone depletion and global warming interact to produce rapid climate change?, *Proc. Natl. Acad. Sci*, **97**:1412-1417.

Hoerling, M., Hurrell, J.W., and Xu, T.Y., 2001: Tropical origins for recent North Atlantic climate change, *Science*, **292(5514):**90-92.

Hurrell, J.W., 1995: Decadal trends in the North Atlantic Oscillation: Regional temperatures and precipitation, *Science*, **269**:676-679.

Jones, P.D., Jonsson, T., and Wheeler, D., 1997: Extension to the North Atlantic Oscillation using early instrumental pressure observations from Gibraltar and South-West Iceland, *Int. J. Climatol*., **17**:1433-1450.

Rogers, J., 1984: The association between the North Atlantic Oscillation and the Southern Oscillation in the Northern Hemisphere., *Mon. Weather Rev*., **112**:1999-2015.

Rogers, J., 1990: Patterns of low-frequency monthly sea level pressure variability (1899-1986) and associated wave cyclone frequencies., *J. Climate*, **3**:1364-1379.

Santer, B.D., 1988: Regional validation of general circulation models., Technical report, University of East Anglia, Norwich, England.

Stephenson, D.B. and Pavan, V., 1999: Is the North Atlantic Oscillation a random walk ?, Submitted to *Climate Dynamics*.

van Loon and Rogers, J.C., 1978: The seesaw in winter temperatures between Greenland and Northern Europe. Part I: General description, *Mon. Weather Rev*., **106**:296-310.

Walker, G.T. and Bliss, E.W., 1932: World Weather V, *Mem. Roy. Meteor. Soc*., **4**:53-84.

Wunsch, C., 1999: The interpretation of short climate records, with comments on the North Atlantic and Southern Oscillations., *Bull. Am. Meteor. Soc*., **80**:5257-270.

Simulated atmospheric response to changed Arctic sea ice conditions

by

N.G. Kvamstø, C. Albertsen and T. Boge

Geophysical Institute, University of Bergen, Norway

1. Introduction

In the present study, we report some preliminary findings from an atmospheric general circulation model (AGCM) experiment, in which we have imposed changes in the annual Arctic sea ice extent- and sea surface temperature (SST) cycle. In general, it is important to explore the influence of the sea-ice on the large scale atmospheric flow since limited attention has been paid to this problem in the literature. In the limited number of studies on this problem sensitivity to highly idealised sea ice changes has been explored (Royer et al., 1990). More recent studies have taken newer more accurate observations (Deser et al 2000) into account and investigated atmospheric response to frequent wintertime anomalies (Honda et al., 1999; Kvamstø et al., 2002; Lopez et al., 2000). In this study as well, recent observations have motivated a sea-ice sensitivity experiment of a slightly different type. Both Rothrock et al. (1999) and Johannessen et al. (1999) show that there is a decreasing trend in the observed summer time Arctic sea-ice extent- and thickness. The other seasons seem not to be affected by this trend to the same degree. In scenario simulations with coupled GCMs, a similar trend is observed. Some of these models predict a short ice-free period in the Arctic during late summer, around the time the CO_2 concentration has been doubled. In the following we have investigated the atmospheric response to a reduced summer time sea ice extent.

2. Experimental design

The model employed in this study is the ARPEGE/IFS model, used by Météo-France and documented in Déqué (1994), Doblas-Reyes et al. (1998). The horizontal resolution used here is a linear T63 truncation ($T63_L$), which has a lat/lon grid spacing of about 2.8° everywhere on the globe. There are 31 levels in the vertical, with 20 in the troposphere and 10 in the stratosphere.

Two 10 years integrations have been carried out:

i) One control experiment, in which the SST and sea-ice conditions consist of monthly climatological values (Reynolds 1988).
ii) One perturbed experiment, in which the same lower boundary conditions as in i, have been applied to winter and spring whereas in summer and autumn the Arctic sea-ice extent has been reduced.

Both experiments have been integrated with a repeated annual cycle of SSTs and sea-ice. In grid points where the sea ice cover has been removed, we specified open ocean conditions just above the freezing point.

The sea ice anomaly in the perturbed experiment has been constructed as follows. First, the time-dependent, climatological distance between the Noth Pole and the Arctic sea ice border was defined at all longitudes $r_i(\lambda,t)$. Subsequently we applied a factor $f_i(t)$ to this distance in order to modify the full Arctic sea-ice extent. Our specific choice of $f_i(t)$ is shown in Figure 1. As can be seen, climatological condition persist through December to May, while the sea ice extent is reduced between June and November.

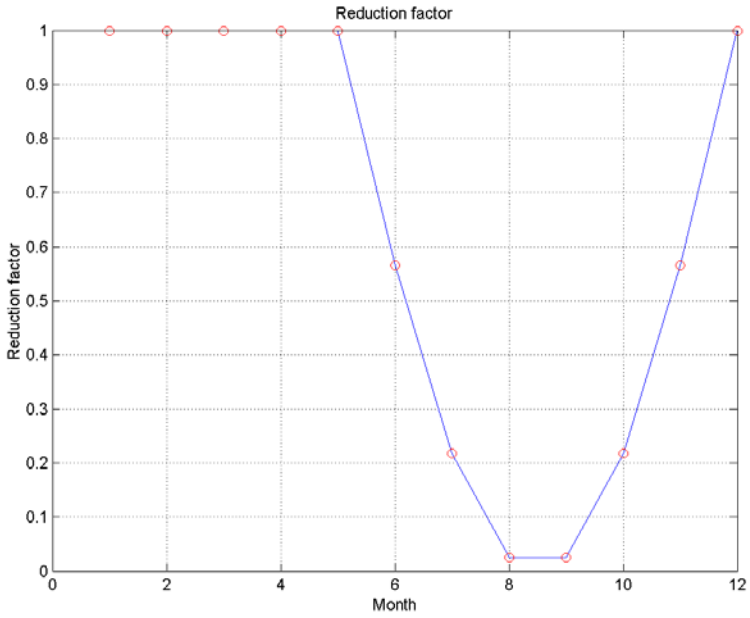

Figure 1: Time dependent reduction factor for sea-ice cover (see text for details).

3. Atmospheric mean response

3.1 Zonal mean temperature response

The zonal mean temperature response for each month of the year in two pressure levels can be seen in Figure 2. The diagrams show the zonal mean temperature difference between the perturbed- and control simulation at two levels 850hPa and 500hPa.

In the lowest layer we find a significant warm anomaly in the perturbed run at the high latitudes, which culminates in November, two months after the ice-free conditions. This local response is statistically significant to 95%. Elsewhere the differences are very small or insignificant.

At 500hPa, the same pattern is more or less apparent, but with significantly smaller differences. This indicates that the response is local and confined to the lowest atmospheric levels.

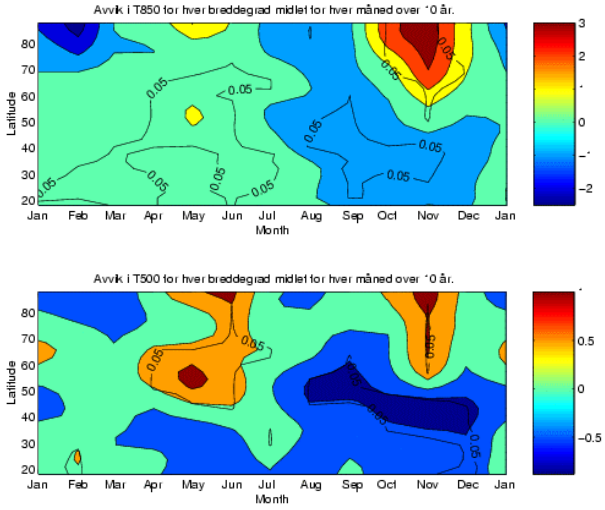

Figure 2: Zonal mean temperature response (in K) in 850hPa (upper) and 500 hPa (lower). The response is taken as perturbed-minus control simulation. The black contour denotes areas where the response is statistically significant (95%, students t-test).

3.2 Zonal mean pressure response

Figure 3 shows the response in the atmospheric mass field. The gross picture is dominated by a local positive (or high pressure) anomaly in the Arctic (with a lagged maximum compared to the time of the ice free conditions) and a more remote, mid-latitude response with a similar time evolution, which is negative.

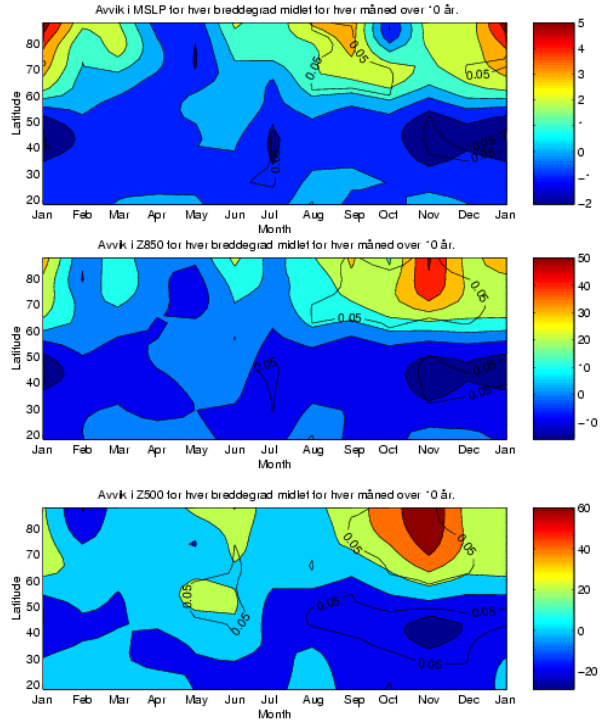

Figure 3: Zonal mean MSLP response (in hPa) (upper panel), zonal mean geopotential response (m) in 850hPa (middler) and 500 hPa (lower). The response is taken as perturbed- minus control simulation. The black contour denotes areas where the response is statistically significant (95%, student t-test).

One may observe that the response at 500hPa is quite close to the one in 850hPa, which indicates that the thickness between 500-850hPa is not affected to the same degree as the layer below.

3.3 Geographical distribution of the low level response

The diagrams in Figure 4 show the geographical distribution in SOND of the low-level atmospheric response. A local, warm, high-pressure response and a more remote mid-latitude low pressure response are clearly apparent. The remote low-pressure response coincides quite closely with the mid-latitude storm tracks, both in the Pacific and in the Atlantic. As mentioned, for the temperature we have mostly a local warm response and weaker mixed anomalies outside the Arctic.

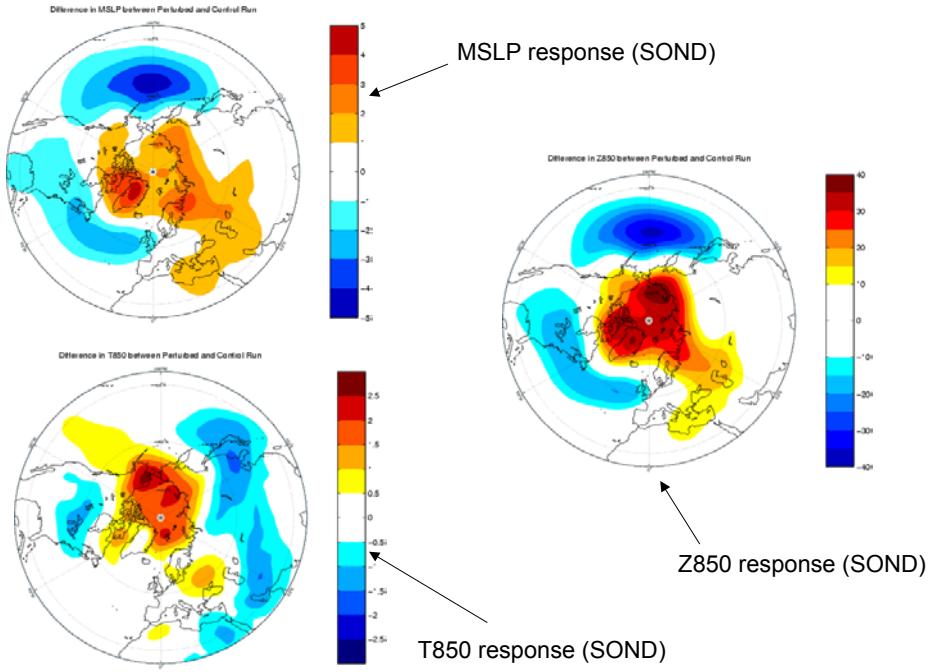

Figure 4: Geographical distribution of MSLP (upper left)-, Z_{850} (middle)- and T_{850} (lower left) responses during SOND. The units are in hPa, m and K respectively.

4. Response in transient characteristics

The only analysis performed on transient properties of the simulations so far is standard principal component analysis on monthly MSLP anomalies. In Figure 5 the characteristics of the first EOF of the MSLP anomalies in late autumn is shown. More specifically, a time sequence of MSLP anomalies for each of the OND months during the two 10 years simulations has been constructed. This time series contains 3*10*2 = 60 anomaly matrixes, where the 30 first matrixes have been collected from the control run and the 30 last matrixes have been collected from the perturbed run. The pattern of the 1st EOF can be considered as the Arctic Oscillation of the model (AO_m), which explains 19.2% of the monthly MSLP variance in the two experiments (Figure 4). The 1st principal component (PC1) describes the time evolution of the AO_m and can be termed the AO_m index. From Figure 5 it is evident that the variability of the AO_m index has been significantly reduced in the perturbed experiment. This can be seen both from the Box plots

and the standard deviations of the AO_m index. It is worthwhile to note that there are no phase changes in the AO_m index between the runs, i.e. none of the experiments prefers a certain phase of the AO_m compared to the other.

Exactly the same diagnostics have been calculated in the North Atlantic sector. The regional counterparts of the AO_m and the AO_m index can be termed the NAO_m and the NAO_m index, respectively. The changes in the NAO_m index characteristics are similar to the AO_m index response. However, the reduction in variability is weaker; a 14% reduction of the standard deviation in the NAO_m case and a 29% decrease in the AO_m case. This indicates that the response in the AO_m variability is due to variability changes in the Pacific sector.

From this analysis it is not possible to state which phenomena that are associated with the variability response. A more thorough variability analysis with band pass filters for example, is needed to give further substantial information on this subject.

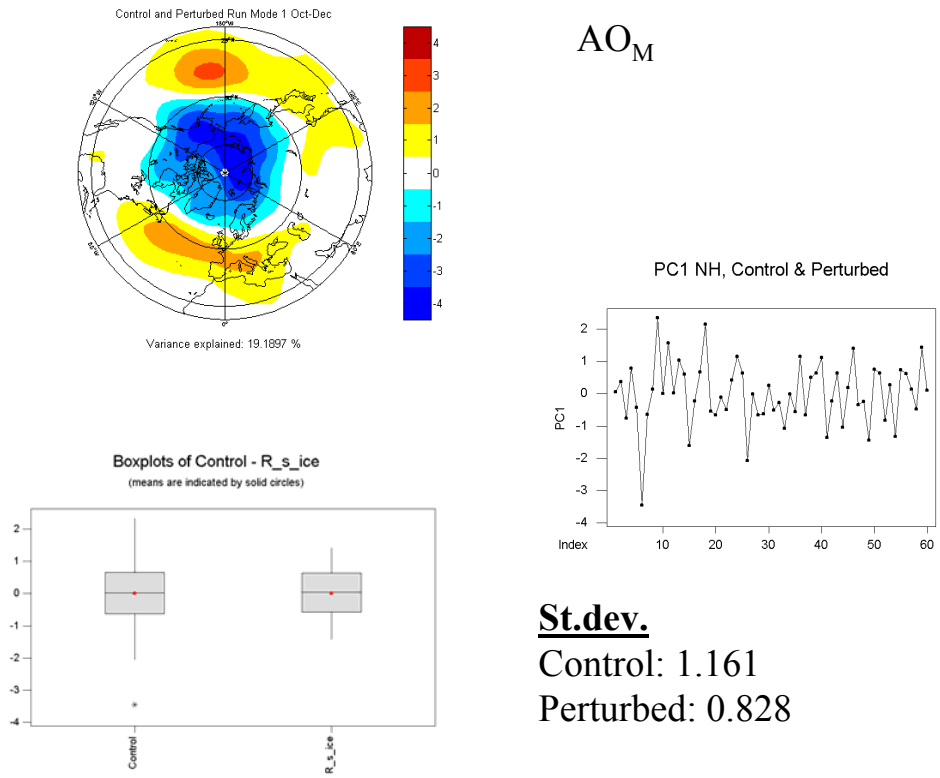

Figure 5: 1st EOF from a standard PCA analysis of the monthly MSLP anomalies (upper left). This pattern may also be termed the AO_m (see text for explanation). Principal component (or AO_m index) of the 1st EOF (right panel). Standard deviations on the vertical axis and months along the horizontal axis (30 first months are from the control run and 30 last months are from the perturbed run. The Boxplot (lower left) shows statistics from each half of the AO_m index; mean value (red), quantiles (horizontal lines and end of whiskers) and outliers (star).

The zonal mean response of some selected physical fields can be seen in Figure 6. Upper left shows the change in latent heat flux. As negative flux is defined to be

negative when directed upward, a lagged increase in latent heat flux can be associated with the imposed decrease in sea ice cover. A similar change is seen in sensible heat flux, which is of the same order of magnitude as the latent heat flux response. Lower panels show the precipitation- and total cloud cover changes, which are positive, occur simultaneously with the energy flux response. The geographical distribution of the response in these fields is more noisy than in the dynamical fields. However, the response in the Arctic is pronounced and has the same sign all over this region.

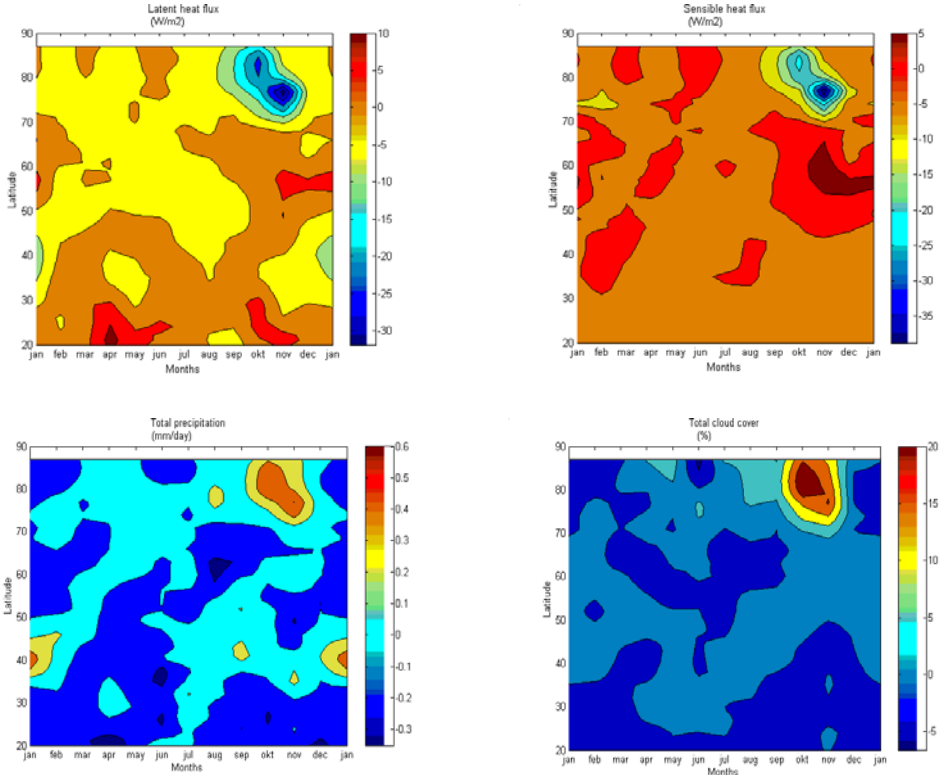

Figure 6: Zonal mean response of latent heat flux (in Wm^{-2}) (upper left), sensible heat flux (in Wm^{-2}) (upper right), total precipitation (in mm/day) (lower left) and total cloud cover (in %) (lower right).

At this stage we think that the explanation for the local Arctic response is straight forward: Increased heat fluxes in the perturbed run heat the lower atmosphere. This leads to a stretching of the lower atmospheric column and a lifting of the pressure surfaces. The stability is probably strong in both experiments so the warming does not trigger any vertical motions associated with horizontal convergence. The mid-latitude (low pressure) response is more difficult to explain and needs closer investigation

Preliminary conclusions

- The decrease or removal of Arctic sea ice in summer leads to a local warm high pressure anomaly that peaks 2 months after the ice free conditions. This can be explained by the increased energy fluxes.
- We get a more remote low pressure response in the mid-latitudes

- The ice reduction seem to cause a reduction in the AO_m variability of the during late autumn/early winter
- We see a similar, but weaker reduction in the NAO_m variability

References

Déqué, M., C. Dreveton, A. Braun, and D. Cariolle, 1994: The ARPEGE/IFS atmosphere model - A contribution to the French Community Climate Modeling, *Clim. Dyn*. **10**, 249-266.

Deser, C., J.E. Walsh, and M.S. Timlin, 2000: Arctic sea ice variability in the context of recent wintertime atmospheric circulation trends. *Journal of Climate* **13**, 617-633.

Doblas-Reyes, F.J., M. Déqué, and F. Valero, 1998: North Atlantic wintertime intraseasonal variability and its sensitivity to GCM horizontal resolution, *Tellus* **50A**, 573-595.

Honda, M., K. Yamazaki, H. Nakamura and K. Takeuchi, 1999: Dynamic and thermodynamic characteristics of atmospheric response to anomalous sea-ice extent in Sea of Okhotsk, *J. Climate*, **12**, 3347-3358.

Johannessen, O.M., E.V. Shalina, M.W. Miles, 1999: Satellite evidence for an Arctic sea ice cover in transformation, *Science* **286 (5446):** 1937-1939.

Kvamstø, N.G., P. Skeie, and D. Stephenson, 2002: North Atlantic Oscillation response to Labrador Sea-Ice. Subm. to *J.Climate*.

Lopez, P., T. Schmith, and E. Kaas, 2000: Sensitivity of the Northern Hemisphere circulation to North Atlantic SSTs in the ARPEGE Climate AGCM, *Clim. Dyn*. **16** 535-547.

Reynolds, R.W., 1988: A real-time global sea surface temperature analysis. *J. Climate*, **1**, 75-86.

Rothrock D.A., Y. Yu, G.A. Maykut, 1999: Thinning of the Arctic sea-ice cover, *Geophys. Res. Lett.* **26 (23):** 3469-3472.

Royer, J.F., S. Planton and M. Déqué, 1990: A sensitivity experiment for the removal of Arctic sea ice with the French spectral general circulation model. *Clim. Dyn*, **5**, 1-17

A possible coupling between the Arctic fresh water, the Arctic sea ice cover and the North Atlantic Drift. A case study

by

Odd Helge Otterå and Helge Drange

Nansen Environmental and Remote Sensing Center, Edv. Griegsvei 3A, N-5059 Bergen, Norway

1. Introduction

It is believed that the transport of fresh water from the high northern latitudes play a major role for the circulation in the Nordic Seas and the Atlantic (and possibly World) Ocean since it passes convective regimes of major importance to the thermohaline circulation (Aagaard and Carmack 1989). The role of high latitude fresh water transport is of interest from both a paleo and future perspective. Simonsen (1996) computed the melt water fluxes into the Atlantic Ocean, the Nordic Seas and the Arctic Ocean based on the paleo topography reconstruction of Peltier (1994). The results suggested at least a doubling of the fresh water fluxes to the Arctic Ocean in short periods during the deglaciation compared to the present.

As for the future perspective, many climate models show a substantial reduction in the Atlantic thermohaline overturning circulation (TOC) with possible large climatic impacts in northern Europe when forced with greenhouse gas and aerosol projections for the current century (e.g., Manabe and Stouffer 1994; Wood et al. 1999). A typical and quite robust response in such simulations is increased evaporation at low latitudes due to heating of the surface ocean, and increased fresh water input to the high northern latitudes from precipitation and continental runoff. It is therefore tempting to believe that increased supply of fresh water and warming at high latitudes will lead to reduced formation rates of intermediate and deep water masses, and consequently to a reduced TOC.

However, a different model response was identified by Latif et al. (2000). Here, Large-scale air-sea interactions in the tropics, lead to anomalously high salinities in the tropical Atlantic. These anomalies are then advected northward into the sinking regions of the North Atlantic , and thereby compensating for the effect of local warming and freshening.

In addition to increased fresh water fluxes at the high northern latitudes, many climate models also show an enhanced greenhouse warming in the polar regions, especially for the Arctic, with a predicted warming of ~3–4 ^{o}C during the next 50 years (Mitchell et al. 1995). This would most likely lead to changes in both the extent and thickness of sea ice in the Arctic, with possible large consequences for the Arctic region (Johannessen and Miles 2000).

In this study we explore the combined effect of increased fresh water input to the Arctic Ocean and Arctic warming, the latter manifested as a gradually reduction in the sea ice thickness, by means of idealized model experiments.

2. The coupled ocean – sea ice model

The OGCM used here is based on the Miami Isopycnic Coordinate Ocean Model (MICOM) (Bleck et al. 1992). To describe the high latitude climate system, dynamic and thermodynamic sea ice modules have been coupled to MICOM (Drange and Simonsen 1997). The dynamic ice model, which transports ice as a result of the applied wind field and the simulated sea surface currents and sea surface tilt, is based on the classical viscous-plastic rheology of Hibler III (1979), but in the modified implementation of Harder (1996).

For this study a regional version of MICOM has been used. The model domain includes the Atlantic Ocean north of 20°S and the entire Arctic Basin (Figure 1). A locally orthogonal curvilinear horizontal grid (Simonsen and Drange 1997) was adapted, with focus in the Nordic Seas (maximum grid resolution about 40 km). Artificial (closed) boundaries occur south of Bering Strait, along the South Atlantic boundary and in the Strait of Gibraltar.

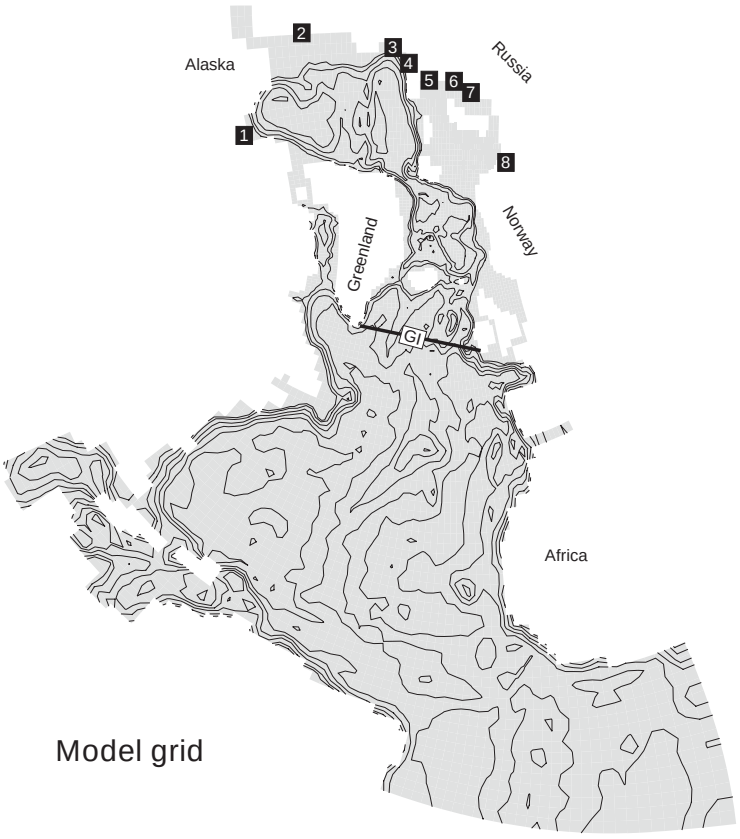

Figure 1: The model grid used in this study. The numbers 1-8 represent the major discharge locations in the Arctic Ocean (MacKenzie, Kolyma, Kotuy, Lena, Ob, Yenisei, Pyasina and Northern Dvina, respectively). Also shown is the Greenland-Ireland (GI) transect.

The model was set up with 23 layers (one mixed layer and 22 isopycnic layers with constant density below) and initialised with temperature and salinity fields for September from the National Oceanographic Data Center (Levitus et al. 1994; Levitus and Boyer 1994). The model was forced with monthly mean climatologic atmospheric data fields as follows:

- Wind stress from ECMWF, merged with data from the Comprehensive Ocean Atmosphere Data Set (COADS) in the Atlantic Ocean (Oberhuber 1988)
- Cloud cover and humidity from COADS
- Air temperature from COADS
- Precipitation is derived from Legates and Willmott (1990)

The major rivers in the model domain are included. The seasonal variation in the river output is adopted from Dümenil et al. (1993). For the Arctic Ocean the river runoff amounts to about 0.1 Sv in the model.

3. Design of the experiments

The model was spun up for 40 years until an annual steady state circulation was achieved. Relaxation of SSS and SST towards Levitus was applied during spin up. After the spin up period of 40 years, the model was run for another 3 years with continued relaxation applied to temperature and salinity. During this period the salt flux implied by the SSS relaxation was diagnosed and monthly mean values were computed and stored. A total of three 50 years long simulations were then carried out. During the three model experiments, the diagnosed monthly mean SSS flux was applied as the SSS relaxation in order to let SSS anomalies freely develop in the model. The three integrations are:

- Control: No change in fresh water flux
- PX2: Doubling of the freshwater fluxes from the Arctic rivers
- PX5: Fivefold increase in the fresh water fluxes from the Arctic rivers

It was further assumed that the additional fresh water supply follows from a warmer climate. For the PX2 and PX5 simulations, the strength of the Arctic warming was assumed to wary in accordance with the change in the fresh water fluxes. An *ad hoc* assumption was made that the warming corresponds to the change in the freezing temperature, T_f ($T_f = 0.066 - 0.057\ S_{mixed\ layer}$). This assumption leads to a reduction in the sea ice thickness of 1.5-2 m in the central Arctic over the 50 years integration period (Figure 2). A changed climate system will necessarily lead to changes in most of the air-sea-ice-sea fluxes. The presented perturbation experiments should therefore be viewed as idealized sensitivity experiments only.

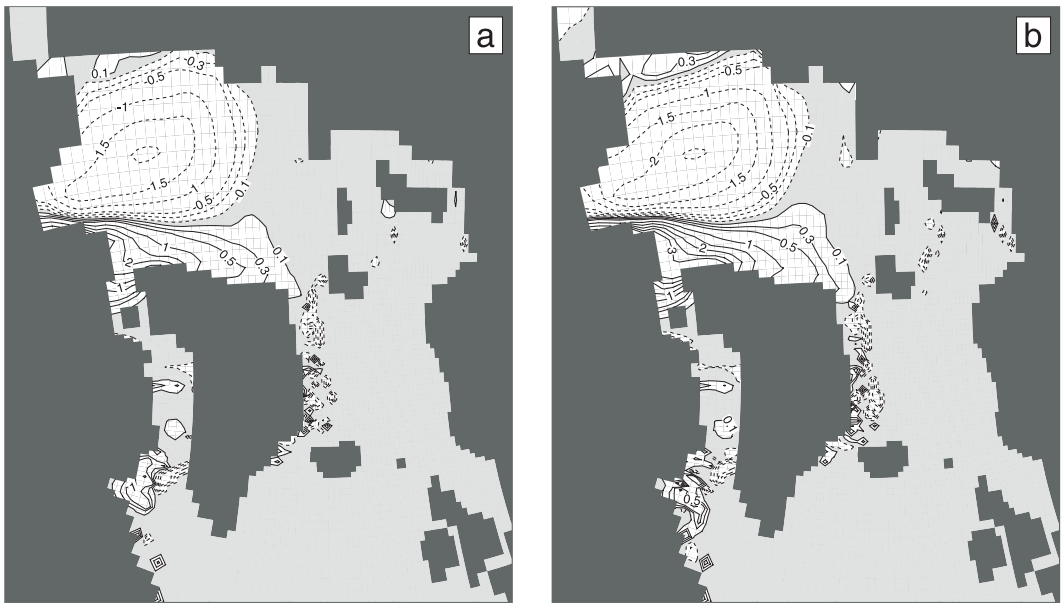

*Figure 2: Difference in sea ice thickness (m) from the control simulation for March for **a** the PX2 simulation and **b** the PX5 simulation. Dotted lines represent reduced sea ice thickness. CI is 0.5 m. In addition the ±0.3 and ±0.1 CI are shown.*

4. Control simulation

The model reproduces the major features of the modern ocean circulation in the North Atlantic, the Nordic Seas and the Arctic Ocean (Figure 3). Some model drift can be seen in the volume transport across the Greenland-Ireland section, while it remains fairly stable for the Faeroe Shetland Channel (FSC) and the Fram Strait (Figure 4).

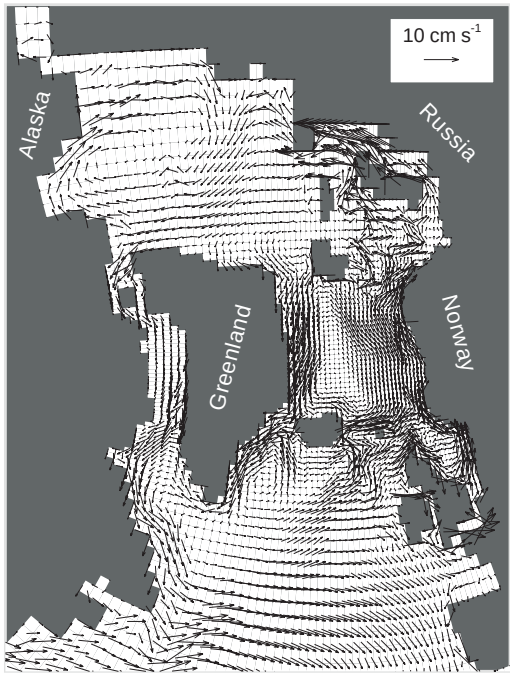

Figure 3: Simulated annual mean sea surface velocity field (cm s^{-1}) at the start of the control simulation.

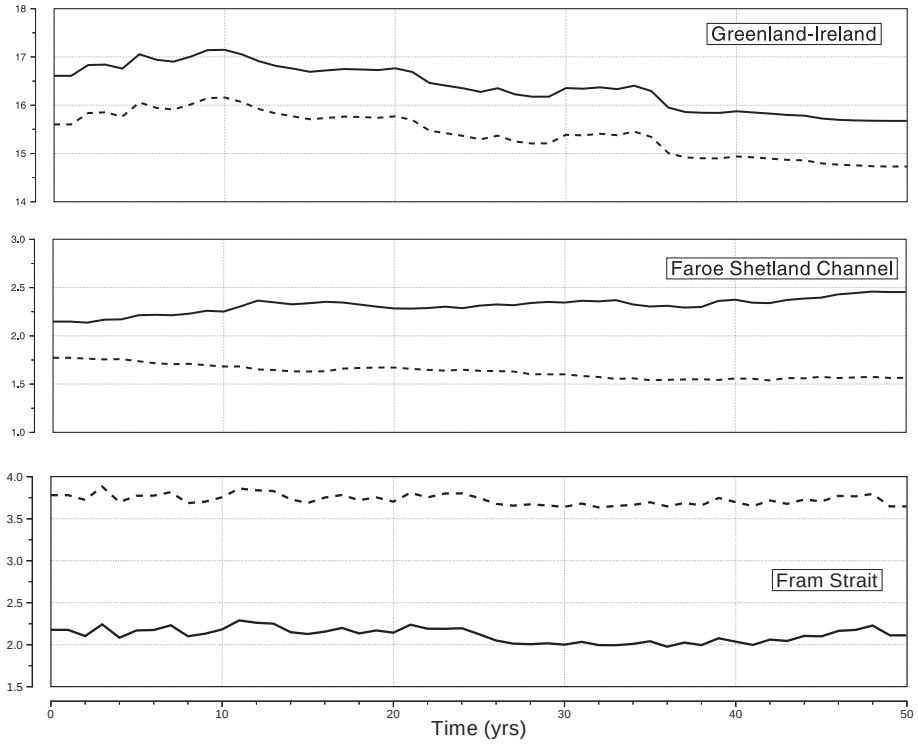

Figure 4: Time series of the net annual mean northward (solid line) and southward transports (Sv) for the Greenland-Ireland section the Faeroe Shetland Channel and the Fram Strait in the control simulation.

The model generate ice cover in fairly good agreement with climatologies derived from observations (Johannessen et al. 1999) (Figure 5) and is at least qualitatively able to reproduce the formation of subsurface water masses in the convective regions of the Labrador and Greenland Seas (Figure 6).

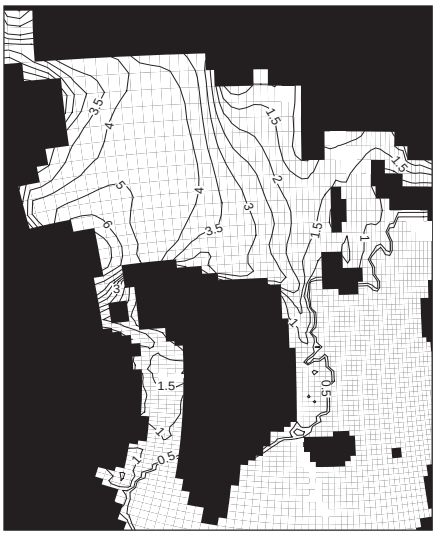

Figure 5: Sea ice thickness (m) in March at the start of the control simulation. CI is 0.5 m in addition the 0.25 m contour level is shown.

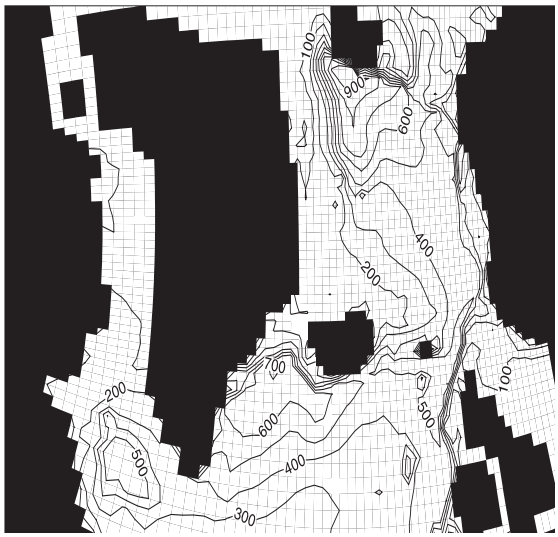

Figure 6: Mixed layer thickness (m) in March at the start of the control simulation. CI is 100 m.

The model has some deficiencies, such as not being able to correctly reproduce the Atlantic layer in the Arctic (not shown). The water at about 500-1000 m depth is too cold by about 1 degree compared to observations. Also the southward transport across the Greenland Strait, and the northward transport across FSC are underestimated in the model. Despite of this, the control run should provide a fairly realistic framework for the perturbation experiments.

5. Perturbed simulations

The major differences in the SSS compared to the control simulation are found down stream of the river discharge areas in Canada, Siberia and Russia, and after 50 years all of the Arctic Ocean is influenced (Figure 7). Furthermore, a fresh water lens can be seen to propagate from the Canadian Archipelago into the Atlantic Ocean. Because of the increased fresh water input to the Arctic Ocean, a strong density gradient is set up along the Transpolar Drift. This in turn influences the horizontal pressure gradient, which is driving the mixed layer flow. Over the Canadian Basin the sea surface height is increased by 40 and 60 cm for the PX2 and PX5 simulations, respectively (not shown). Since the sea surface height reflect the pressure gradient, this points to intensified geotropic currents in the central Arctic Ocean.

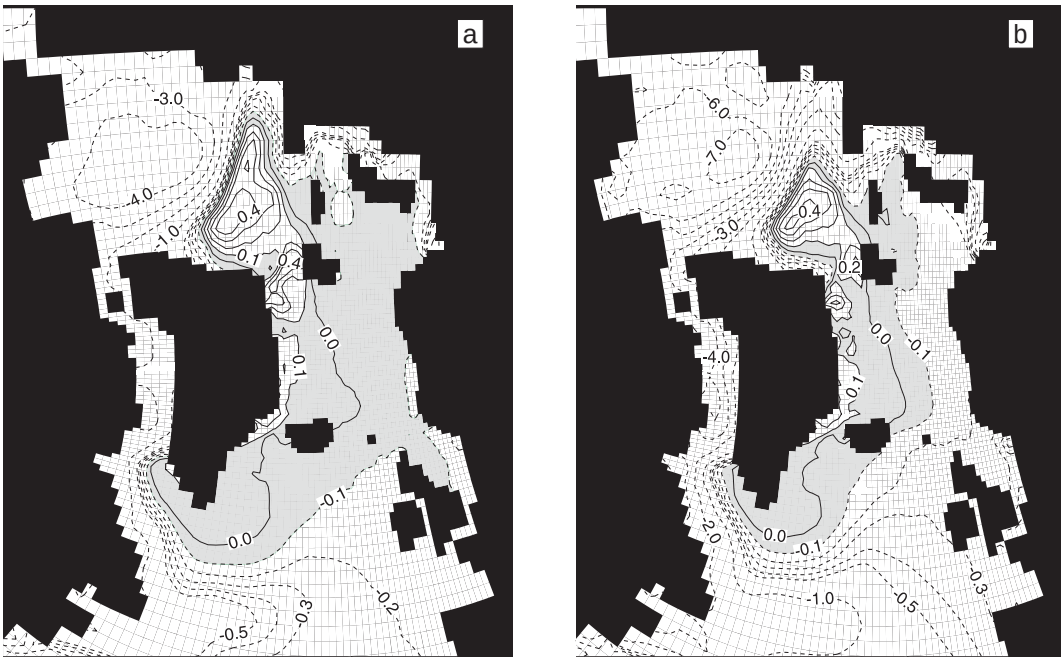

*Figure 7: Difference from the control simulation in annual mean SSS in year 50 for **a** the PX2 simulation, and **b** the PX5 simulation. Dotted lines represent negative anomalies. CI is 0.1 psu. In addition the contour lines from –0.5 to 0.5 psu are shown in CI of 0.1 psu.*

The artificially reduced sea ice thickness of between 1.5-2 m in the central Arctic Ocean has a strong impact on the obtained sea ice velocity fields (Figure 8). The increase in sea ice velocity is particular evident in the Beaufort Gyre (BG), where increases of about 3-5 cm s^{-1} can be found. As a consequence of this, momentum transfer from the atmosphere to the ocean is increased, leading to an intensified BG in the Arctic Ocean (Figure 9). Due to the intensified BG, there is a gradual

increase in the net southward transport of mass across the Canadian Archipelago throughout the 50 years integration period for both the perturbed simulations (Figure 10). In the Atlantic, the net northward transport of Atlantic water with the NAD across the section from Greenland to Ireland also increases gradually throughout the period (Figure 10), thus compensating for the increased southward transport across the Canadian Archipelago.

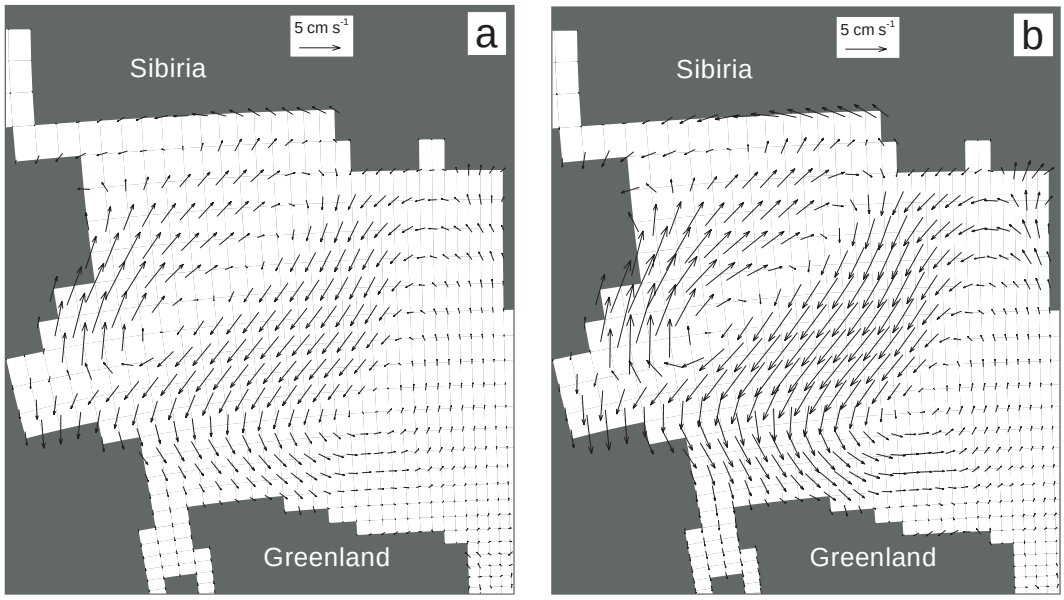

*Figure 8: Difference from the control simulation in the annual mean sea ice velocity (cm s^{-1}) in year 50 for **a** the PX2 simulation and **b** the PX5 simulation.*

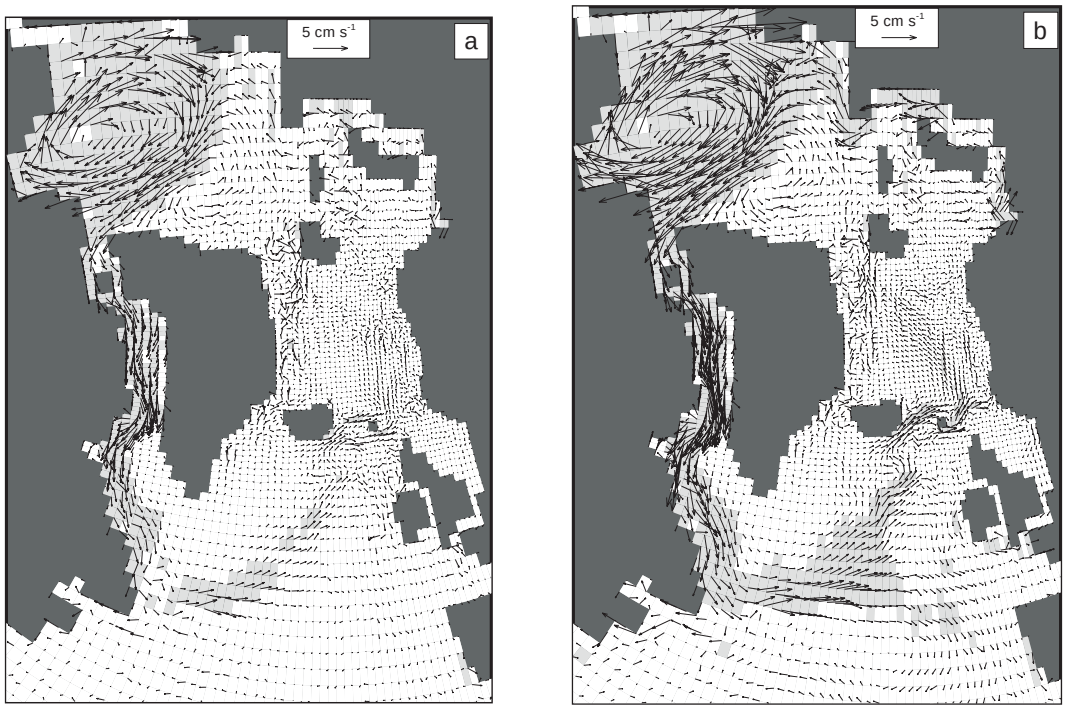

*Figure 9: Difference from the control simulation in the annual mean surface velocity (cm s^{-1}) in year 50 for **a** the PX2 simulation and **b** the PX5 simulation. Shaded areas indicate an increase in absolute velocity greater than 1 cm s^{-1}.*

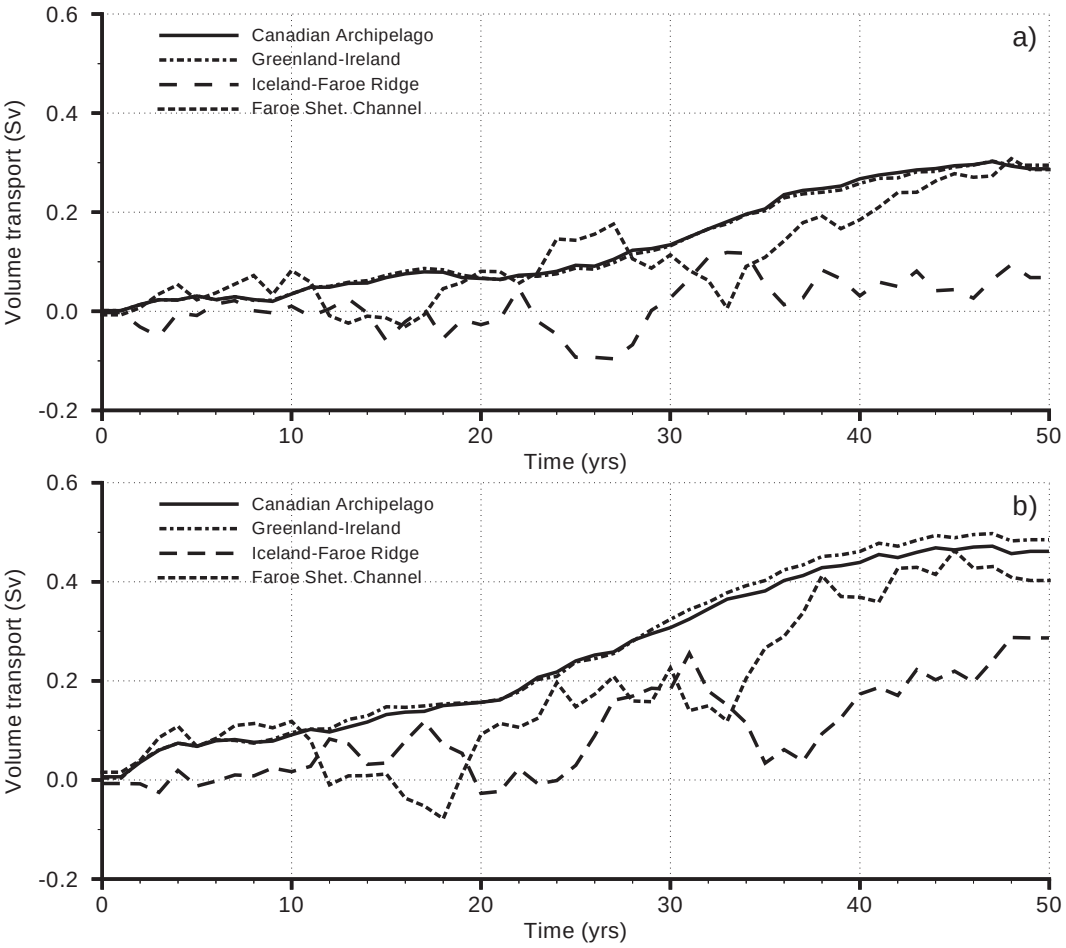

*Figure 10:Time series showing the difference from the control simulation in the annual mean net volume transport (Sv) for **a** the PX2 simulation and **b** the PX5 simulation through the Canadian Archipelago (solid line), Greenland-Ireland section (dash-dotted line), Iceland Faeroe Ridge (dashed line) and Faeroe Shetland Channel (dotted line). Negative values indicate reduced transport.*

The modelled mixed layer thickness is the best measure of the formation of subsurface water masses in the model. In the Greenland Sea, the major reduction in the mixed layer thickness takes place between year 14 to 20 in the perturbed simulations, while for the rest of the period a recovery and stabilization can be seen (Figure 11a). In the Labrador Sea, the initial response to the increased fresh water input is a rapid decrease in the mixed layer thickness (Figure 11b). However, from year 10 and onwards a gradual recovery can be seen almost restoring the mixed layer to its original thickness in year 50. The reason for this recovery and stabilization of the mixed layer thickness in the convective regions, are the increased northward transport of Atlantic water with the NAD. As a result of this, more salt are transported into the Labrador and Nordic Seas, increasing the density, and thus compensating for the increased fresh water input from the Arctic.

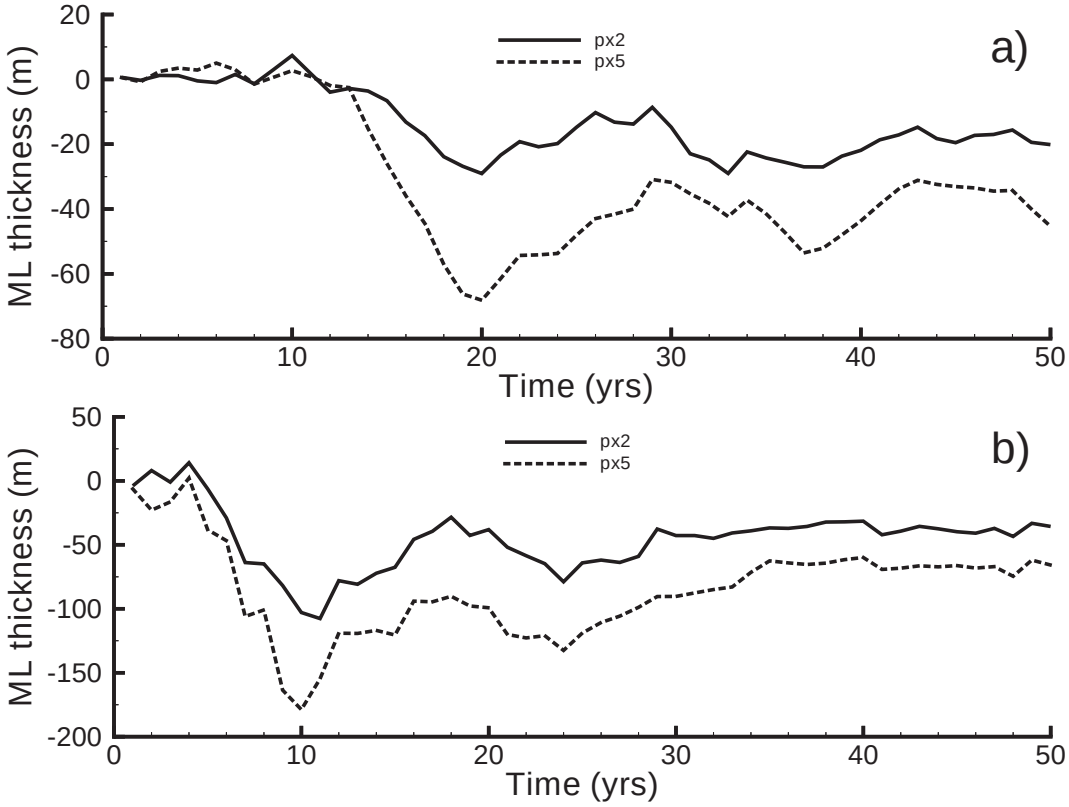

*Figure 11: Time series showing the deviation in the winter mixed layer thickness (m) compared to the control simulation in **a** the Greenland Sea and **b** the Labrador Sea. Solid lines are the PX2 simulation.*

6. Concluding remarks

The obtained model response indicates that the combined effect of increased fresh water supply to the Arctic Ocean and a reduced sea ice thickness may have a near stabilizing effect on the NAD. The reason for this is linked to the opposite responses of the two perturbations: Firstly, the increased fresh water released in the Arctic Ocean leads to a stabilization of the water column in the Atlantic subpolar gyre and in the Nordic Seas, resulting in a weakened NAD. Secondly, the reduced sea ice thickness leads to more efficient transfer of momentum to the Arctic surface waters, and consequently to an intensified BG. Intensified geostropic currents due to increased density gradients along the TD reinforce this. The intensified BG in turn increases the southward transport of mass through the Canadian Archipelago. Since the Arctic Ocean, the Barents Sea and the Nordic Seas constitute a closed system in the model (assuming that the flow through the Bering Strait remains fairly constant), this loss of water has to be replaced. In the model, this is accomplished through an intensified NAD, resulting in an ocean state close to the state characterized by the control integration.

In a global warming simulation, Latif et al. (2000) found an interesting response on the Atlantic TOC. Her large-scale air-sea interactions in the tropics lead to anomalously high salinities in the tropical Atlantic. These anomalies are then advected northward into the sinking regions, thereby increasing the density and compensating the effects of the local warming and freshening. An alternative mechanism is operating in the model experiments presented here.

The obtained model results furthermore highlight the potential importance of the Canadian Archipelago in controlling the fresh water budget of the Arctic and Atlantic Oceans. Coarse resolution ice-ocean and climate models are usually set up with a closed Canadian Archipelago (e.g., Prange and Gerdes 1999). However, several studies (e.g., Aagaard and Carmack 1989; Steele et al. 1996) suggest that the fresh water flux through this passage is larger than the one associated with the water export through the Fram Strait. This underline the need for representing this passage correctly in global models used for climate studies.

The presented study has focused on the circulation and thermodynamics of the North Atlantic-Arctic climate system. A continuation of the study is planned with a truly global, medium resolution model, where the NAD and the Atlantic TOC can be studied on centennial time scales. Such studies will be useful to examine theories on glacial circulation, to identify the origin, propagation and decay of dynamic and thermodynamic anomalies in the Arctic, and to further explore the role of flow of water through the Canadian Archipelago in climate modelling.

References

Aagaard K, Carmack EC (1989) The role of sea ice and other fresh water in the Arctic circulation. *J Geophys Res* **94**:14485-14498

Bleck R, Claes Rooth DH, Smith LT (1992) Salinity-driven thermocline transients in a wind –and thermohaline-forced isopycnic coordinate model of the North Atlantic. *J Phys Oceanogr* **22**:1486-1505

Drange H, Simonsen K (1997) Formulation of air-sea fluxes in the ESOP2 version of MICOM, Tech. Rep. 125, Nansen Environmental and Remote Sensing Center, Bergen, Norway

Dümenil L, Isele K, Liebscher HJ, Schröder U, Wilke K (1993) Discharge data from 50 selected rivers for GCM validation, Tech. Rep. 100, Mac Planck Institute, Hamburg, Germany

Harder M (1996) Dynamik, Rauigheit und alter des Meerises in der Arktis, Ph.D thesis, Alfred-Wegner-institute für Ploar –und Meeresforschung, Bremerhaven, Germany

Hibler III WD (1979) A dynamic thermodynamic sea ice model. *J Phys Oceanogr* **9**:815-846

Johannessen OM, Miles M (2000) Arctic sea ice and climate change – will the ice disappear in this century? *Science Prog* **83(3):**209-222

Johannessen OM, Shalina EV, Miles M (1999) Satellite evidence for an Arctic sea ice cover in transformation. *Science* **286(5446):**1937-1939

Latif M, Roeckner E, Mikolajewicz U, Voss R (2000) Tropical stabilization of the thermohaline circulation in a greenhouse warming simulation. *J of Climate* **13**:1809-1813

Legates DR, Willmott CJ (1990) Mean seasonal and spatial variability in gauge-corrected, global precipitation. *Int J Climatol* **10**:111-127

Levitus S, Boyer TP (1994) World Ocean Atlas 1994 Volume 4: Temperature, NOAA Atlas NESDIS 3, Washington, D.C.

Levitus S, Burgett R, Boyer TP (1994) World Ocean Atlas 1994 Volume 3: Salinity, NOAA Atlas NESDIS 3, Washington, D.C.

Manabe S, Stouffer RJ (1994) Multiple-century response of a coupled ocean-atmosphere model to an increase of atmospheric carbon dioxcide. *J of Climate* **7**:5-23

Mitchell JFB, Johns TC, Gregory JM, Tett SFB (1995) Climate response to increasing levels of greenhouse gases and sulphate aerosols. *Nature* **376**:501-504

Oberhuber JM (1988) An atlas based on the 'COADS' data set: The budgets of heat, buoyancy and turbulent kinetic energy at the surface of the global ocean, Tech. Rep. 15, Max Planck Institute, Hamburg, Germany

Peltier WR (1994) Ice age paleotopography. *Science* **265**:195-201

Prange M, Gerdes R (1999) Influence of Arctic river runoff on the circulation in the Arctic Ocean, the Nordic Seas and the North Atlantic. ICES ASC Council Meeting L/11:5 pp

Simonsen K (1996) Heat budgets and fresh water forcing of the Nordic Seas and the Arctic Ocean, Ph.D thesis, Nansen Environmental and Remote Sensing Center, Bergen, Norway, September, 1996

Simonsen K, Drange H (1997) Surface forcing and initialisation of the ESOP2 version of MICOM, Tech. Rep. 116, Nansen Environmental and Remote Sensing Center, Bergen, Norway

Steele M, Thomas D, Rothrock D (1996) A simple model study of the Arctic Ocean fresh water balance, 1979-1985. *J Geophys Res* **101**:20833-20848

Wood RA, Keen AB, Mitchell JF, Gregory JM (1999) Changing spatial structure of the thermohaline circulation in response to atmospheric CO_2 forcing in a climate model. *Nature* **399**:572-575

Simulations of sulphate and black carbon aerosols: Sensitivity to the treatment of aerosol-cloud-chemistry interactions

by

Øyvind Seland and Trond Iversen

Department of Geophysics, University of Oslo, Norway

1. Introduction

There is increasing evidence that anthropogenic aerosols significantly disturb the forcing of the climate system, but quantified estimates are considerably more uncertain than for greenhouse gases. While the level of scientific understanding of the radiative forcing from greenhouse gases is classified as high (IPCC (2001)), the level of understanding assigned to aerosols ranges from low to very low. In the case of indirect effects of aerosols the uncertainty estimate is almost as large as the forcing from greenhouse gases. The low level of knowledge includes the entire lifecycle of the aerosol from emission to deposition, as well as the aerosol physical properties with regard to radiation and effect on clouds. Even for a long-studied component as sulphate, models give a wide span of results, both for the distribution in the atmosphere as well as radiative effects.

A common factor in many of these uncertainties is the understanding of clouds. Clouds and their effect on climate are among the most uncertain parameters in a climate model as shown in page 430 in IPCC (2001). Understanding and parameterising the cloud-processes is important also when studying aerosols. Cloud microphysics and chemistry determines both the production and removal of particles, and the way aerosols perturb climate forcing. In Iversen and Seland (2002) we also showed that the cloud dynamics, in particular the treatment of convective clouds, contributes considerably to the uncertainty. Although these results only include calculations of sulphate and black carbon (BC), the conclusions should be valid also for other aerosol components, such as organic carbon, nitrates, seas-salt and dust.

In this paper we will present results from 3 sensitivity tests using a model for calculating black carbon and sulphate within the NCAR CCM3 general circulation model. The results are also compared to a base-run as described in Iversen and Seland (2002).

2. Description

The model set-up for the experiments is the same as in Iversen and Seland (2002), and briefly presented in Seland and Iversen (2000). An aerosol-chemistry scheme for calculating black carbon and sulphate is included in NCAR CCM3.2, with the extension prognostic cloud water from Rasch and Kristjansson (1998). The model resolution is T42 with 18 layers in the vertical, extending up to 1 kPa.

The aerosol-chemistry scheme includes chemical reactions, transport and deposition of dimethylsulphide, SO_2, sulphate and BC. The aerosol components SO_4 and BC are further divided into modes, depending on the process creating the aerosol. This separation of modes enables off-line reconstruction of the size distribution and composition of the aerosol. The main simulations as described in Iversen and Seland (2002) are two 5 year runs using IPCC emissions scenarios for 2000 and 2100. With regards to the sensitivity experiments, we have chosen to use year 3 of the IPCC2000 base-run.

An important exception in the base case model is that we neglect the vertical transport in convective clouds. The reason for this was a previous work using the CCM3, Barth et al. (2000), had much too high vertical transport of boundary-layer air. This has also been pointed out as a major source of error in other GCMs (Barrie et al., 2001). To test this assumption two sensitivity tests were made. The first test uses full convective transport and the second using 10 % of the full transport. The latter is thought to represent the situation that a large fraction of the air is exchanged throughout the entire updraft plume. Another point of uncertainty is that the mixing will also expose a larger fraction of air to scavenging processes, than the fraction that at a given time-step is inside the cloud-volume. A test was therefore made where we assumed that the entire grid volume below the cloud-top is exposed to precipitation. This test only included SO_4 and BC.

3. Results

Table 1 shows turnover-times for the base run and the sensitivity tests. The calculated turnover times for SO_2, SO_4 and BC are 1.5, 3.5 and 4.7 days respectively, which is within the range of other models. Test 1 uses full convective transport and the turnover times increased markedly. As expected, test 2 gave a smaller increase in lifetimes than test 1, but it is still considerable. Test 3 on the other hand gave a drastic reduction in the lifetime of the particles. These drastic consequences are caused by the high concentrations at lower levels due to the neglected transport in convective clouds. Hence, these effects must be combined consistently.

Table 1: Calculated turnover times for SO_2, SO_4 and sulphate.

	T (SO2) days	T(SO4) days	T (BC) days
Base run	1.5	3.5	4.7
Test 1	2.0	9.3	9.2
Test 2	1.6	4.6	5.5
Test 3	1.5	1.7	2.8

Vertical distribution and transport was the main reason for omitting the convective transport in the base run. Figure 1 shows zonal concentration averages of sulphate for the base run and sensitivity tests. Comparing test 1 to the base run we see an increase in concentration of more than a magnitude over huge parts, but also test 2 give a large increase compared to the main run. Test 3 shows a very similar

pattern to the base-run but with generally lower values. Results for BC are similar to sulphate.

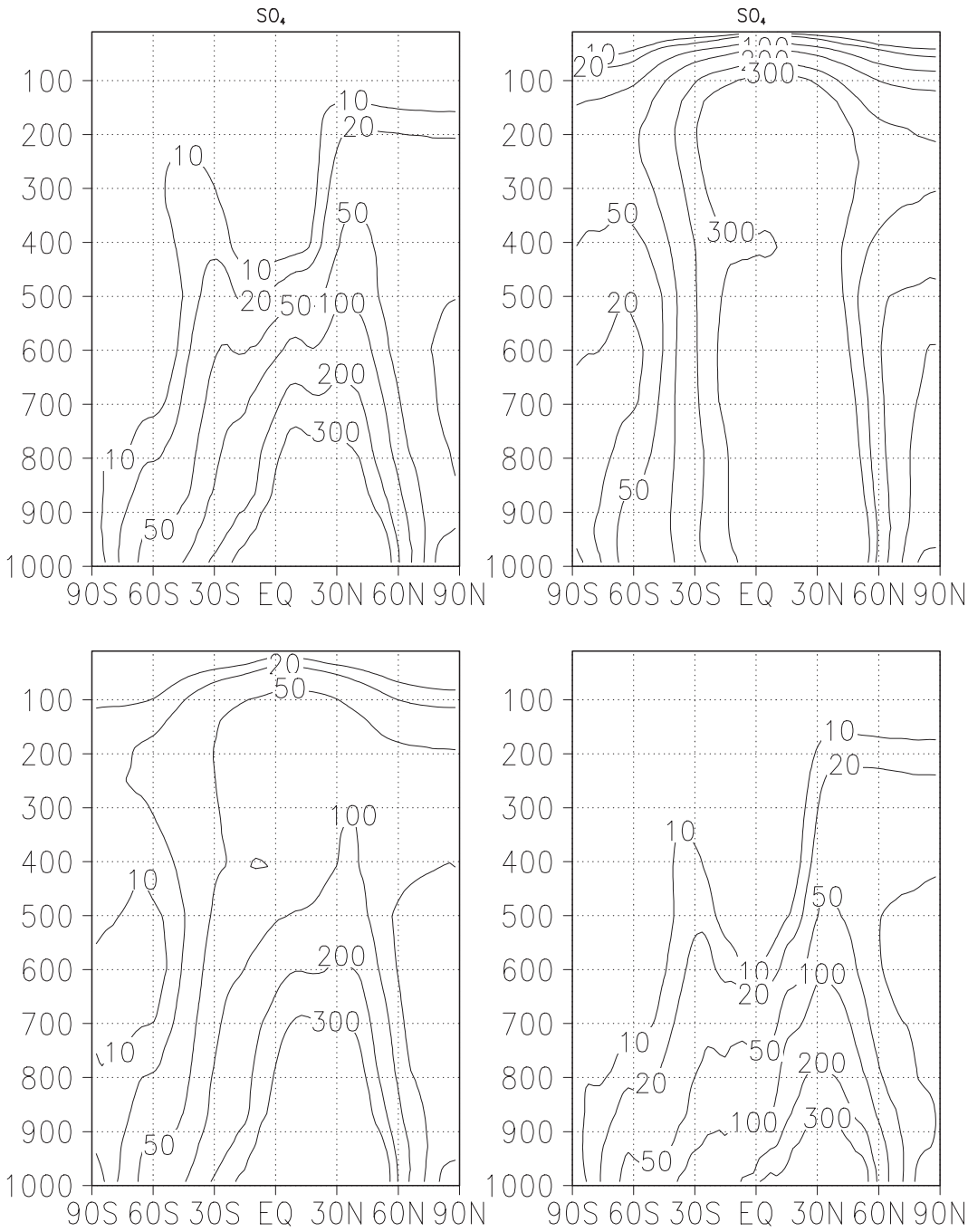

Figure 1: Zonal averages of volume mixing ratios (pptv) of annually averaged sulphate for base run and the sensitivity tests described in the article. The base case is shown in the upper left part of the figure, test 1 upper right, test 2 lower left, and test 3 on the lower right side.

These are all model results. To be able to assess the quality, we also need to compare with measurements. There are very few measured vertical profiles of sulphur, and even less of other components, and all are measured during campaigns. Figure 2 shows a comparison with measurements for the base run,

test 1 and test 2. For sulphate test 1, differs uniquely from the others, with almost uniform mixing rate through the entire troposphere. The base run without convective transport and test2 follow the measurements much more closely. The too high concentrations near the ground in the base run still points out that there should have been some transport, or larger scavenging. For SO2 the opposite is true. Here the test with full convective transport is closer to the measurements in the upper part of the troposphere. We believe the reason for this difference is partly inefficient convective cloud scavenging.

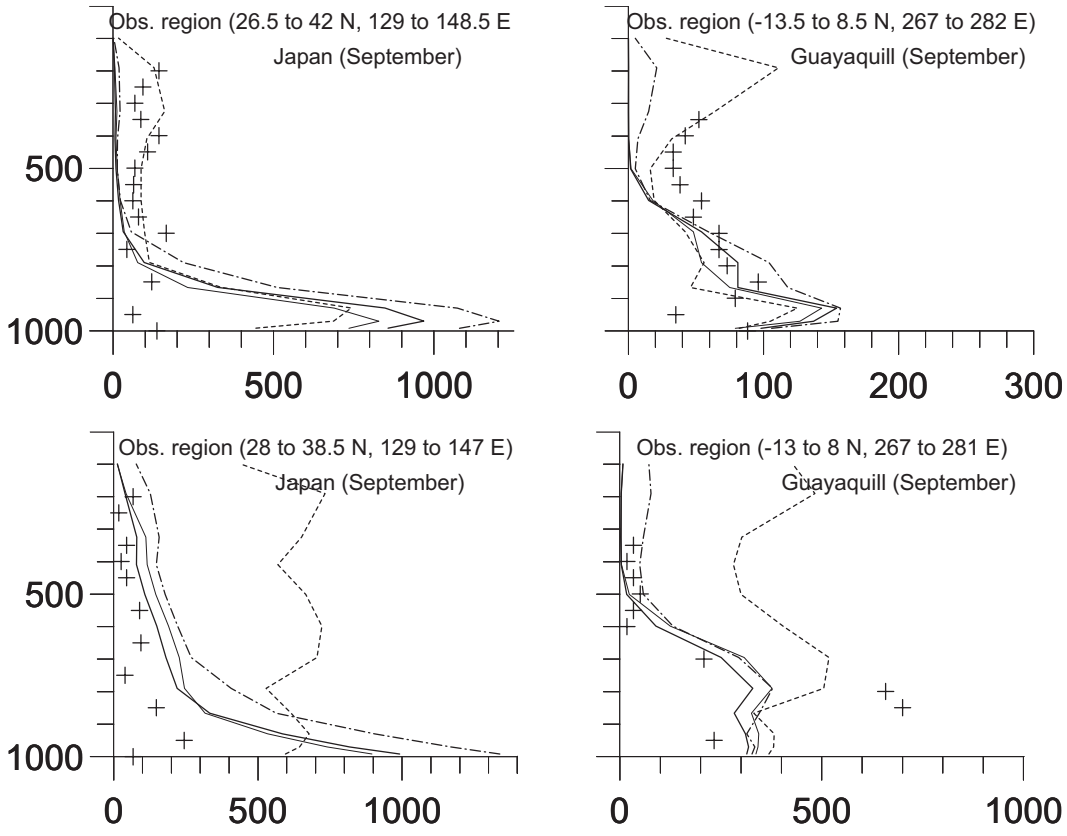

Figure 2: Vertical profiles of SO_2, upper part, and SO_4, lower part of figure compared to measurements at two stations in the Pacific. The measurements are taken from Barth et al. (2000). Thick solid line: base-run over three years; thin solid line: Base-run for the year used in the sensitivity tests; dashed line: sensitivity test 1 with full convective transport; dash-dotted line: sensitivity test 2 with 10 % of convective transport.

4. Conclusion

Three sensitivity tests have been performed in order to estimate the uncertainties due to convective transport and scavenging. The tests showed that atmospheric burdens of SO_4 and BC depend heavily on the parameterisation of vertical transport and scavenging in deep convective clouds. These processes must be parameterised consistently, otherwise factor 2 errors in global burdens may arise, vertical profiles will be wrong, and the potential for climate perturbation erroneous.

References

Barrie, L.A., Yi, Y., Leaitch, W.R., Lohmann, U., Kasibhatla, P., Roelofs, G.-J., Wilson, J., McGovern, F., Benkovitz, C., Melieres, M.A., Law, K., Prospero, J., Kritz, M., Bergmann, D., Bridgeman, C., Chin, M., Christensen, J., Easter, D., Feichter, J., Land, C., Jeuken, A., Kjellstrom, E., Koch, D. and Rasch, P. (2001) A comparison of large-scale atmospheric sulphate aerosol models (COSAM): overview and highlights. *Tellus*, **53B**, 615-645.

Barth, M.C., Rasch, P.J., Kiehl, J.T., Benkowitz, C.M. and Schwartz, S.E.(2000) Sulfur chemistry in the National Center for Atmospheric Research Community Climate Model: Description, evaluation, features, and sensitivity to aqueous chemistry. *J. Geophys. Res.*, **105**, 1387-1415.

IPCC (2001) Climate Change 2001. The Scientific Basis. Contribution of working Group I to the Third Assessment Report of the Intergovernmental Panel on Climate Change. Cambridge University Press, United Kingdom. 881p.

Iversen, T. and Seland, Ø. (2002) A scheme for processs-tagged SO4 and BC aerosols in NCAR CCM3. Validation and sensitivity to cloud processes. *J. Geoph. Res*. Accepted

Rasch, P.J. and Kristjánsson, J.E. (1998) A comparison of the CCM3 model climate using diagnostic and predicted condensate parameterizations. *J. Cl.imate*., **11**, 1587-1614

Seland, Ø. And Iversen, T. (2000) Modelling black carbon and sulphate under different IPCC emission scenarios. Regclim General Technical Report **4.** p 99-105

Zhang, G.J. and McFarlane, N.A. (1995) Sensitivity of climate simulations to the parameterization of cumulus convection in the Canadian Climate Centre general circulation model. *Atmos. Ocean.,* **33**, 407-446

How large is the direct effect of black carbon and sulphate aerosols?
Results from sensitivity experiments and response simulations

by

Alf Kirkevåg, Trond Iversen, and Espen Biseth Granan

Department of Geophysics, University of Oslo, Norway

1. Introduction

A parameterization of aerosol optical parameters has been developed and implemented in an extended version of the Community Climate Model version 3.2 of the US National Center for Atmospheric Research (NCAR CCM3) (Kirkevåg and Iversen, 2002, hereafter KI02). The most important extension for this work is the sulphur and black carbon life-cycle scheme by Iversen and Seland (2002) (hereafter IS02). Estimates of direct radiative forcing (DRF) by non-sea-salt sulphate (SO_4) and black carbon (BC) for baseline calculations and for a set of sensitivity experiments (KI02) are presented, as well as some results from response simulations.

Inputs to the parameterization scheme are production specific concentrations of SO_4 and BC, background aerosol size distribution and composition, and ambient relative humidity. The scheme interpolates between tabulated values to obtain the aerosol *single scattering albedo*, *asymmetry factor*, *extinction coefficient* and *specific extinction coefficient*. The tables are constructed by full calculations of optical properties for an array of aerosol input values, for which size distributed aerosol properties are estimated from theory for condensation and Brownian coagulation, assumed distribution of cloud-droplet residuals from aqueous phase oxidation, and prescribed properties of the background aerosols. Humidity swelling is estimated from the Köhler equation, and Mie calculations finally yield spectrally resolved aerosol optical parameters for 13 solar bands. The scheme has been shown (KI02) to give excellent agreement with non-parameterized DRF calculations for a wide range of situations.

2. Some results

2.1 Forcing experiments

Using IPCC A2 emission scenarios for the years 2000 and 2100, our calculations yield a global net anthropogenic DRF of $-0.11 Wm^{-2}$ and $0.11 Wm^{-2}$ respectively, when 90% of BC from biomass burning is assumed anthropogenic, see Figure 1. In the 2000 scenario the individual DRF due to SO_4 and BC are separately estimated to $-0.29\ Wm^{-2}$ and $0.19\ Wm^{-2}$, respectively, see Figure 2. In the baseline forcing experiments the GCM is run 12 months (plus 3 months spin-up) with prescribed monthly SST, using monthly averaged aerosol concentrations.

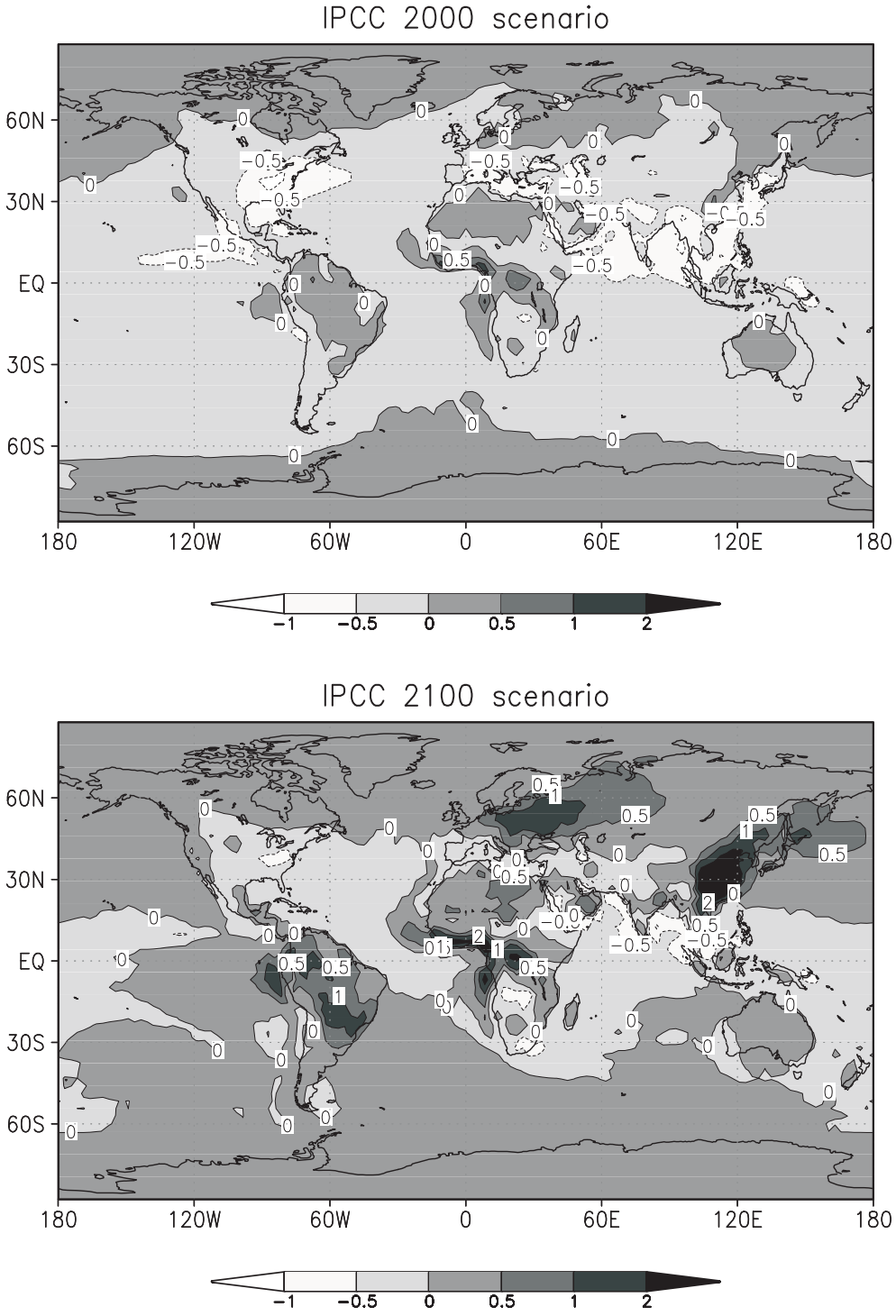

Figure 1: DRF due to anthropogenic sulphate and BC for IPCC scenarios for year 2000 (upper panel, global mean: -0.11Wm^{-2}) and 2100 (lower panel, global mean: 0.11Wm^{-2}). Note: 90% of BC from biomass burning is assumed to be anthropogenic.

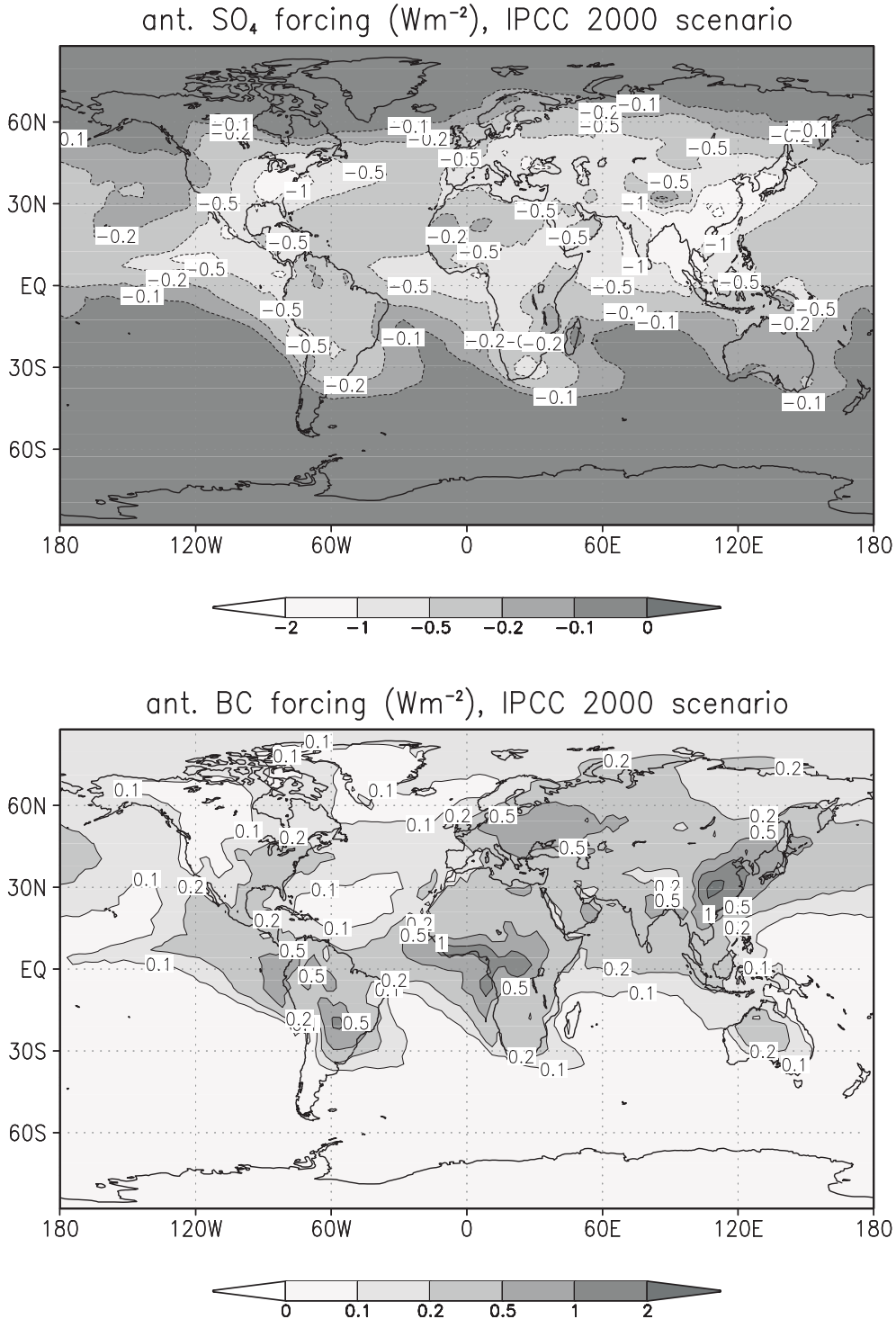

Figure 2: Individual DRF by anthropogenic sulphate (upper panel, global mean: -0.29Wm^{-2}) and BC (lower panel: global mean: 0.19Wm^{-2}) for the IPCC 2000 emission scenario.

These forcing estimates fall within the range of published estimates (IPCC, 2001) for both sulphate (-0.82 to -0.26 Wm^{-2}) and BC (0.16 to 0.54 Wm^{-2}). However, the DRF of BC per BC mass burden of 622 Wg^{-1}, is typically half of earlier published results. Partly to understand why, a number of sensitivity experiments have been performed. Some of the results are summarized in Table 1. The model was run for

April month only, and except for two experiments (6 and 7), also here using monthly averaged aerosol concentrations.

Table 1: Globally averaged direct radiative forcing (DRF) for April (IPCC 2000 emissions) due to SO_4 and BC in the baseline and sensitivity experiments. In experiments 6 and 7, concentrations were taken directly from the life-cycle scheme, while monthly averages were used in the others. D is the fractal dimension for particles of the externally mixed accumulation mode (ax) BC. ΔDRF is the change in DRF from baseline calculations.

Case	DRF (Wm^{-2})	ΔDRF (case-baseline) (Wm^{-2})
Anthropogenic BC and SO_4:		
0) Baseline: r_M(n-mode BC)=0.0118μm, ρ(n-mode BC)=2.3gcm^{-3}, r_M(ax-mode BC)=0.2μm, D=1.8	-0.11	0
1) ρ(n-mode BC)=1.0gcm^{-3}	-0.07	0.04
2) ρ (n-mode BC)=1.0gcm^{-3}, all BC in the n-mode	0.00	0.11
3) r_M(n-mode BC)=0.04μm	-0.12	-0.006
4) r_M(a-mode BC)=0.1μm	-0.11	-0.0001
5) r_M(a-mode BC)=0.1μm, D=2.5	-0.12	-0.004
Natural + anthropogenic BC and SO_4:		
6) Baseline: No convective transport of aerosol and precursors	-0.19	0
7) 10% of full convective transport of aerosol and precursors	-0.22	-0.03
8) SO_4 and BC concentrations monthly averaged from 6)	-0.20	-0.01

The assumed BC mass density ρ=2.3gcm^{-3} (as for pure graphitic particles) may be too high in our calculations, causing a too low BC forcing. This is not clear, however, and is something we will study in more detail in future work. Martins et al. (1998) use a value of 1.8gcm^{-3} for the BC core particles, while some papers, e.g. Myhre et al. (1998), use 1.0gcm^{-3}. In test 1 we ascribe the n-mode BC particles a mass density of 1.0gcm^{-3}. This increases the global anthropogenic forcing from –0.11 to –0.07 Wm^{-2}. Also in test 2 ρ=1.0gcm^{-3}, but here we additionally let all BC reside in the n-mode, as in e.g. Myhre et al., (1998). We then end up with 0.00 Wm^{-2} for our partly externally and partly internally mixed aerosol, close to their 0.01 for an external mixture, and 0.19 Wm^{-2} for internal mixture. Our normalized DRF for BC is more than doubled, and is now close to theirs. Evidently the degree of internal vs. external mixing is an important factor also, as are a number of other model assumptions not discussed here.

As seen from Table 1, the sensitivities to assumed modal radius (r_M) of the n-mode BC in test 3 and the externally mixed ax-mode BC in test 4 are not as high as the density effect. Even when the fractal dimension D of the ax-mode particles (Ström et al, 1992) is changed from 1.8 (corresponding to quite fluffy aggregates) to 2.5 (more densely packed), the effect on the forcing is still small in test 5. The mass density of these particles, which are assumed to be aggregates of core particles with air filling the empty space in between, is for radii exceeding the modal radius given by (gcm^{-3}): $\rho(r) = 2.3(r/r_M)^{3-D}$. Hence, the particles become solid (fully packed) at D=3.

The extended CCM3 version we use has no vertical transport of aerosols and their precursors in convective clouds. For practical reasons we calculate DRF from

both natural and anthropogenic SO_4 and BC in the new baseline experiment 6, using concentrations taken directly from the life-cycle scheme. In test 7 we increase the convective transport to 10%, which gives significantly higher aerosol concentrations in the upper troposphere (IS02). Probably as a result of the cancelling radiative effects of scattering SO_4 and mainly absorbing BC, the combined effect on the forcing, $-0.03 Wm^{-2}$ globally averaged, is not as large as expected. However, regionally the effect varies from 0.5 down to $-1.0 Wm^{-2}$. For the indirect aerosol effect the sensitivity to this assumption is expected to be larger (Kristjánsson, 2002). Test 8 finally illustrates the sensitivity to using monthly averaged aerosol concentrations. The effect is a bit smaller than in the previous test, but also here we find changes in DRF of about 0.5 to $-0.3 Wm^{-2}$ regionally.

2.2 Response experiments:

Two 5-year runs with dynamic feedback (but prescribed monthly SST) have also been performed, using online concentrations of SO_4 and BC calculated from IPCC 2000 emissions: one with the pure background plus natural aerosol; and one with the pure background plus natural and anthropogenic aerosol. The change in net shortwave irradiance at the top of the atmosphere between the two runs (a "quasi-forcing") is very similar to the forcing in the baseline experiment described above. This calculated forcing pattern yields significant changes in the solar heating rate, especially in the middle and lower troposphere at northern hemispheric (NH) mid-latitudes.

The resulting responses on sea-level pressure and near surface temperature in NH winter are shown in Figure 3, where also the statistic significance is indicated. Most important for our region is the decreases in the sea-level pressure of about 2-3 hPa in the northern Atlantic Ocean and in the Arctic. In the Arctic, near surface temperatures are also higher than in the control run by about 1-2°C. In the future we also plan to do similar response experiments with a slab-ocean version of the extended CCM3, to allow for interaction with the ocean.

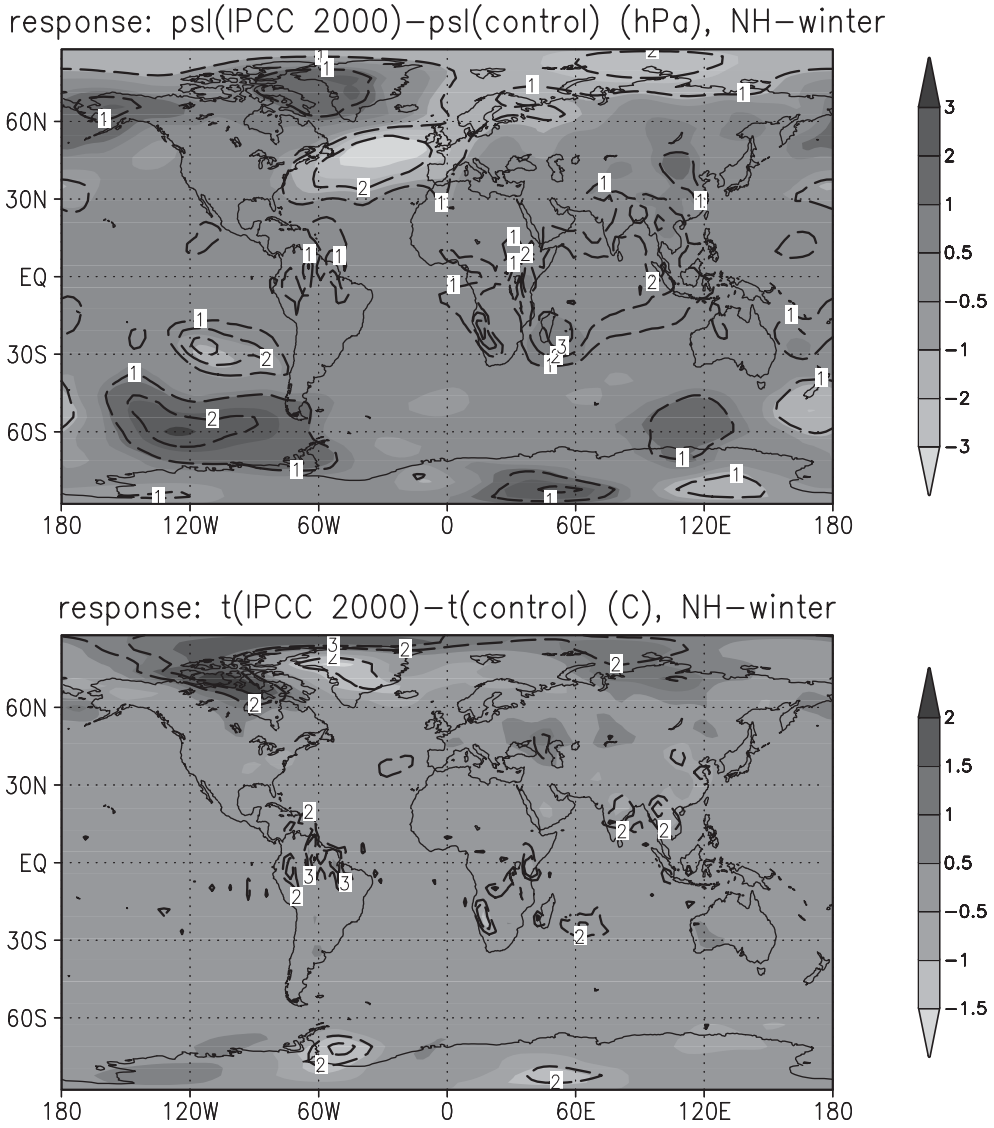

Figure 3: Response of anthropogenic sulphate and BC forcing on sea level pressure (upper panel) and near surface temperature (lower panel) in NH winter (10 October – 20 April), year 2000. The long-dashed curves and labels show the corresponding t-distribution values, where 2 corresponds to ~ 95% confidence.

References:

IPCC (2001) Climate Change 2001, The Scientific Basis. Contribution of WGI to the CLIMATE CHANGE 2001 of IPCC. Cambridge University Press, UK.

Iversen, T., and Seland, Ø. (2002) Life cycle modelling of SO_4 and BC for on-line climate impacts. *J. Geophys. Res.,* Accepted.

Kirkevåg, A., and Iversen, T. (2002) Global direct radiative forcing by process-parameterized aerosol optical properties. *J. Geophys. Res.,* Accepted.

Kristjánsson, J.E. (2002) Studies of the aerosol indirect effect from sulfate and black carbon aerosols. *J. Geophys. Res*., Accepted.

Martins, J.V., Artaxo, P., Liousse, C., Reid, J.S., Hobbs, P.V., and Kaufman, Y.J. (1998) Effects of black carbon content, particle size, and mixing on light absorption by aerosols from biomass burning in Brazil. *J. Geophys. Res.* **103**, 32041-32050.

Myhre, G., Stordal, F., Restad, K., and Isaksen, I.S.A. (1998) Estimation of the direct radiative forcing due to sulfate and soot aerosols. *Tellus*, **50B**, 463-477.

Ström, J.S., Okada, K., and Heintzenberg, J. (1992) On the state of mixing of particles due to Brownian coagulation. *J. Aerosol Sci.* **23**, 467-480.

Simulations of the aerosol indirect effect in RegClim – Sensitivity to parameterization assumptions

by

Jón Egill Kristjánsson

Department of Geophysics, University of Oslo, Norway

1. Introduction

We have previously [e.g., Kristjánsson et al., 2000a, 2000b; Kristjánsson, 2002] described simulations of the aerosol indirect effect within the RegClim project. A new parameterization scheme has been developed and implemented in a version of the NCAR CCM3 climate model. The purpose of this study is to investigate the sensitivity of the main results obtained so far to some of the assumptions that went into the development of the modules for calculating the indirect effect. For instance, it is of interest to know how uncertain our estimate of a globally averaged indirect forcing of –1.8 W/m^2 is.

The calculations of aerosol indirect effect consist of three modules; aerosol and chemistry modules described by Iversen and Seland [2002] and Kirkevåg and Iversen [2002], and thirdly, modifications of the microphysics and radiation schemes of the NCAR CCM3. The first of these three modules consists of a process-oriented life-cycle scheme for sulfate and black carbon (BC) aerosols, accounting for natural emissions of DMS and anthropogenic emissions of SO_2, SO_4 and BC through industrial emissions and biomass burning. The IPCC A2 emission scenario is used, and monthly means of the chemical fields of sulfate and black carbon (nucleation and accumulation modes) from Iversen and Seland [2002] are then used in the present study. As in Kirkevåg and Iversen [2002], they are combined with background aerosols, varying between continental, maritime and polar environments, and size distributions are calculated.

2. Sensitivity to autoconversion threshold

The third module for computing the indirect effect uses the prognostic cloud water scheme of Rasch and Kristjánsson [1998]. In this scheme, release of precipitation is described by five processes, two of which only operate in ice clouds (PSACI, PSAUT), one operates in clouds of mixed phase (PSACW), while the remaining two describe precipitation release from warm clouds (PWAUT, PRACW). The warm cloud auto-conversion process (PWAUT) is parameterized as a function of cloud droplet number concentration, N, and mean volume droplet radius ($r_{3l} = [(3\ q_l\ \rho_a) / (4\ \pi\ \rho_w\ N)]^{1/3}$) through the equation:

$$\mathrm{PWAUT} = [(C_{l,aut}\ q_l^2\ \rho_a) / \rho_w]\ [(q_l\ \rho_a) / (\rho_w\ N)]^{1/3}\ \ H(r_{3l} - r_{3lc}) \qquad (1)$$

where q_l denotes in-cloud liquid water mixing ratio, ρ_a is air density and ρ_w water density; while H is the Heaviside function and r_{3lc} denotes a threshold value for

mean volume radius, discussed in the next section. In Rasch and Kristjánsson [1998] N values of 400 cm^{-3} over land (decreasing with height to 150 cm^{-3}) and 150 cm^{-3} over ocean were used. Now, on the other hand, the droplet number concentration is determined from activation of the largest hygroscopic aerosols, based on Based on assumptions on supersaturation (see section 3), Köhler theory is then applied to determine the number concentration of cloud droplets that are initiated. This is set equal to N.

As explained in Kristjánsson [2002] the parameter r_{3lc} in (1) was changed from 5 μm to 10 μm, based on the results of sensitivity experiments and the results of Delobbe and Gallée [1998]. We now explore the sensitivity to this change. Comparing the 1st and 3rd lines of Table 1, we see that if the autoconversion threshold is reset to 5 μm, the cloud liquid water path is reduced by more than 10 %, since thin clouds (low LWP => low r_{3l}) now precipitate more than before. More importantly, however, the *change* in liquid water path due to anthropogenic aerosols is halved. On the other hand, the cloud droplet radius in general, and its change are not affected much by the change in autoconversion threshold. This has interesting implications for the radiative forcing. The indirect effect consists of a sum of two effects, a Radius Effect, due to reduction in droplet size and a Lifetime Effect caused by an increase in cloud liquid water path. A novelty in Kristjánsson [2002] is that both effects are computed as pure forcing terms. The relative value of the two effects varies considerably between different studies, and it has been suggested that this may be related to the treatment of clouds in the models [Rotstayn, 2000]. To investigate this, we have made simulations with Radius or Lifetime Effects turned off, and repeated this set of experiments after modifying the value of the autoconversion threshold. The results are shown in Figure 1 and in Table 1 (rows 4-7). In the control run, the Radius Effect contributes almost 3 times as much as the Lifetime Effect, globally averaged. When a lower autoconversion threshold is used, this ratio increases to more than 4. The reason is the reduction in ΔLWP, discussed at the beginning of this paragraph. As Figure 1 shows, there are large horizontal variations in the ratio between Radius and Lifetime radiative forcing. The largest ratios tend to be found in the storm tracks and the tropics, while much smaller ratios dominate the marine stratus regions. In the latter regions, PWAUT is the dominating mechanism for precipitation release. As seen by (1), this mechanism is very sensitive to cloud water amounts (q_l). Conversely, in regions containing high clouds and many cloud layers, collection (PRACW) and ice phase processes (PSACI, PSAUT, PSACW) tend to dominate. This would explain the much weaker significance of the Lifetime Effect in those regions.

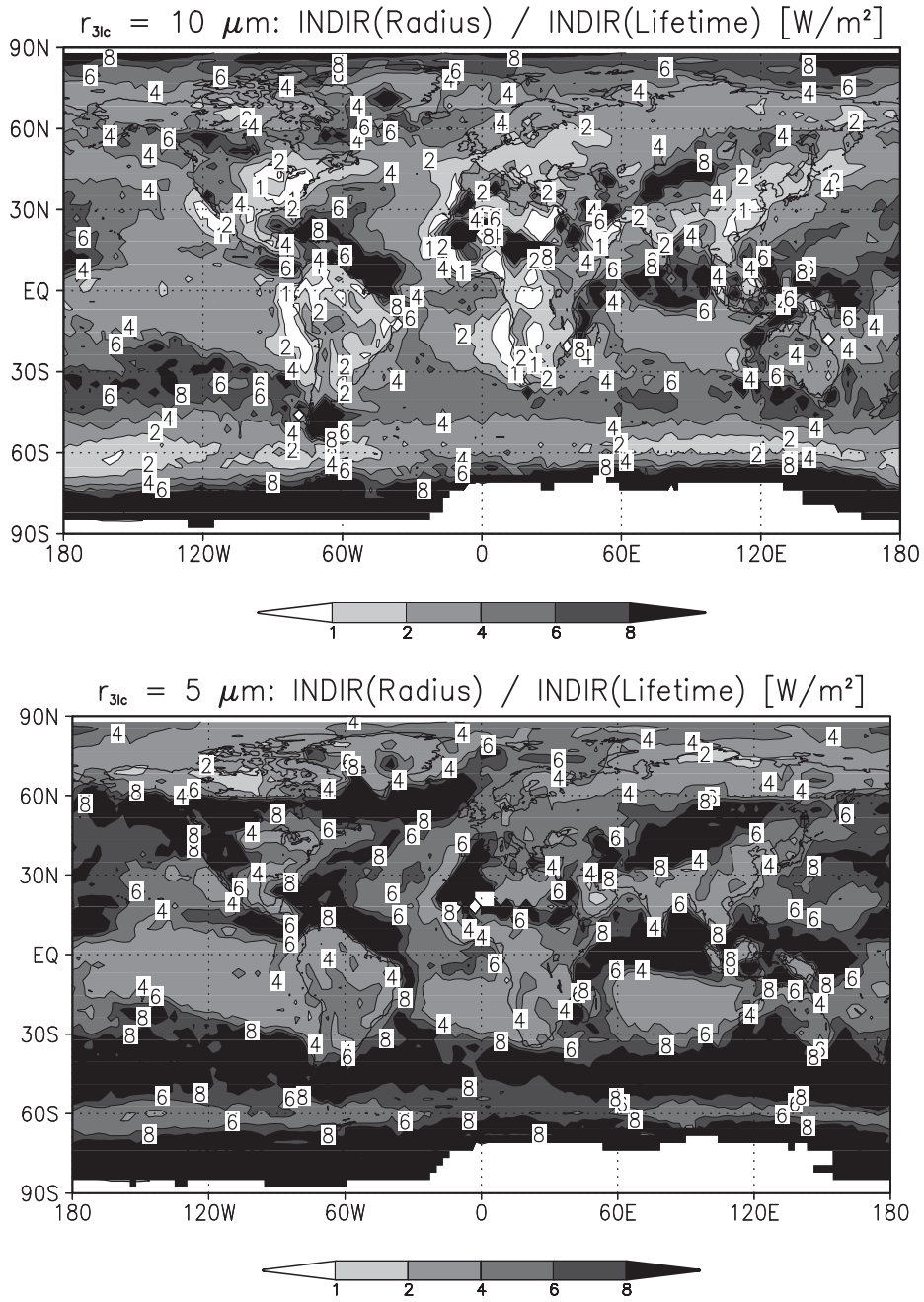

Figure 1: The ratio of the radiative forcing associated with the Radius Effect and the Lifetime Effect. a) Control run. b) Run with reduced autoconversion threshold

Table 1: Global and annual averages from sensitivity runs. INDIR is the change in cloud radiative forcing at TOA due to anthropogenic aerosols [Units: W m^{-2}]; Δr_e is the change in cloud droplet effective radius ($r_e \approx 1.1\ r_{3l}$) due to anthropogenic aerosols [Units: μm]; ΔLWP is the change in cloud liquid water path due to anthropogenic aerosols [Units: g m^{-2}].

	INDIR	Δr_{ev}	ΔLWP	r_{ev}	LWP
Control	-1.76 W m^{-2}	-0.55 μm	1.93 g m^{-2}	10.20 μm	41.8 g m^{-2}
S*2	-1.75 W m^{-2}	-0.37 μm	2.58 g m^{-2}	8.53 μm	51.0 g m^{-2}
$r_{3lc}/2$	-1.63 W m^{-2}	-0.59 μm	0.90 g m^{-2}	10.12 μm	37.3 g m^{-2}
Control (RAD)	-1.25 W m^{-2}	-0.55 μm	-	10.20 μm	41.8 g m^{-2}
Control (LIF)	-0.46 W m^{-2}	-	1.93 g m^{-2}	10.20 μm	41.8 g m^{-2}
$r_{3lc}/2$ (RAD)	-1.34 W m^{-2}	-0.59 μm	-	10.12 μm	37.3 g m^{-2}
$r_{3lc}/2$ (LIF)	-0.27 W m^{-2}	-	0.90 g m^{-2}	10.12 μm	37.3 g m^{-2}
SULFATE CONST.	-1.27 W m^{-2}	-0.32 μm	1.07 g m^{-2}	10.57 μm	40.7 g m^{-2}
SULFATE / 2	-1.11 W m^{-2}	-0.34 μm	1.12 g m^{-2}	10.54 μm	40.6 g m^{-2}
LAND AEROSOL	-1.18 W m^{-2}	-0.35 μm	1.85 g m^{-2}	8.46 μm	48.8 g m^{-2}
OCEAN AEROSOL	-2.17 W m^{-2}	-0.79 μm	1.76 g m^{-2}	11.12 μm	38.2 g m^{-2}
WINDS	-1.42 W m^{-2}	-0.45 μm	1.54 g m^{-2}	10.30 μm	41.4 g m^{-2}

3. Sensitivity to assumed supersaturation at cloud formation

In the control run, a super saturation (S) of 0.05 % is assumed for stratiform clouds, while for convective clouds, S is set to 0.10% over ocean and 0.15 % over land. We now explore the sensitivity to these assumptions by multiplying all these values by 2. The results are shown in the second row of Table 1 and in Figure 2. With higher super saturation, a larger fraction of the cloud condensation nuclei (CCN) is activated, resulting in generally smaller cloud droplet radii and larger liquid water paths. Compared to the control run, the anthropogenic reduction in cloud droplet radius is now reduced (Table 1), while the anthropogenic increase in liquid water path is enhanced. This suggests an enhanced Lifetime Effect and a weakened Radius Effect, according to the arguments presented in the previous section. In a global average these two effects cancel, so that the Total Indirect Effect is unchanged, i.e., -1.75 W/m^2, as compared to –1.76 W/m^2 in the control run. However, as Figure 2 shows there are large regional differences. The Indirect Effect is reduced in the storm track regions in the northern hemisphere and along the Pacific Intertropical Convergence Zone (ITCZ), while the marine stratus regions, the South Pacific Convergence Zone (SPCZ), as well as large of the Indian Ocean show an enhanced short wave cloud radiative forcing. More investigations are needed to fully explain the geographical patterns of Figure 2, but a partial explanation is that the clouds in the marine stratus regions are particularly sensitive to a doubling of S, since S is so low there in the control run. The opposite holds true in the convective regions of the ITCZ and over the continents in summer.

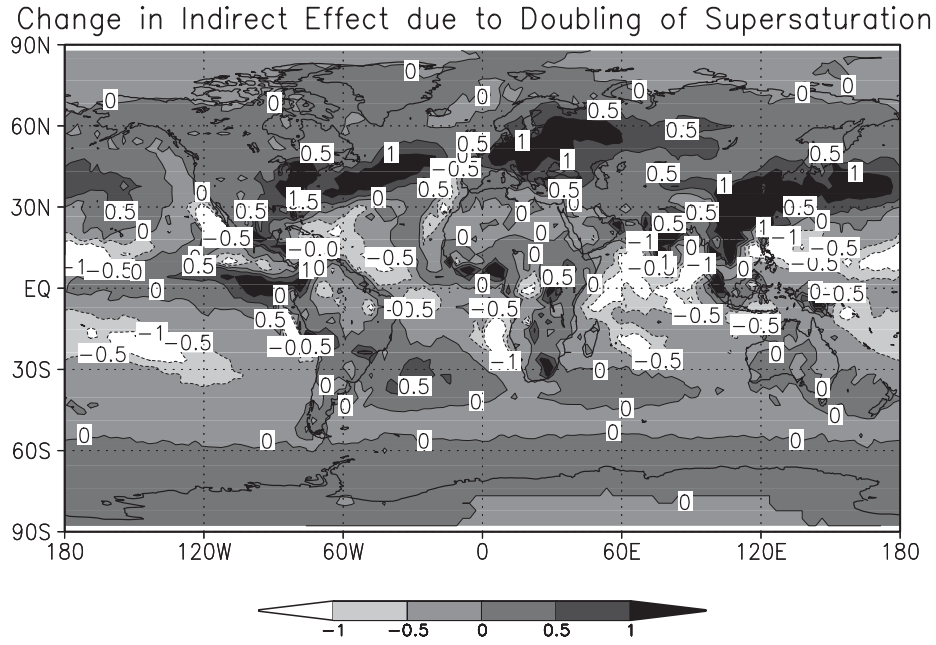

Figure 2: Difference between total Indirect Forcing between run with doubled super saturation at cloud formation and the control run.

4. Sensitivity to assumed background aerosol

An important component of the aerosol treatment that we have used is an elaborate treatment of background aerosols (sea salt, soil particles, DMS, etc.). An important question that arises is how sensitive the simulations of aerosol indirect effect are to the assumptions that went into this treatment. To get a rough answer to this question, we now describe two sensitivity experiments, one termed LAND, where the current treatment of continental aerosols is used everywhere, and another termed OCEAN, where a maritime aerosol is assumed everywhere. In the LAND simulation, cloud droplets over ocean become much more numerous, and hence smaller than in the control run. The difference increases from about 1 μm near the coast to about 3 μm over the main ocean regions (not shown). At the same time there are large increases in the liquid water path over ocean, the largest differences of about 40 gm^{-2} being found over the storm track regions at 50-60° latitude. Associated with these changes there is a large reduction in the indirect effect, as seen in Table 1 and Figure 3a. This is because both the anthropogenic reduction in cloud droplet size and the anthropogenic increase in liquid water path are reduced compared to control. This is most clearly seen in the Arctic, where an even more pristine aerosol than the ocean aerosol [see Kirkevåg and Iversen, 2002 for details] has been replaced by the land aerosol. The fact that the radius change is largest in pristine areas can be understood by considering the relation:

$$\Delta r_{3l} \sim - 1/3 \, r_{3l} \, \Delta N / N \qquad (2)$$

Both ΔN and 1 / N are largest in the pristine areas, resulting in a large Δr_{3l} change there. By comparison, Figure 3b shows the difference between the results of simulation OCEAN and control. Now the aerosol indirect effect is greatly enhanced and is almost twice as large as from the simulation LAND (Table 1). This is because now the anthropogenic reduction in cloud droplet size is greatly

enhanced compared to CONTROL, at the same time as the sensitivity to such a change is enhanced.

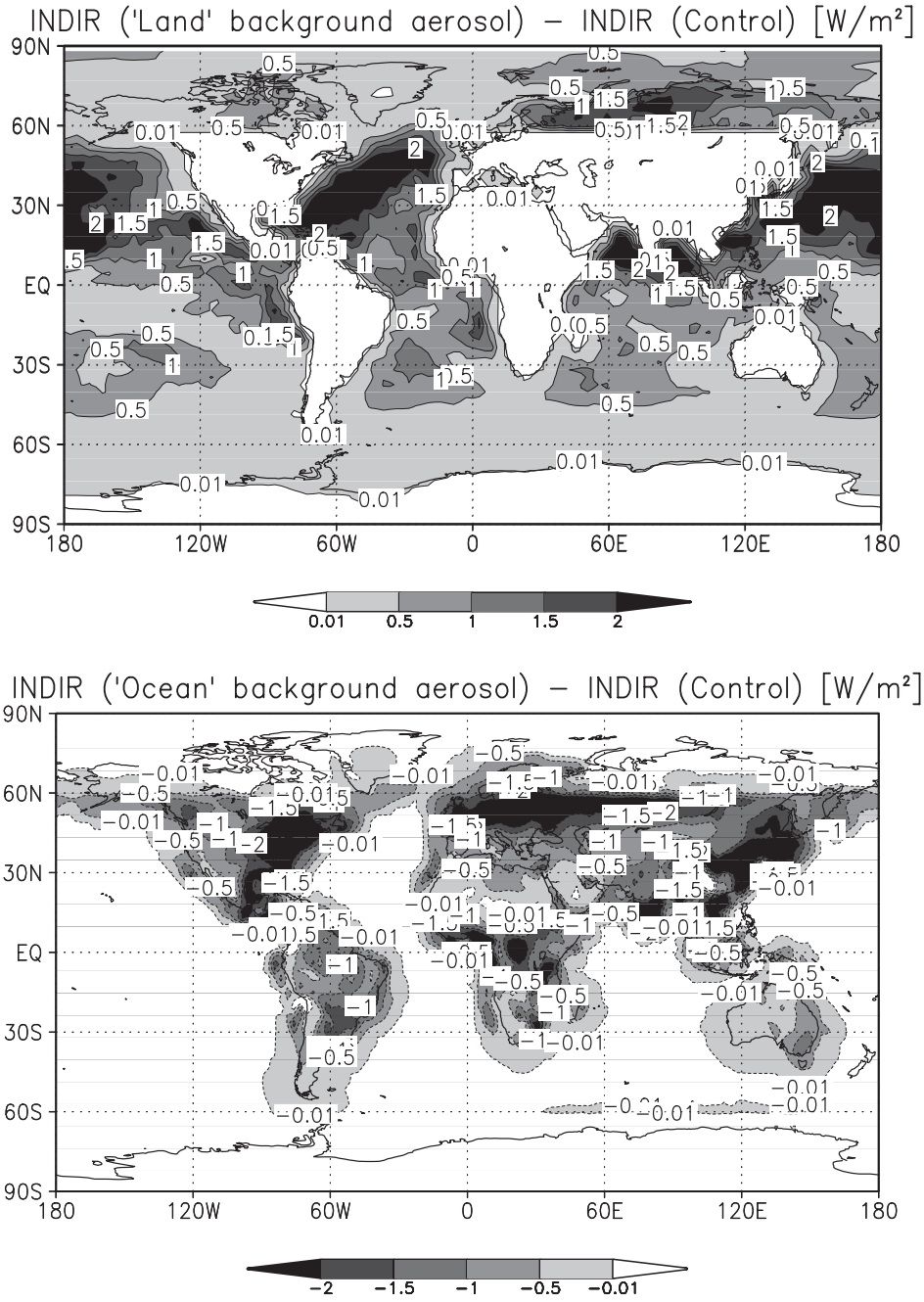

Figure 3: Sensitivity of aerosol indirect forcing to treatment of background aerosols. a) Difference between simulation with continental aerosols everywhere and the control run. b) Difference between simulation with maritime aerosols everywhere and the control run.

5. Sensitivity to vertical distribution of sulfate

Since we only compute the aerosol indirect effect of warm clouds, located near the surface, the vertical distribution of sulfate will be of great importance. This is highlighted in a sensitivity experiment in which the mixing ratio of sulfate was artificially set constant with height everywhere, keeping the vertically integrated

sulfate burden unchanged at every grid point. A summary of the results is given in line 8 of Table 1. Most importantly, the indirect effect is reduced by almost 1/3. This result is more important than it may appear at first sight, since Iversen and Seland [2002] demonstrated a great uncertainty in the treatment of vertical transport of chemical species by moist convection in the tropics. Their findings indicate that many models may be significantly overestimating this transport, leading to too weak vertical gradients in sulfate mixing ratios. By comparison, Iversen and Seland [2002] neglected this transport altogether, and our results use the monthly averaged concentration from that study, hence boosting the indirect effect estimates in our control run.

6. Competition between sea salt and sulfate aerosols

Recent studies by Ghan et al. [1998] and O'Dowd et al. [1999] suggest a possible mechanism by which the indirect effect may be greatly reduced locally, due to competition between background and anthropogenic aerosols. In the latter paper observations from the North Atlantic show that in light wind conditions the cloud droplet number concentration increases with increasing aerosol burden, as expected, due to a larger number of CCN. However, with strong near-surface winds, large sea salt particles are effectively transported upward towards cloud base. These particles are much more effective CCN than the sulfate particles, and grow at the expense of the latter by reducing the peak supersaturation. The result is a reduction in cloud droplet number concentration by a factor of about 3-4 compared to the light wind case.

Such a mechanism is not parameterized in our scheme at present. In order to get a crude picture of the possible significance of this omission, an experiment has been carried out, in which all anthropogenic aerosols were ignored whenever near-surface winds over ocean exceeded 10 m/s. As shown in Figure 4 this leads to a reduction of the indirect effect by as much as 2.5 W/m^2 in certain regions, mainly in the northern hemisphere storm tracks. In a globally averaged sense a 20% reduction was found (last line of Table 1), with contributions from both components of the indirect effect (Radius Effect and Lifetime Effect).

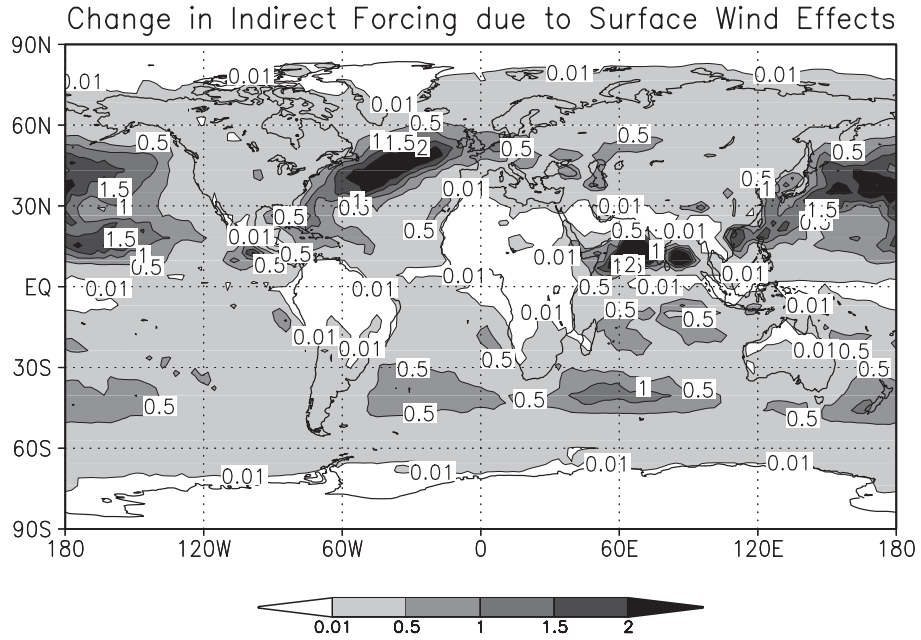

Figure 4: Change in aerosol indirect forcing due to competition between sea salt and sulfate in high wind conditions.

Acknowledgments

Alf Kirkevåg kindly provided the scheme for computing the CCN activation. Monthly mean fields of sulfate and black carbon from multi-year simulations were kindly provided by Øyvind Seland. Discussions with Alf Kirkevåg, Øyvind Seland and Trond Iversen are gratefully acknowledged.

References

Delobbe, L., and Gallée, H., 1998. Simulation of marine stratocumulus: Effect of precipitation parameterization and sensitivity to droplet number concentration. *Boundary-Layer Met.*, **89**, 75-107.

Ghan, S., Guzman, G., and Abdul-Razzak, H., 1998. Competition between sea salt and sulfate particles as cloud condensation nuclei. *J. Atmos. Sci.*, **55**, 3340-3347.

Iversen, T., and Seland, Ø., 2002. Life cycle modelling of SO_4 and BC for on-line climate impacts. *J. Geophys. Res*., in press.

Kirkevåg, A., and Iversen, T., 2002. Global direct radiative forcing by process-parameterized aerosol optical properties. *J. Geophys. Res*., in press.

Kristjánsson, J.E., Kirkevåg, A. Seland, Ø., and Iversen, T., 2000a. Studies of the aerosol indirect effect using the NCAR CCM3. RegClim General Technical Report No. 4, Presentations from Workshop 8-9 May 2000 at Jevnaker, Norway, pp. 105-111.

Kristjánsson, J.E., Kirkevåg, A. Seland, Ø., and Iversen, T., 2000b. Report from PT5: Clouds and indirect effect of aerosols. RegClim General Technical Report No. 5, Presentations from Workshop 20-21 November 2000 at Geilo, Norway, pp. 59-75.

Kristjánsson, J.E., 2002. Studies of the aerosol indirect effect from sulfate and black carbon aerosols. *J. Geophys. Res*., in press.

O'Dowd, C.D., Lowe, J.A., Smith, M.H., and Kaye, A.D., 1999. The relative importance of non-sea-sulphate and sea-salt aerosol to the marine cloud condensation nuclei population: An improved multi-component aerosol-cloud droplet parameterization. *Q. J. R. Meteorol. Soc.*, **125**, 1295-1313.

Rotstayn, L., 2000. On the "tuning" of autoconversion parameterizations in climate models. *J. Geophys. Res.*, **105**, 15495-15507.

Interactive global modelling of regional SO_2 and sulphate trends until 1996

by

Tore F. Berglen & Ivar S.A. Isaksen

Dept. of Geophysics, University of Oslo

Introduction

The sulphur cycle is important both concerning the atmospheric chemistry and concerning climate (radiative forcing). The main constituents in the sulphur cycle are SO_2 and sulphate (SO_4^{2-}), although DMS (dimethylsulphide, CH_3SCH_3), H_2S, and MSA (methanesulphonic acid, CH_3SO_3H) also play a certain role. In the stratosphere photolysis of COS contributes to the formation of sulphate particles (not included in here). 75% of the total emissions of sulphur are anthropogenic. In populated areas in the Northern Hemisphere anthropogenic emissions of SO_2 and its' oxidation to sulphate are predominant, in background areas in the Southern Hemisphere oceanic emissions of DMS and oxidation to SO_2 and finally to sulphate are most important.

Sulphate forms particles in the atmosphere and hence alters the radiative balance of the atmosphere both through direct and indirect effects. The importance of direct radiative effect is that sulphate particles scatter solar radiation. Through the indirect effects sulphate particles reduce the cloud droplet size and change the optical properties of clouds. Sulphate particles also reduce precipitation efficiency and hence increase cloud water content and the lifetime of clouds. Both direct and indirect effects of sulphate aerosols lead to a decrease of the earth's surface temperature (IPCC, 2001). The lifetime of SO_2 and sulphate in the atmosphere is on the order of days so the largest impact of sulphur is seen close to its' sources.

To study the sulphur cycle we use the OsloCTM2. It is a Chemical Transport Model developed at the Dept. of Geophysics, Univ. of Oslo. The horisontal resolution is either T21 (5,625° × 5,625°), T42 (2,8125° × 2,8125°), or T63 (1,875° × 1,875°) with 19 or 40 vertical σ-p layers. For this study the T21/19 layers version is used. The meteorological input data driving the OsloCTM2 is generated especially for this model by the Integrated Forecast System (IFS) model at the ECMWF. Input data are updated every 3rd hour and they are all internally consistent. The background chemical scheme from Berntsen and Isaksen (1997) includes 51 components. The concentrations of the gases are calculated using the QSSA solver from Hesstvedt et al. (1978).

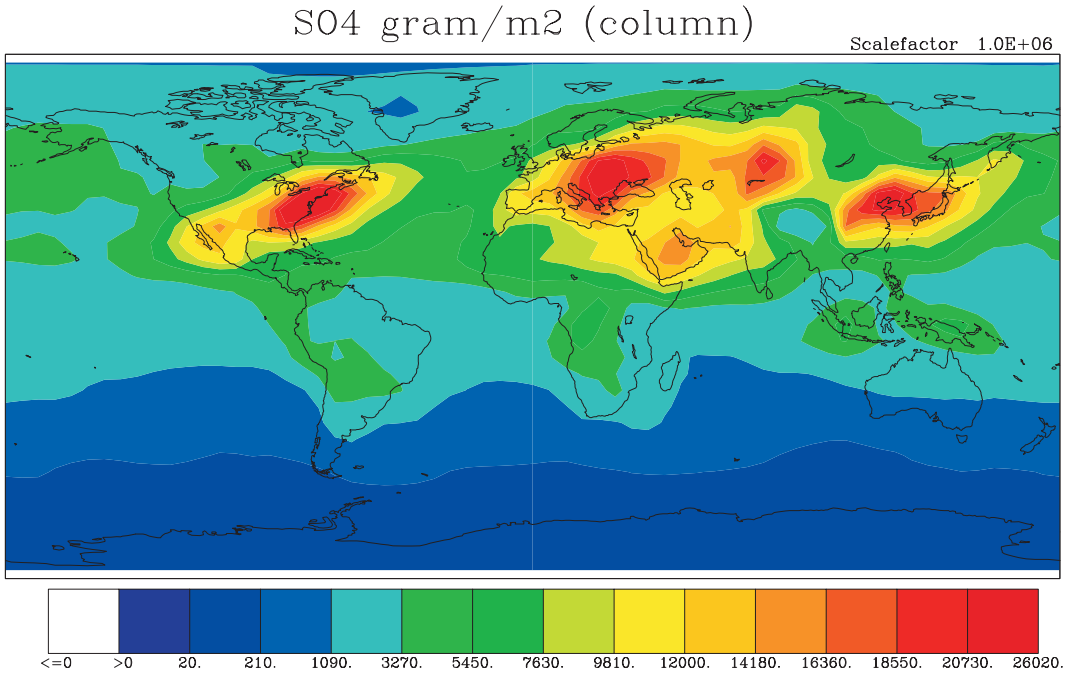

Figure 1: Total burden of sulphate in July, unit: $\mu g\ m^{-2}$. We clearly recognise the anthropogenic areas in the Northern Hemisphere.

The sulphur cycle; emissions, oxidation and deposition

We have introduced 5 sulphur components to the OsloCTM2 (SO_2, sulphate, DMS, H_2S and MSA). The anthropogenic emissions of SO_2 are taken from GEIA for the year 1985 (Benkovitz et al., 1996). For 1996 the EMEP emission inventory is used for Europe and the US while we scale the emissions to fossil fuel use elsewhere as suggested by Karlsdóttir and Isaksen (2000). The anthropogenic emissions of SO_2 have decreased in Europe and in the US during the last 15 years due to better cleansing technology whereas they have increased in South East Asia due to economic growth. SO_2 emissions from ships are elaborated by Det Norske Veritas (AMVER). 5% of anthropogenic SO_2 is emitted as sulphate assuming instant oxidation in the plume.

SO_2 is oxidised to sulphate both in the gas phase and in the aqueous phase (by H_2O_2, O_3 and HO_2NO_2). For the aqueous phase chemistry a scheme described in e.g. Jonson et al. (2000) is applied. We use meteorological data (T, cloud cover fraction, cloud water content), Henry's law constants, equilibrium rates and gas phase reaction rates to calculate a set of modified reaction rates used in the QSSA solver. It is important to emphasise that the oxidants and the sulphur compounds are calculated interactively, they are not prescribed as with other models. We will thus be able to study the interaction between the sulphur cycle and the oxidants.

About 50% of SO_2 is removed due to dry deposition. SO_2 is scarcely soluble so that little SO_2 is lost by wet deposition. On the other hand sulphate is very soluble and over 85% of sulphate is estimated to be lost by wet deposition, either by large-scale precipitation, by convective precipitation or by sub-cloud deposition. Concerning the convection the model calculates the vertical transport by using a so-called "elevator". A new iterative method has been developed (T.K. Berntsen,

Dept. of Geophysics) to calculate how much of the water put into this elevator is actually condensed, and how much remains in gas phase.

When we are to compare model results with observations to validate our model we often compare with stations located at the ground. This implies that the treatment of the boundary layer mixing in the model is important. Several boundary layer schemes have been tested and we have found that a Holtslag K-profile scheme gave the most reasonable results.

Influence of the sulphur cycle upon atmospheric chemistry

To study the influence of the sulphur cycle upon the oxidants it is most convenient to look at H_2O_2 and O_3. 30% of OH is lost by reaction with CH_4 and 70% by reaction with CO while sulphur hardly influences OH. Two strategies are possible: either we can investigate the chemistry with and without the sulphur cycle or we can investigate how the changes in the anthropogenic emissions from 1985 to 1996 have altered the chemistry. Here we focus on how the changes in the emissions have influenced H_2O_2 and O_3. Results for layer 3 in the model (~400m) for July are shown. The difference between a model run with emission inventory for 1996 and a run with the GEIA 1985 inventory is presented. For H_2O_2 the picture is straightforward: the emissions and concentrations of SO_2 have decreased in Europe and increased in Asia and consequently the abundance of H_2O_2 has increased in Europe and decreased in Asia.

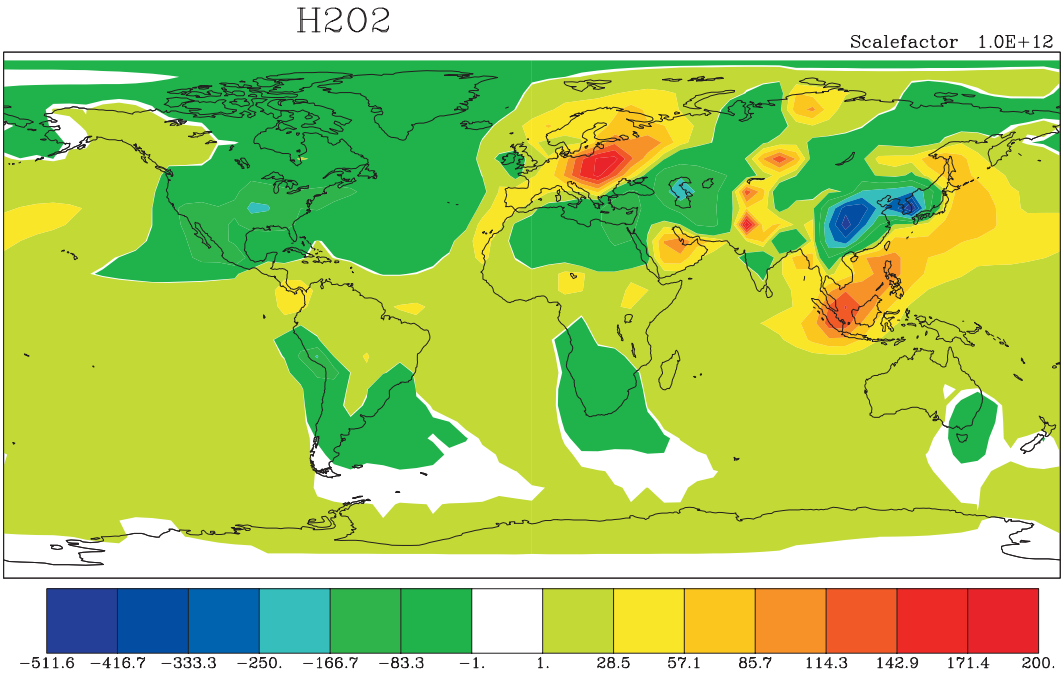

Figure 2: Difference in H_2O_2 between 1985 and 1996 (i.e. 1996 ÷ 1985) for July, layer 3 (~400m) in the model, unit: ppt. We observe how the changes in the emissions of SO_2 have changed the level of H_2O_2.

For O_3 the picture is reversed: if we change the emissions of SO_2, hydrocarbons and NO_x we get a decrease in Europe and increase in Asia. This has to do with

secondary effects of the emissions. If we change the emissions of SO_2 only we get the same results as with H_2O_2 (not shown). A model run without the sulphur included where we change hydrocarbons and NO_x would give an even larger decrease in Europe and increase in Asia. To conclude we may say that the changes in the emissions of SO_2 contribute to a damping of the effect caused by the changes in emissions of hydrocarbons and NO_x.

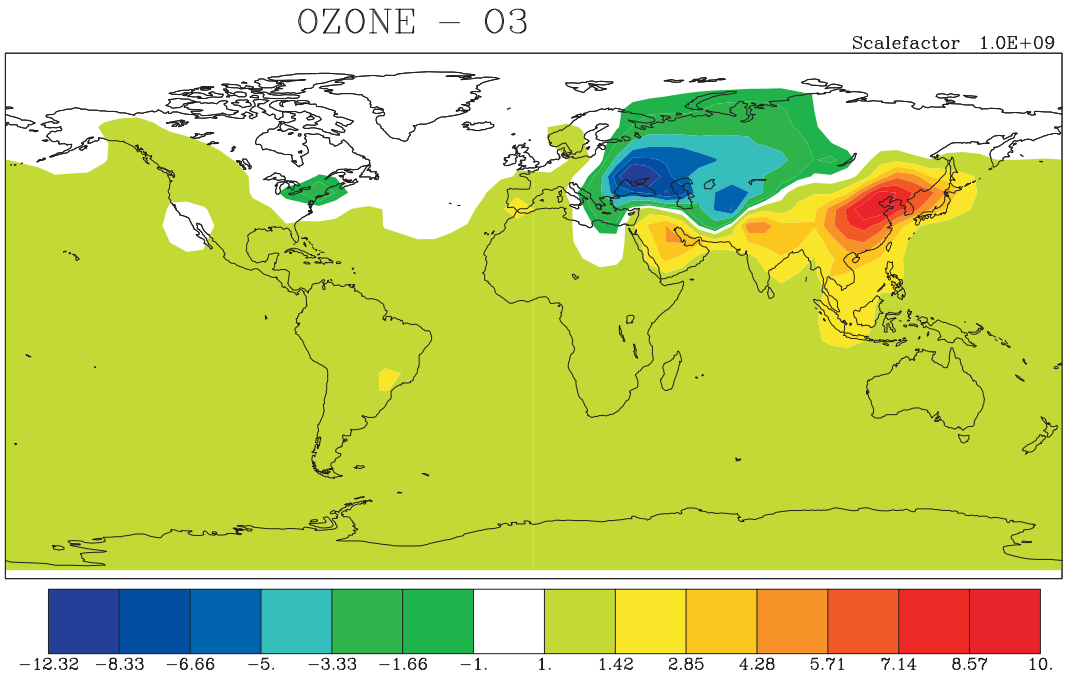

Figure 3: Difference in O_3 between 1985 and 1996 (i.e. 1996 ÷ 1985) for July, layer 3 (~400m) in the model, unit: ppb. The sign of the changes in O_3 is opposite the sign of the changes in H_2O_2 due to secondary effects in the hydrocarbon-NO_x chemistry.

Comparison with observations

Comparing observations with models is our best way to validate model results. We have compared our results with stations within the EMEP network, both as monthly averages and on a day-to-day basis. The model concentrations reproduce fairly well (within a factor 2) the observations of SO_2 and sulphate. The calculations catch the overall level and the model is able to reproduce the seasonal variations and specific episodes. The results of the model run using the 1996 emission inventory fit better with observations than the run using GEIA 1985. In grid boxes covering several stations we take the average of these stations and compare with the model result. This averaging process smoothes out any particular features for each specific station. Grid boxes containing several stations fit better with observations than grid boxes with only one observation site.

The analysis shows that it is difficult to reproduce the wet deposition in the model with observations from one single station. To get sensible results we have to compare yearly average of all stations to see whether the model underestimates / overestimates the observed wet deposition.

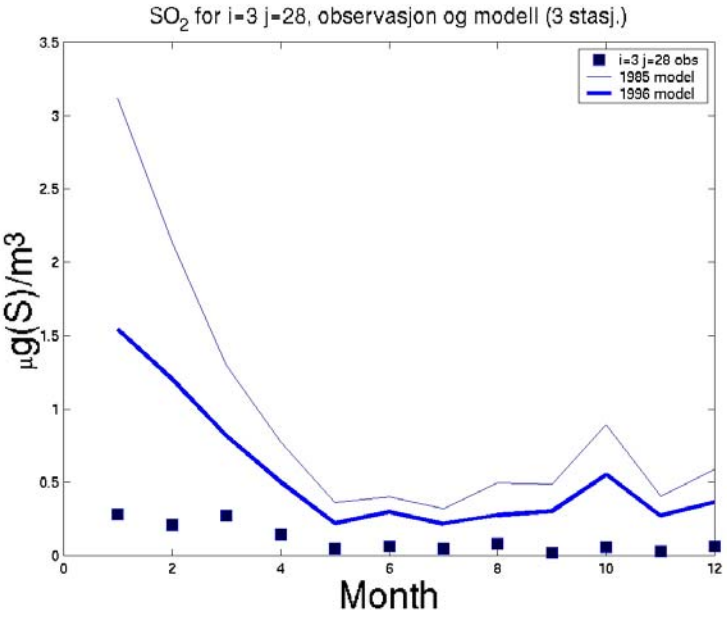

Figure 4: SO_2 for the three Norwegian stations Tustervatn (NO15), Krvatn (NO39) and Osen (NO41), unit: µg(S) m^{-3}. Results for a model run using 1996 emission inventory fit better with observations than a model run using GEIA 1985 emission inventory.

References

Benkovitz, C.M., Scholtz, M.T., Pacyna, J., Tarrasón, L., Dignon, J., Voldner, E.C., Spiro, P.A., Logan, J.A. and Graedel, T.E., 1996: Global gridded inventories of anthropogenic emissions of sulfur and nitrogen, *J. Geophys. Res.* **101**, 29239-29253.

Berntsen, T.K. and Isaksen, I.S.A., 1990: A 3-D chemical transport model for the troposphere: Model description and CO and O_3 results, *J. Geophys. Res.* **102**, 21239-21280.

Hesstvedt, E., Hov, Ø. and Isaksen, I.S.A., 1978: Quasi steady-state approximation in air pollution modelling: Comparison of two numerical schemes for oxidant prediction, *Int. J. Chem. Kinet.,* **X**, 971-978.

IPCC, 2001: Climate Change 2001: The Scientific Basis. Contribution of Working Group I to the Third Assessment Report of the Intergovernmental Panel on Climate Change [Houghton, J.T., Y. Ding, D.J. Griggs, M. Noguer, P.J. van der Linden, X. Dai, K. Maskell, and C.A. Johnson (eds.)]. Cambridge University Press, Cambridge, United Kingdom and New York, NY, USA, 881pp.

Jonson, J.E., Kylling, A., Berntsen, T.K., Isaksen, I.S.A., Zerefos, C.S. and Kourtidis, K., 2000: Chemical effects of UV fluctuations inferred from total ozone and tropospheric aerosol variations, *J. Geophys. Res.* **105**, 14561-14574.

Karlsdóttir, S and Isaksen, I.S.A., 2000: Changing methane lifetime: Possible cause for reduced growth, *Geophys. Res. Lett.,* **27**, 93-96.

Radiative forcing from sulphate with uncertainty estimates

by

Gunnar Myhre

Dept. of Geophysics, University of Oslo, Norway

ABSTRACT

Radiative transfer calculations based on a sulphate distribution from regional and global chemistry-transport model simulations have been performed. A wide range of sensitivity experiments has been performed to illustrate the large uncertainty in the radiative forcing due to sulphate aerosols. The most important factors seem to be processes involved in mixing of sulphate aerosols with other particles and uncertainties in the relative humidities. These uncertainties can explain much of the earlier large range in the radiative forcing due to sulphate. In this study we have included a simple sub-grid scale parameterisation of relative humidity to illustrate a potentially large uncertainty in the radiative forcing due to sulphate aerosol.

Results

In a high resolution regional model for sulphate aerosols it is investigated the effects of spatial and temporal averaging of radiative forcing. Haywood et al. (1997) have earlier shown that the radiative forcing due to sulphate in global models can be significant underestimate due to nonlinearities in the hygroscopic effect of sulphate aerosols using a limited area model with high resolution (2km by 2km). In this work we use a regional model (covering Europe and much of the north Atlantic) with 50km by 50km spatial resolution. Figure 1 shows the radiative forcing due to sulphate for different horizontal resolutions for clear sky and when clouds are included in the calculations. The forcing is strongly dependent on the horizontal resolution, which is almost entirely due to the hygroscopic effect of the sulphate aerosols, as the radiative forcing for dry sulphate shows little spatial variability. Generally, the patterns for the clear sky and the calculations including clouds are similar. However, for the highest horizontal resolutions the rate of change of forcing with resolution in the radiative forcing is slightly stronger in the clear sky case than in the case including clouds. This is mainly due to the fact that the strongest non-linear effect of the sulphate aerosols is for high relative humilities, which are often in cloudy regions. For lower horizontal resolutions, averaging is made over larger spatial regions and the collocation of relative humidity and clouds is weaker and results for the clear sky and the cloudy cases are more similar. The dependence of the radiative forcing on horizontal resolution is strongest for low resolutions, but also significant at higher resolutions indicating a need for further investigations with even better horizontal resolution than used in this study.

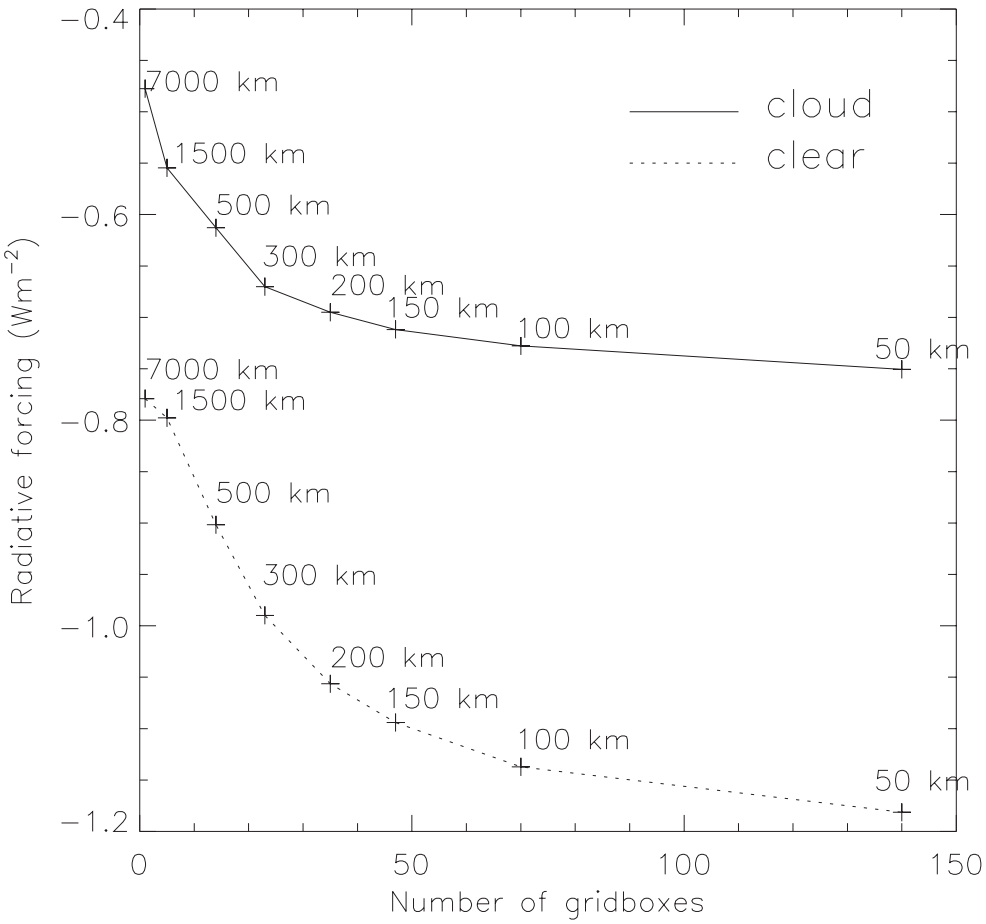

Figure 1: Radiative forcing due to sulphate (in Wm-2) as a function of horizontal resolution. Radiative transfer calculations are performed for horizontal resolution marked with +. The resolution is indicated (in km).”Clear” indicates that clouds are excluded in the calculations and ``cloud'' indicates that clouds are included.

A comparison in a global model with T21 horizontal resolution (about 5.6 x 5.6 degrees) with a calculation using the T63 (about 1.9 x 1.9 degrees) spatial resolution is made using ECMWF meteorological data such as relative humidity and clouds. The sulphate distribution is the same in both calculations (T21 resolution). Simulations are performed for clear sky and calculations including clouds in both cases for hygroscopic sulphate aerosols and dry aerosol (no hygroscopic growth).

The results shows that the radiative forcing due to sulphate aerosols is insensitive to spatial resolution for dry aerosols. However, significant deviations are found when humidity is taken into account. The impact of humidity is larger for clear sky (12%) than when clouds (5%) are included, as high relative humidity and clouds are often collocated and as clouds strongly reduce the forcing. The results are in accordance with the results found in Myhre et al. (2002) for a similar difference in spatial resolution in relative humidity.

In an attempt to take into account the variability in relative humidity in global models we have made a simple sub-grid scale parameterisation. Also with the sub-

grid scale parameterisation we find a larger effect when clouds are excluded than included in the calculations.

The results of Haywood et al. (1997) and Myhre et al. (2002) showed that relative humidity variations is of importance for spatial resolutions higher than T63. We have thus used the same sub-grid scale parameterisation method for the 50km x 50km relative humidity data as for T63 spatial resolution. The radiative forcing is strengthened by about 15% (slightly more for clear sky condition) using the 50km sub-grid scale variability in relative humidity compared to the reference calculation (T21).

Figure 2 shows the global and annual mean vertical profiles of the relative humilities for the five data sets. Noticeable and important differences in relative humidity in the lowest few kilometres can be seen. In the upper troposphere the differences in relative humilities are larger, but as the sulphate concentration is much lower here this is of much less importance for the radiative effect of sulphate aerosols.

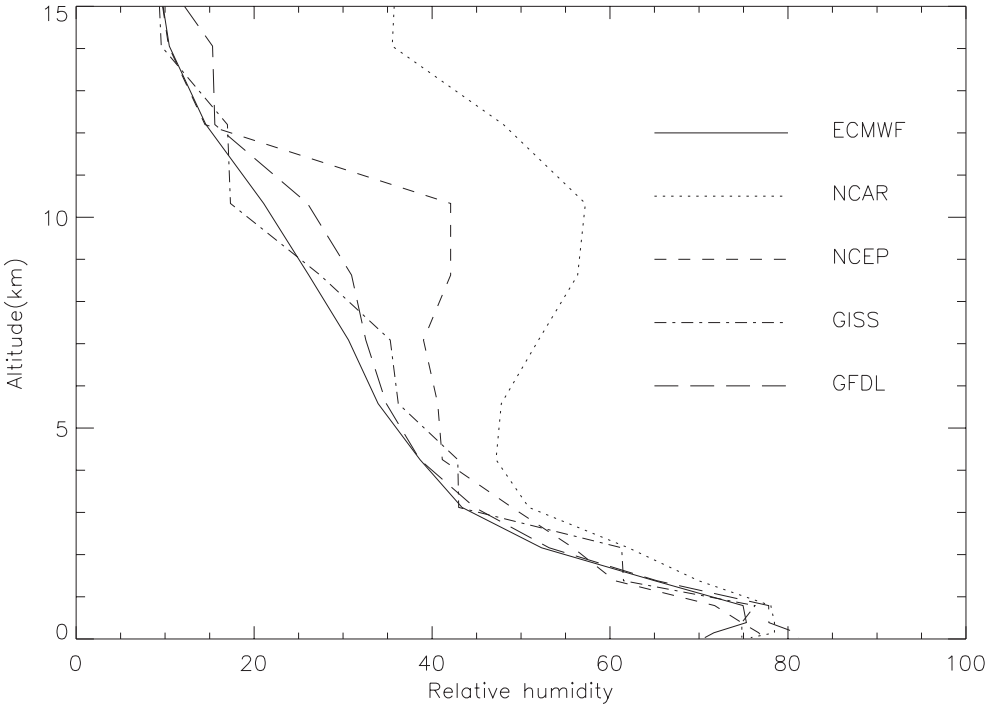

Figure 2: Relative humidity as a function of altitude for five different data sets.

The differences in relative humidity introduce a large variation in the radiative forcing and its geographical distribution. The radiative forcing due to sulfate with relative humilities from NCAR, NCEP, GISS, and GFDL are shown in Figure 3. The global mean radiative forcing due to sulfate using the NCAR relative humilities increases with 60% compared to the reference calculation with ECMWF humilities. For the three other data sets the global mean radiative forcing is between the values based on NCAR and ECMWF. Regionally the NCAR relative humilities result in particularly strong forcing at high latitudes, but also over Europe, North America, and south East Asia the forcing is in some regions

more than twice as strong as in the reference case. With the GISS relative humilities the radiative forcing is particularly strong over south East Asia. With the GFDL data this is the case over Europe.

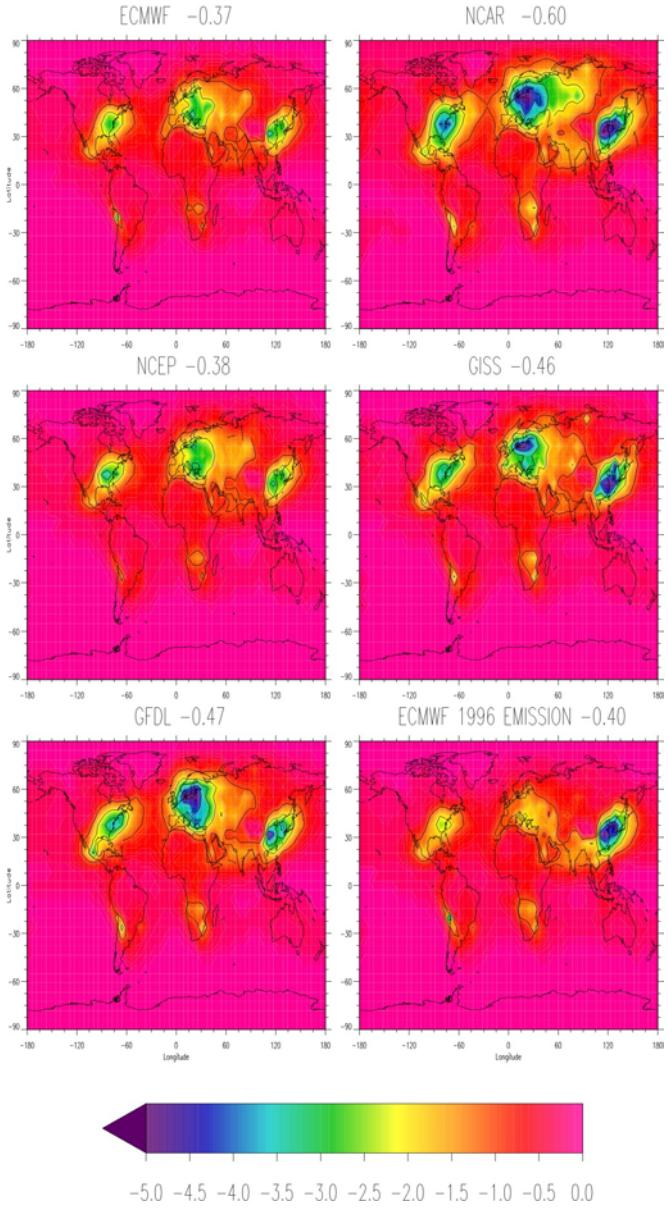

Figure 3: Radiative forcing due to sulphate for five different data sets of relative humilities.

References

Haywood, J.M., V. Ramaswamy, L.J. Donner, 1997. A limited-area-model case study of the effects of sub-grid scale variations in relative humidity and cloud upon the direct radiative forcing of sulfate aerosol. *Geophys. Res. Lett.,* **24**, 143-146.

Myhre, G., J.E. Jonson, J. Bartnicki, F. Stordal, and K.P. Shine, 2002, Role of spatial and temporal variations in the computation of radiative forcing due to sulphate aerosols: A regional study, *Q.J.R.Meteorol.Soc..,* **128**, 973-989.

An update on the future wind, wave and surge climate using the dynamical downscaling of the global MPI GSDIO scenario as forcing

by

Jens Debernard, Øyvind Sætra and Lars Petter Røed

Norwegian Meteorological Institute

Considered is a possible change in the future wind, wave, and surge climate for a regional area roughly covering the Northern Seas. Conclusions are drawn based on a statistical analysis of changes in the results derived with state of the art wave and storm surge models run for two 20-year time-slice periods, one for the period 1980 - 2000 (control climate) and one for the period 2030 - 2050 (future climate). Forcings were derived by extracting atmospheric wind and sea level pressure from a state of the art regional atmospheric climate model, which in turn constitutes a dynamical downscaling of Max-Planck Institute's global GSDIO scenario for the same two 20-year periods.

Generally the trends found are small and mostly insignificant. However, there are some important exceptions. For instance, a significant increase in all variables in the Barents Sea and a significant reduction in wind and waves north and west of Iceland is found. Also, there is a significant increase in wind speed in the northern North Sea and westwards in the Atlantic Ocean, and a comparable reduction southwest of the British Isles in the autumn. The same change is found in wave height, but is not statistically significant. There is also a significant increase in the seasonal 99 percentile of the sea level in autumn in the southwest part of the North Sea. These results are in line with earlier studies reporting a roughening of the maritime climate in the northern North Sea in autumn, although the uncertainties in the data are considerable. These finding is fully reported in Debernard et al. (2002).

One particular strong storm that occurs in the future scenario period is also studied. The storm gives extremely high waves at Ekofisk in the North Sea. The conclusion from evaluation of the development of the storm is that the storm could also occur in the present climate. Indeed, it may be regarded as a nearly worst case scenario for waves at Ekofisk. This study is fully reported in Debernard and Saetra (2001).

Reference

Debernard J, Saetra Ø (2001) Future wave and storm surge climate in Norwegian waters. Research Report No. 130, Norwegian Meteorological Institute, Oslo, Norway.

Debernard J, Saetra Ø and Røed LP (2002) Future wind, wave and storm surge climate in the Northern Seas. Submitted to Climate Research

Empirical Orthogonal Function analysis applied to MSLP from regional climate simulations

by

Dag Bjørge and Viel Ødegaard

Norwegian Meteorological Institute

1. Introduction

The questions addressed are:

- Will some weather regimes have increased frequency in the future, provided a change in radiative forcing?
- To what extent can the changes be allocated to the effect of down-scaling, to errors in the climate models or to global climate change.

The characteristics of the weather in the weather regimes might be relatively stable. However the atmosphere is more sensitive to external forcing in intermediate phases between weather regime. Thus external forcing can be responsible for how often the atmosphere is pushed over to a certain weather regime.

2. Description

Data used in this study are:

- Max Planck Institute ECHAM/OPYC model, GSDIO scenario global simulations 1980-99 and 2030-49 (MPI)
- HIRHAM model forced by boundaries, sea surface temperature and sea ice from the above (HIRHAM)
- ERA15 ECMWF reanalysis 1979-93 (ERA15)
- HIRHAM forced by ERA15 as above (HIRHAM)
- MSLP fields for each 12 hour in the winter months December to March are used for creating a 5 day averages of mslp.

3. Results

Common EOF

The eigenvectors of the varians-covarians matrix of the following pairs of data are common basis in which each of the datasets can be studied:

MPI - HIRHAM, now
MPI - HIRHAM, scenario
HIRHAM now - HIRHAM scenario
ERA15 - HIRHAM

The first two pairs are expected to reveal the effect of doing simulations on a higher resolution, in terms of stream patterns on a smaller scale, the third pair will reveal the effect of changed greenhouse forcing and the fourth pair will reveal the effect of the model error compared to observations.

The four first EOFs are as follows:

EOF1 is the Iceland anomaly with a high NAO-index, figure 1a.
EOF2 is an anomaly over the British Islands with a low NAO-index, Figure 1b
EOF3 reveals the north-south streamlines, Figure 1c

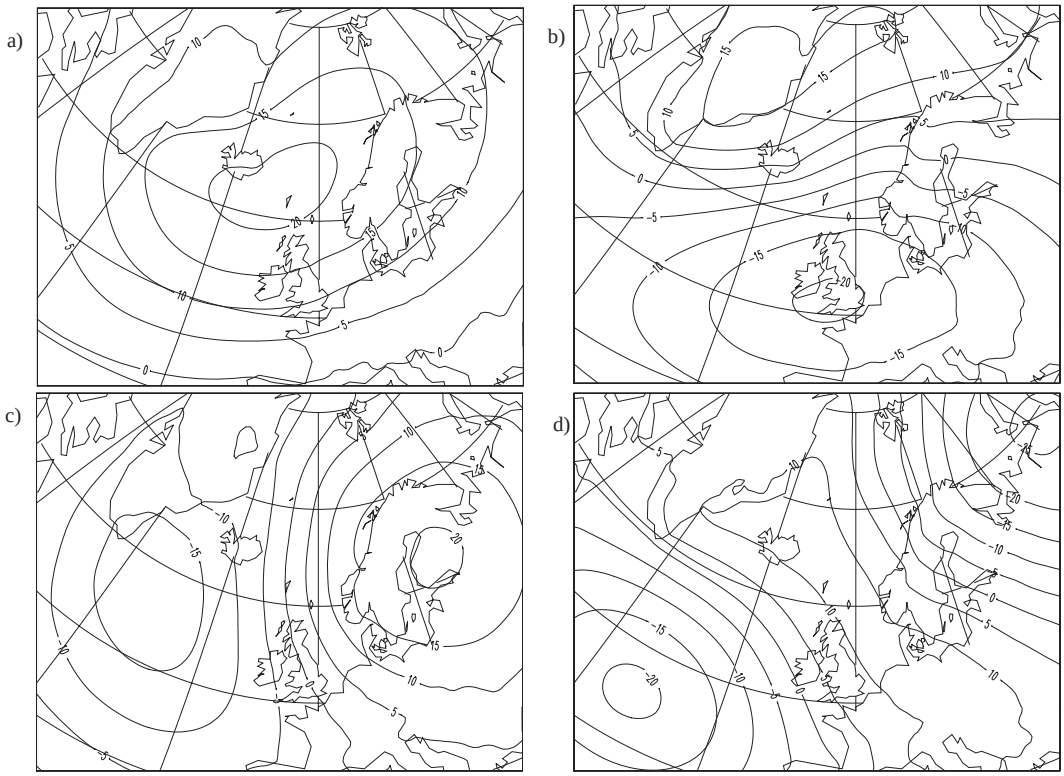

Figure 1

The individual weather regimes are represented by 5-days averaged mslp, and can be distributed in the plane spanned by EOF1 - EOF2. Each plot contains the points from one dataset, MPI simulations are denoted BND and HIRHAM simulations are denoted REG. The density of points is contoured. Common for all plots containing simulation of future climate is a bimodal distribution of weather regimes, Figure 2.

The average of the value of all points along one axis shows the representation of the EOFs in each of the datasets. Most pronounced is the difference of the representation of EOF1 in the ERA15 dataset compared to the ERA-forced HIRHAM simulations, Figure 3a.

The interpretation is a strengthening of the cyclonic circulation in the Iceland area (EOF1 has a negative sign) in the ERA data compared to HIRHAM, Figure 3b.

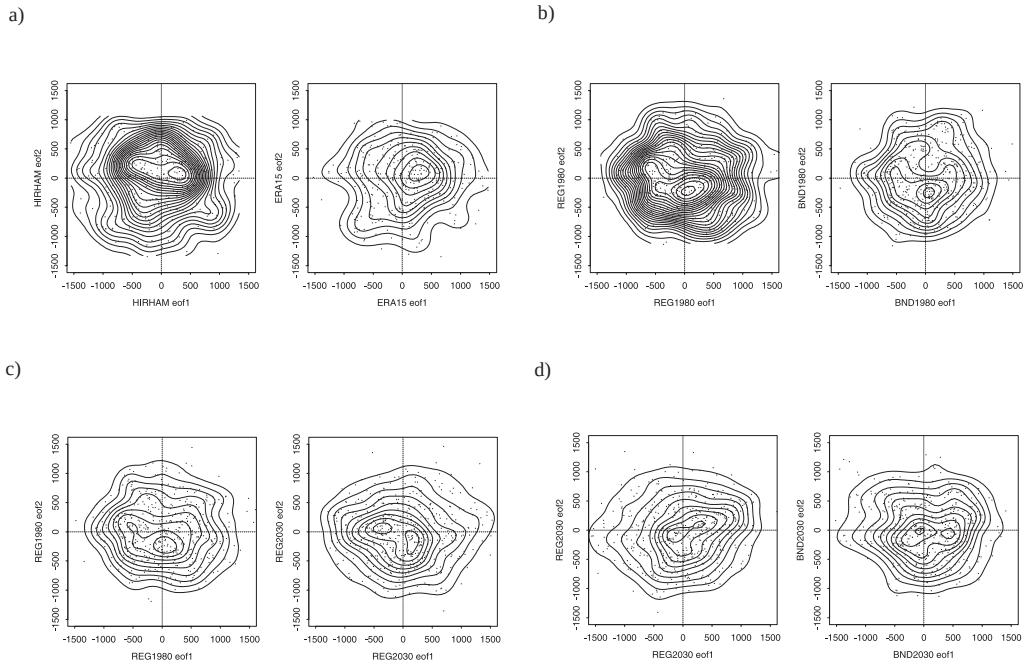

Figure 2

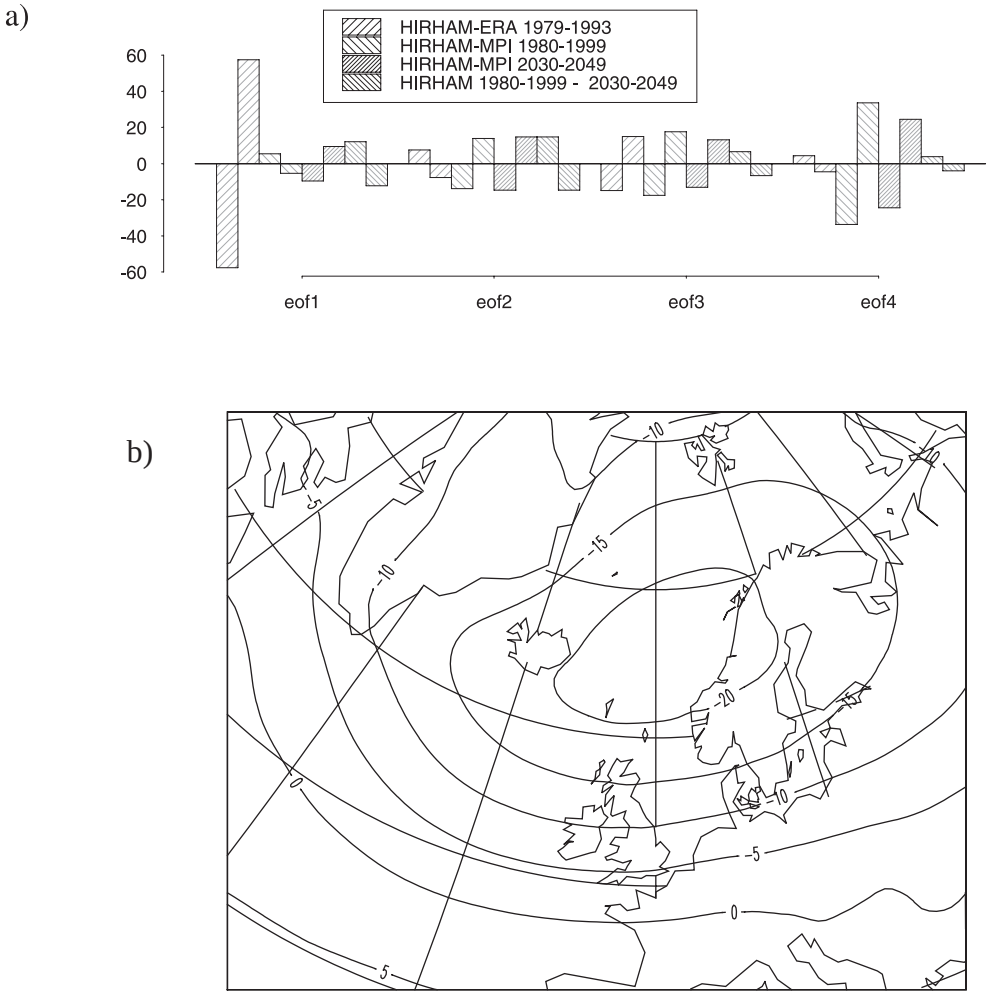

Figure 3

Individual weather regimes representative for those with the highest frequency in present and future climate are identified. An example of weather regime with high frequency in today's climate is in 4a), 4b) is an example from future climate which is very similar to 4a) while 4c) shows the weather regime that seems to be more frequent in the future than it is today.

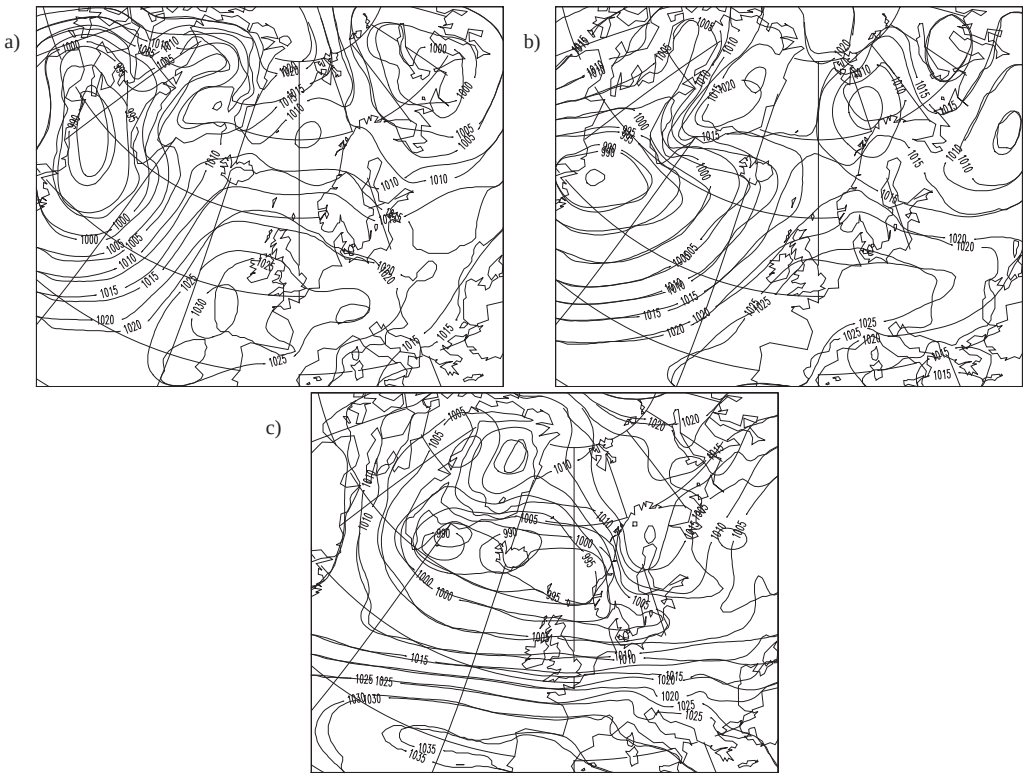

Figure 4

4. Conclusion

- The models have limited ability to reproduce the main stream pattern seen in the observations. The non-linearity of the weather model (and the atmosphere) makes it difficult to correct for this bias.
- The "new" about the future climate, is an increased frequency of weather regimes with a strong westerly wind between 45 and 60 deg. north, and a trough/low west of or over Scandinavia.
- The effect of higher resolution is seen only EOF4. High resolution does not seem to represent the solution to the main problem of the model's difficulties with the Icelandic Low.

Implementation of rivers in met.no's MICOM-version by surface fluxes

by

Jens Debernard and Lars Petter Røed

Norwegian Meteorological Institute (met.no)

The inclusion of river discharges into the met.no MICOM-version when this is coupled to an ice model is documented. The rivers are included as fluxes of mass, salt and heat through the ocean surface into the upper mixed layer of MICOM. In the current implementation, a flux-coupler or ice model converts the river inflow to surface fluxes. Rivers in this context also includes the influx of water through straits, e.g. the Bering Strait.

Introduction

The freshwater balance and distribution of salinity is of utmost importance for the predictive skills of ocean models utilized in cold regions. Due to the nonlinear equation of state for seawater, the density of cold seawater is mainly determined by the distribution of salinity. In the Arctic Ocean, a considerable part of the freshwater forcing is due to river runoff. In addition, there are very distinct inflow straits, e.g., the Bering Strait. In a regional model these inflow may advantageously be treated as rivers. It is important to note that river inflows do not only influence the hydrography of the ocean through fluxes of salt and heat. They also add mass (volume) into the ocean. For small rivers, this contribution is usually negligible. However, for “rivers” like the Bering Strait, this effect is the most important contribution. In the Bering Strait, there is a nearly barotropic inflow of about 1-1.5 Sv (10^6 m^3/s).

The implementation in MICOM

In MICOM (Miami Isopycnic Coordinate Ocean Model), the upper layer is usually a mixed layer with horizontal varying density. This is in contrast to the remaining layers in the model that have fixed, prescribed densities. Therefore, it is most flexible to input the water supplied by the rivers in the mixed layer. The straightforward approach is to implement it as a specified influx (advection) through its lateral boundaries. However, here another approach is chosen, namely to simulate it as surface fluxes of salt, heat and mass. This equals the method MICOM uses to include precipitation, evaporation and heat fluxes from the atmosphere. However, the treatment of the lateral transport trough major straits at the boundary of the regional model as river input requires that the important contribution of the added mass must be taken into account.

The dilution effect of a flux of water through the surface is usually included in ocean models as a salt flux

$$F_s = w_f (S_i - S), \tag{1}$$

where w_f is the rate of freshwater input (in m/s) through the surface, S is the surface salinity of the ocean and S_i is the salinity of the added water (e.g. Gill, 1982). To better understand this effect it is instructive to examine the mixing of to distinct water masses with volume V_1 and V_i, and salinity S_1 and S_i respectively. Neglecting for the moment the difference in density between these two volumes, the mixtures creates new water mass with volume $V_2 = V_1 + V_i$ and salinity

$$S_2 = \frac{V_1 S_1 + V_i S_i}{V_1 + V_i}. \tag{2}$$

If the added mass to the layer is freshwater only, that is, $S_i = 0$, then (2) shows that the salinity change is solely due to the change in water volume and hence that it is the change in water volume that dilutes the water mass. Consider that the added volume of water V_i is inserted in the small time period Δt. Then if V_i is much smaller than the original water volume V_1 the change in salinity as given by (2) to first order can be approximated as

$$\frac{S_2 - S_1}{\Delta t} V_1 = \frac{V_i}{\Delta t}(S_i - S_1) \tag{3}$$

Note that the right-hand side of (3) is the equivalent of the salinity-flux shown in (1). This also conforms to the salinity flux used in MICOM to calculate the new salinity, and hence the dilution effect of adding water mass is taken into account automatically. However, when also the volume contribution of the added discharge is included in MICOM, this has to be regarded as a process separated from the change in salinity. This means that in the step where the salinity of the mixed layer in MICOM is changed due to the added salt-flux, no change in the mixed layer thickness (volume) is allowed. Thereafter, the change in volume is added to the mixed layer thickness, and to the total water column depth to ensure a consistent increase in volume. The increase in mixed layer thickness affects the baroclinic mode of the model and the added thickness anomaly tends to spread out as internal waves or baroclinic currents. The change in total water depth alters the barotropic component of the model and propagates into the rest of the model domain proper as fast barotropic signals.

The implementation into MICOM is done as follows. The inclusions of the salt- and heat fluxes are unchanged. This is done in the mixed-layer routine, which also calculates changes in mixed-layer depth due to entrainment and detrainment. The changes in mixed-layer thickness and total water depth are divided into two different steps determined by the physical characteristics of the processes they affect. MICOM invokes a time-split scheme that separates the depth independent (barotropic) mode from the depth dependent (baroclinic) mode. Due to the fast propagation of barotropic waves in the ocean a much shorter time-step is used for

the barotropic part than for the baroclinic part. This difference is also reflected in the implementation of the change in layer thickness. The change in mixed layer thickness is therefore done for each baroclinic time step, while the change in total water column depth is done on each barotropic time step. The latter change is added directly into the continuity equation for the barotropic component.

The calculation of the fluxes for heat, salt and mass is at present administrated by an ice model or flux-coupler and transferred to MICOM together with atmospheric fluxes and fluxes from the ice model. At present the rivers include a climatologically, monthly mean temperature and volume flux. Their salinity is at present prescribed as a value constant in time, but a time-varying salinity is easily incorporated. For true rivers, the salinity is set to zero, while for the "river" discharge through straits it is given an annual mean value.

Because the flux-coupler is administrating the fluxes it is relatively easy to incorporate a river routing system (hydraulic cycle), which takes into account the precipitation from the atmosphere model and then transforms it into subsequent river run-off fluxes for the ocean model.

The Bering Strait influx

As a demonstration of the effects of including mass from rivers or straits, an implementation of the Bering Strait as a large, salty river is given here. Figure 1 shows a snapshot picture of the sea surface elevation and vertical averaged horizontal current from MICOM in a region of the Arctic Ocean, near the Bering Strait. The land mask of the model is seen as rectangles. The inflow through the strait is included as surface fluxes into the seven grid points marked 1, 2, . . . , 7 in the strait. Together, approximately 1 Sv of water is included into the model through these points. The monthly mean temperature of the inflow water is specified from the EKASC climatological archive (Engedahl et al. 1997). The salinity of the inflow water is constant and is derived as the yearly mean salinity from the EKASC archive.

As seen from the Figure 1, there is a strong barotropic current flowing from the strait into the Arctic Ocean. In the present situation, the inflow is so strong that the mixed layer extends to the bottom in the inflow region (~50 meter). This is not a problem in the Bering Strait. In other inflow areas such as the Belts between Denmark and Sweden, it constitutes a problem since the above implementation of flow through straits as a surface flux does not capture the two-layer structure with light water flowing in one direction at the top and denser water underneath flowing in the opposite direction. In situations where this situation is important, an open boundary condition with vertical varying inflow and outflow should be utilized.

In the Bering Strait, the mean transport of sea ice is generally directed into the Arctic Ocean. However, in situations with the wind blowing out of the strait also the ice is transported out of the strait. With the configuration shown in Figure 1, this is not possible and the ice tends to pile up in the strait during such periods. Therefore, it seems advantageous to open up a larger part of the strait to allow the outflow of sea ice.

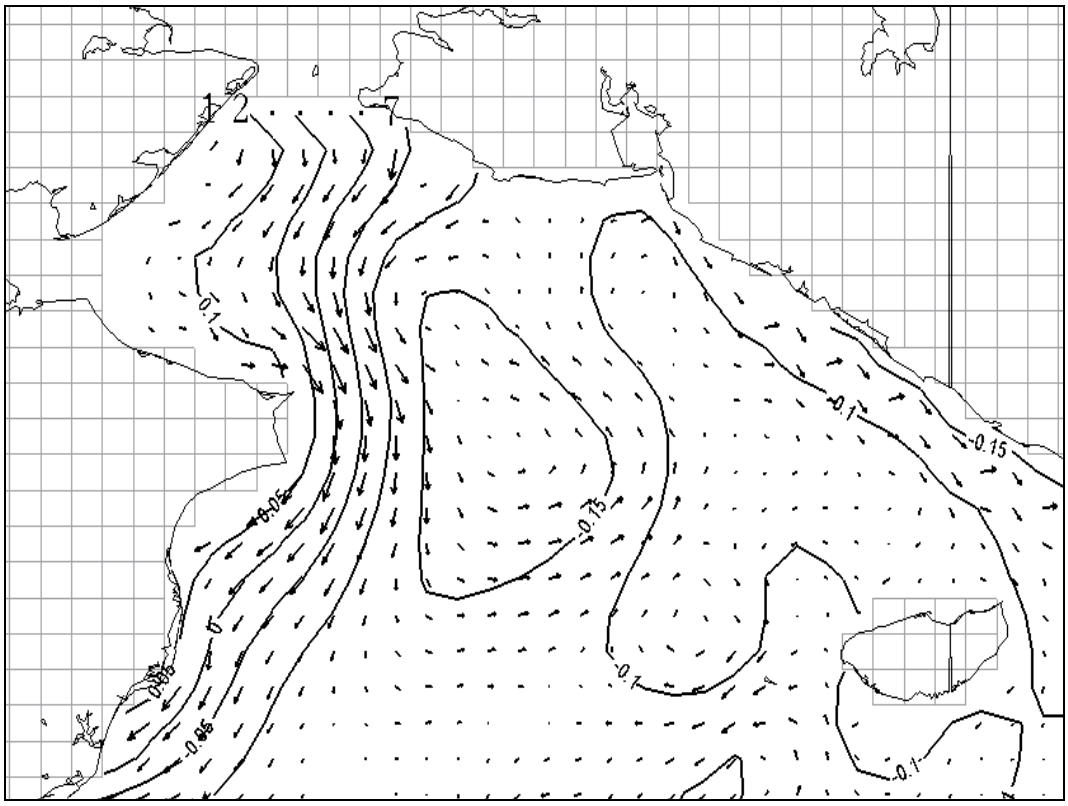

Figure 1: Inflow of salt water through the Bering Strait. The influx is computed as fluxes of heat, salt and mass through the surface of the mixed layer. Isolines show the sea surface elevation (contour interval 0.05 cm), while the arrows show the depth independent (barotropic) current. The flow into the Arctic is mainly a barotropic current caused by the inclusion of mass through the surface of the mixed layer.

References

Engedahl H, Eriksrød G, Ulstad C, Ådlandsvik B (1997) Climatological oceanographic archives covering the Nordic Seas and the Arctic Ocean with adjacent waters. Research Report No. 59, Norwegian Meteorological Institute, Oslo, 69 pp.

Gill, AE (1982) Atmosphere-Ocean Dynamic. International geophysics series, Vol 30, Academic Press, ISBN 0-12-283522-0.

Scenarios for heating and growing seasons in Norway

by

Torill Engen Skaugen and Ole Einar Tveito

Norwegian Meteorological Institute, P.O.Box 43 Blindern, N-0313 Oslo, Norway

ABSTRACT

This paper presents an impact study of the change in the length of the heating and growing season, the heating degree-days (HDD) and growing degree-days (GDD) due to global warming. The time slice periods analysed is the standard normal period 1961-90 and the scenario period, 2021-2050.
The temperature for the scenario period is expected to increase, especially in the winter. This will lead to a decrease in the length of the heating season all over the country up to 2050. The HDD will decrease at the most with more than 20 % in costal areas.
Even though the temperature is supposed to increase most in the wintertime, the expected temperature increase in the summertime (and spring and autumn) will lead to longer growing season all over the country up to year 2050. The GDD will increase with more than 100 % in the mountain area. In Northern Norway the GDD will increase with between 30-100 % and at the coastal belt from Trondheimsfjorden to the Swedish border it will increase with less than 30 %.

1. Introduction

The heating season is here defined as the period of the year when the daily mean air temperature is below 10 ^{o}C. The growing season is the period of the year when the daily mean air temperature is above 5 ^{o}C. The length of these seasons depends on the air temperature, which again varies in space with altitude, latitude, distance from the coast etc.

The HDD and the GDD are the accumulated sum of ^{o}C between the daily mean temperature and a threshold temperature. This temperature is for HDD below 17 ^{o}C, for the GDD it is defined to be above 5 ^{o}C. HDD and GDD is a good estimate on respectively accumulated cold and heat. HDD is therefore a useful index of energy available for heating energy consumption and thus to power production planning. Hence GDD is a useful index of biological growth.

This paper presents the results of a study of the assumed change in the heating season and the GDD due to a warmer climate for Norway in the next 50 years. The work presented in this paper is fully described in Skaugen and Tveito [3] and Skaugen and Tveito [4].

Temperature data and methods used are presented. The length of the heating and growing seasons and HDD and GDD for the normal period and the scenario period 2021-2050 are discussed.

2. Data

For the standard normal period 1961-90 temperature observations are used. For the scenario period 2021-2050, temperature data are calculated from the empirical downscaling of the GSDIO integration [2]. The empirical downscaling apply empirical links between large –scale fields and local variables to deduce estimates of the local variables.

For the normal period, data for 421 stations is available [5]. Temperature estimates for the scenario period is carried out for fifty stations in Norway, four of these is located in the Arctic [1].

3. Methods

3.1 Daily mean temperature

The smoothed daily mean temperature is interpolated from monthly mean temperature applying a cubic spline algorithm [3]. A constraint is added to the spline equation to ensure that the deviation between the gridded monthly mean temperature and the mean monthly temperature based on the estimated daily temperature values not exceeds 0.001 ^{o}C.

3.2 Spatial interpolation

Mean monthly temperature maps are established for the last normal period for Fennoscandia by Tveito et al. [5]. The maps are obtained by using residual kriging. The grid resolution is 1 x 1 km^2.

Interpolation of absolute temperature values is difficult due to sparse station density and its large variability over short distances. This is in conflict with the assumptions using spatial interpolation methods that usually are based on the assumption of second order stationarity. By normalising the mean temperature value for the 2021-2050 period, these assumptions are almost fulfilled. The normal value is subtracted from the mean temperature values for the respective periods, and the resulting residual value is used as the regionalized variable. By interpolating the residuals, the variability due to climatology is removed, and more robust estimates are obtained compared to interpolation of absolute temperature values.

Temperature maps the scenario period are obtained by adding the residual maps for the scenario period to the temperature maps for the normal period (1961-1990). (The maps are represented as grids in a Geographical Information System (GIS)).

3.3 Heating season and heating degree-days (HDD)

The heating season is defined to be the period of the year when the mean daily temperature is below 10°C.

The heating degree-days (HDD) are defined as the accumulated degree sum above a defined reference temperature, $\hat{T}$. Mathematically this can be expressed throughout the whole year (or within a defined season) as:

$$HDD = \sum_{i=1}^{365} (\hat{T} - T_i), T_i \le \hat{T} \qquad (1)$$
$$HDD = 0, T_i > \hat{T}$$

where T_i is the daily normal temperature for day number *i,* $\hat{T}$ is the reference temperature (17 ^{o}C).

3.4 Growing season and growing degree-days (GDD)

The growing season for grass is defined to be the period of the year when the mean daily temperature is above 5°C.

The growing degree-days (GDD) are defined as the accumulated degree sum above a defined reference temperature, $\hat{T}$. Mathematically this can be expressed throughout the whole year (or within a defined season) as:

$$GDD = \sum_{i=1}^{365} (T_i - \hat{T}), T_i \ge \hat{T} \qquad (2)$$
$$GDD = 0, T_i < \hat{T}$$

where T_i is the daily normal temperature for day number *i,* $\hat{T}$ is the reference temperature (5 °C).

4. Heating season

4.1 Length of the heating season

The length of the heating season in the normal period increases with altitude (m. a. s. l.) and latitude from less than 240 days in the coastal area in the southwestern and southeastern part of Norway (Figure 1a). In a belt from the Swedish border in the southeastern part of Norway along the coast to the Trondheimsfjord area, and in a tiny belt further north up to Lofoten, the heating season lasts up to 300 days. This belt is widest in the southeast and gets thinner along the west coast and further north. It widens in the low altitude area around Trondheimfjorden. The black areas in the map indicate that the heating season lasts from 300 up to 364 days of the normal year. This are the areas located at the high altitudes and in the northern Norway. In the high mountain areas and northernmost parts of the country, the temperature never exceeds 10 ^{o}C during the summer and thus the heating season is defined throughout the normal year (365 days).

The white area in Figure 1b indicates where there will be no change in the length of the heating season in the scenario period (2021-2050) compared to the normal period. This is the high mountain area where the heating season lasts throughout

the whole year. Compared to the normal period, this area will decrease with nearly 60 %.

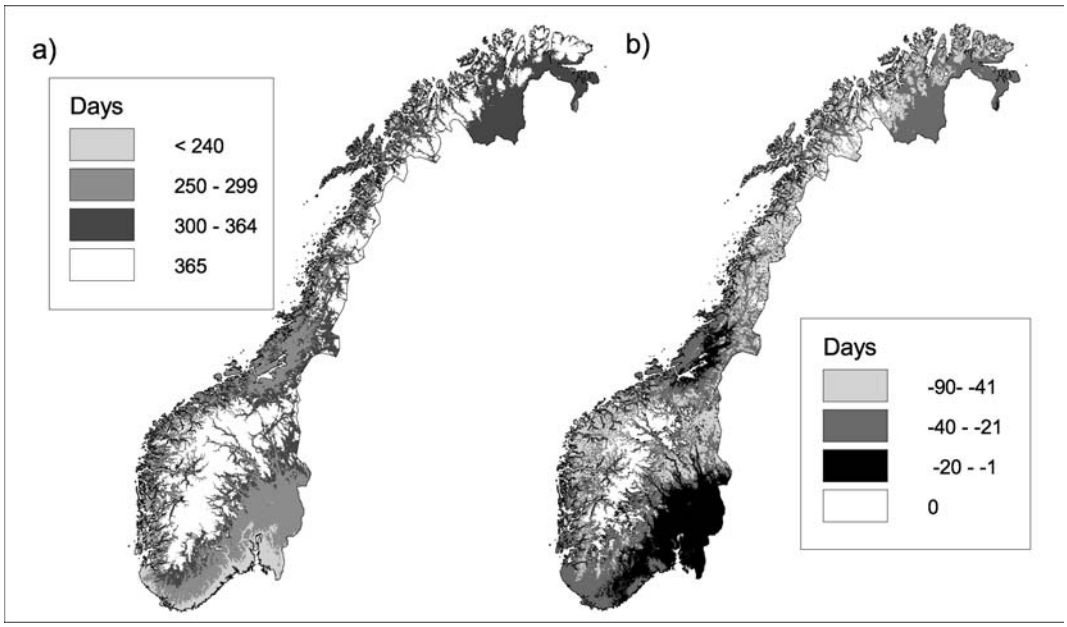

Figure 1: The length of the heating season in the normal period 1961-1990 is presented to the right. Changes in the length of the heating season in the scenario period compared to the normal period are presented to the right.

In the southeastern part of Norway and the area around Trondheimsfjorden, the heating season will be up to 20 days shorter. For the costal part of the southwest, the coastal part of the Trondheimsfjord area and the inner part of Finnmarksvidda, the heating season will decrease with between 20 and 40 days. In the western part of the country, in the mountain areas and in the north the heating season will decrease with more than 40 days. The temperature increase will delay the beginning of the heating season and it will end earlier.

4.2 Heating degree-days (HDD)

The HDD within the heating season increase with negative °C. For Norway this means that the HDD increases with altitude and latitude. The distributed HDD map over Norway in the normal period (Figure 2a) is divided into three regions. The first region is the belt along the coast from the Trondheimsfjord area to the Swedish border. This belt has a rather linear distributed increase in HDD according to the area, ranging from less than 3000 and up to 4500 ^{o}C. The next region has almost the same amount of area within each HDD-value, ranging from 4500 to 6000. This area is the high land area from the Swedish border in the east within the belt between the high mountain area and the first region. From Trondheimsfjorden the belt gets thinner along the coast up to Finnmark. The third region, with the highest estimates of HDD, more than 6000 ^{o}C, coincides with the high mountain areas and Finnmarksvidda.

As a consequence of increasing temperatures, especially in wintertime, the HDD is supposed to decrease all over the country in the scenario period (2021-2050) compared to the normal period (Figure 2b). The changes in HDD in percent are

largest along the west coast and the costal line in the northern part of Norway, where the HDD will decrease with more than 20 %. Finnmark will have a reduction in HDD between 15-20 %. In the eastern part of the country and the Trondheimfjord area, the reduction in HDD is expected to be between 10 and 15 %. In the high mountain area in southern Norway, the decrease is smallest, less than 10 %.

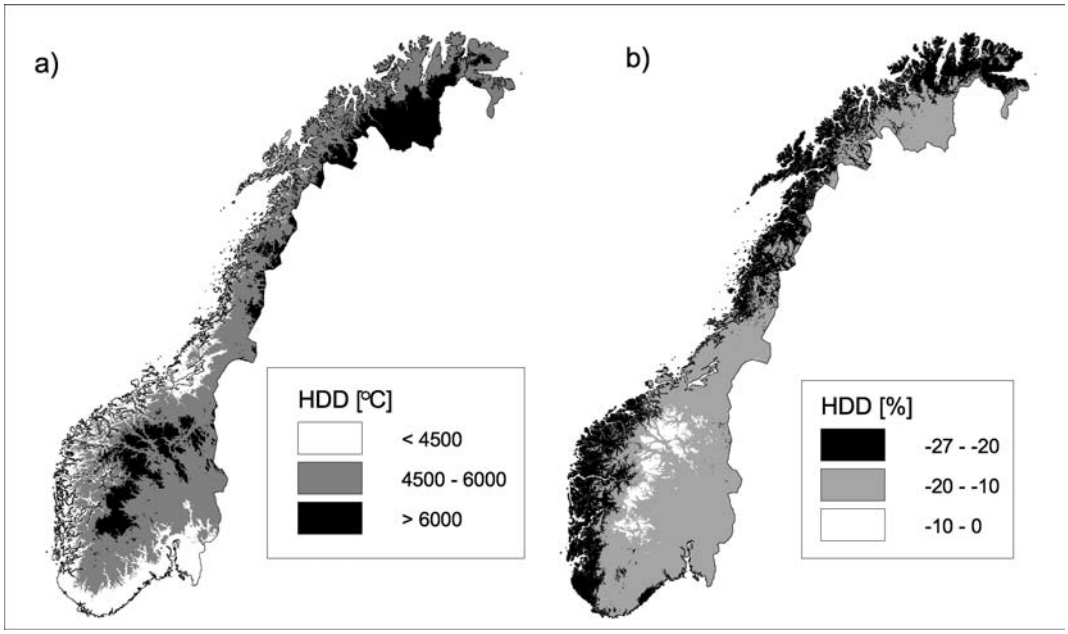

Figure 2: The HDD within the heating season in the normal period 1961-1990 is presented to the left. Changes in the HDD within the heating season, in the scenario period compared to the normal period, are presented in percent to the right.

5. Growing season

5.1 Length of the growing season

The duration of the growing season decreases with altitude (m a. s. l.) and latitude (Figure 3a). In the northern part of Norway, the duration of the growing season for the normal period (1961-1990) varied between 50 – 150 days. In the coastal area in the area from the Trondheimsfjord to Lofoten, it lasted up to 150 days. In this area the length of the growing season decreased towards east. A rather large part of Finnmarksvidda, the growing season lasted between 100-125 days. In the rest of Finnmark the growing season lasted between 75 – 100 days. The growing season lasted less than 75 days only in minor areas in Finnmark. In the coastal area in the southwestern and southeastern part of Norway from the Swedish border to the Trondheimsfjord area, the growing season lasted between 150 and 200 days. Only a narrow zone at the southwestern coast it lasted more than 200 days. In the mountain area in the southern Norway, the growing season lasted between 100-150 days. The area where the growing season was shortest, less than 50 days, is at the high mountain area in the western part of Norway.

The length of the growing season in the scenario period compared to the normal period (Figure 3b) is supposed to increase with less than 20 days in the eastern part of Finnmarksvidda, the Trondheimfjord area and the Oslofjord area. In the

southern part of the country, the mountain area in the south and the coastal area further north, the growing season will increase with more than 20 days. In the coastal part of Finnmark, the area from Trøndelag to Lofoten, and the high mountain area in the weastern part of Norway, the growing season will increase with more than 30 days. This is in accordance with the increase in the summer temperature scenario [2].

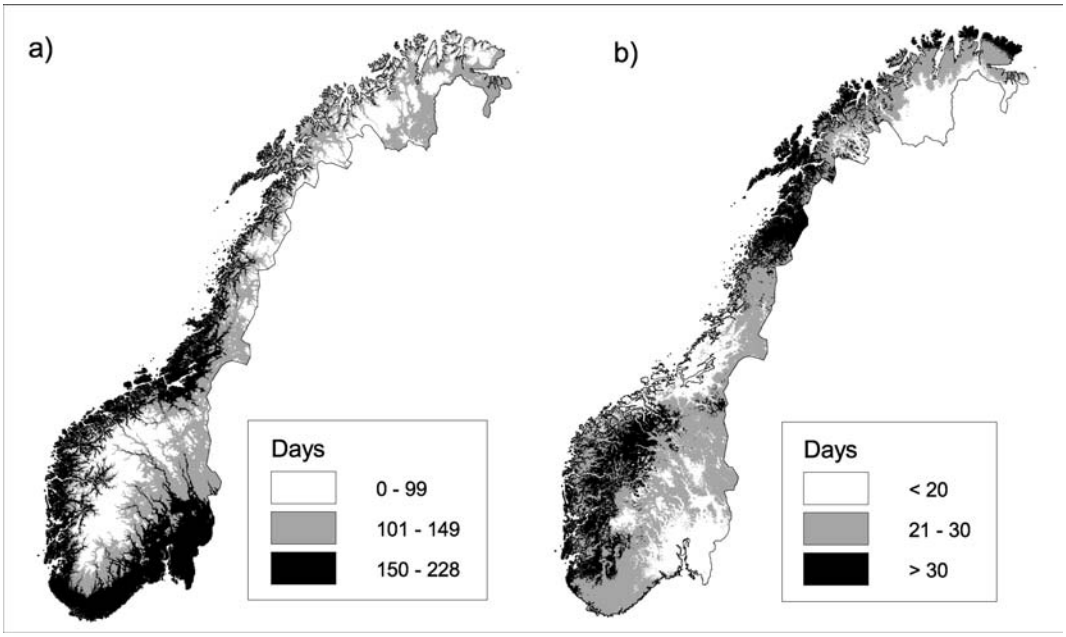

Figure 3: The length of the growing season in the normal period 1961-1990 is presented to the right. Changes in the length of the growing season in the scenario period compared to the normal period are presented to the right.

5.2 Growing degree-days (GDD)

The GDD estimate corresponds with the length of the growing season and with the temperature within the season. In Figure 4a, the GDD within the growing season in the normal period, 1961-1990, is shown. The area at the southwestern and southeastern coast of the Oslofjord had the largest GDD value, more than 1200 °C. A belt along the coast, from the Swedish border in the east to the area around Trondheimsfjorden, had a GDD value between 700-1200 ^{o}C. From here this belt gets thinner, and it is only a small belt up along the coast to the Lofoten area. The mountain area in southern Norway, the costal part of the northern Norway, and Finnmark had a GDD value between 200 and 700. The high mountain area had the lowest GDD estimate, less than 200.

As a consequence of increasing temperatures, especially in wintertime, the GDD is supposed to increase all over the country in the scenario period (2021-2050) compared to the normal period (1961-1990). This is shown in percent in Figure 4b. The area where the change is supposed to be more than 100 % is the high mountain area where the growing season was short in the normal period. A few days increase in the growing season in this area will lead to a great change in percent. The mountain area and Finnmarksvidda will have the largest change in percent the next 50 years, up to 100 % change. The area around the Trondheims-

fjord, a tiny belt along the coast that widens further east to the Swedish border will have a change in the GDD with less than 30 %.

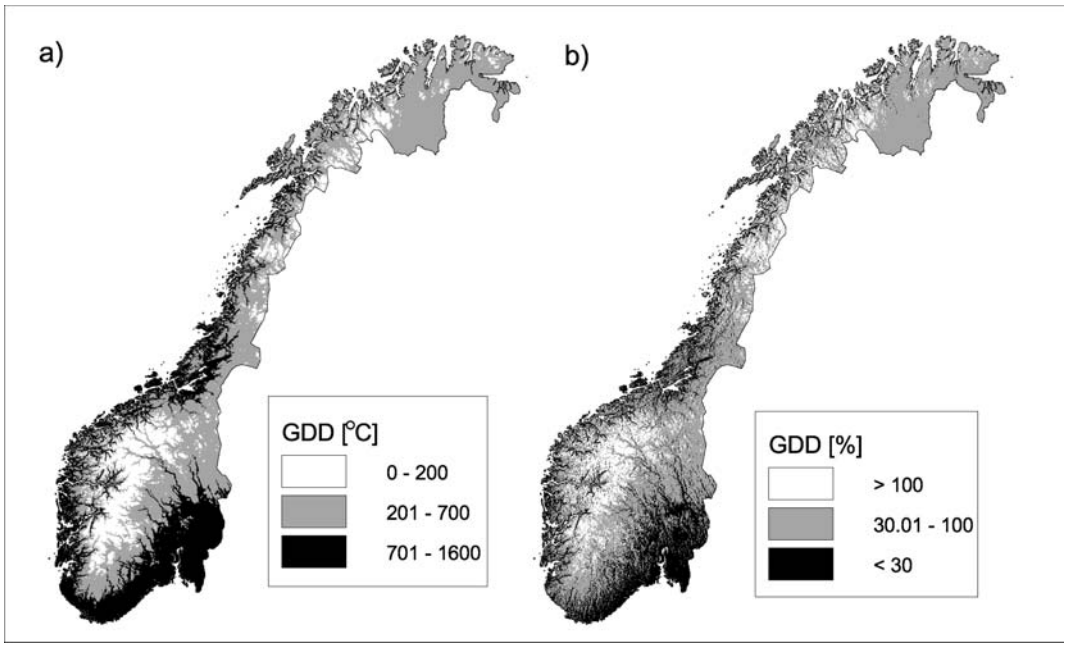

Figure 4: The GDD within the growing season in the normal period 1961-1990 is presented to the left (a). Changes in the GDD within the growing season, in the scenario period compared to the normal period, are presented in percent to the right (b).

6. Summary

6.1 Heating season

The normal heating season (1961-1990) varies from less than 240 days in the coastal lowland up to 365 days in the high mountain areas and the northernmost part of Norway.

For the period 2021-2050, the scenario shows that the temperature will increase, and thereby result in a reduced heating season. The heating season will decrease with more than 40 days in the western part of the country and in the mountain area. In the coastal part of the southwestern area and the inner part of Finnmarksvidda, the heating season will decrease with between 20 and 40 days compared to the normal period. The smallest changes will occur in the southeastern part of Norway and in the Trondheimsfjord area were the heating season will be less than 20 days shorter.

The heating degree-days (HDD) in the heating season for the normal period varies from less than 4500 in the southern coastal area to more than 6000 in the high mountain area and in northern Norway.

For the scenario period, the HDD decreased with more than 20 % at the west coast and the coastal area in Finnmark. In the eastern part of the country and the Trondheimfjord area, the scenario indicates a reduction in HDD between 10 and 20 %. Finnmarksvidda will have a reduction in HDD of between 15-20 %. In the

high mountain area in the southern Norway, the decrease is smallest, less than 10 %.

6.2 Growing season

The high mountain area in southern Norway, the growing season in the normal period (1961-1990) lasted less than 50 days. The area from the Trondheimfjord to the Swedish border had the longest growing season, between 150-200 days. Only in a narrow zone at the west coast, the growing season lasted longer than 200 days. The growing season in Northern Norway lasted between 50 - 150 days.

The length of the growing season in the scenario period (2021-2050) is supposed to increase all over the country compared to the normal period. The temperature increase in the summer period is supposed to be largest in Nordland and in the high mountain area in the western part of Norway, with an increase in temperature of 0.3 - 0.4 °C per decade from the period 1961-1990 to the period 2020-2049. The same area is supposed to have the largest increase in the growing season, more than 30 days. At Finnmarksvidda, the Trondheimfjord area and the Oslofjord area, it is supposed to be an increase in the growing season with less than 20 days. The rest of the country will have an increase in the growing season between 20 - 30 days.

The growing degree-days, GDD, in the normal period (1961-1990) varied from less than 200 to more than 1200 °C over the country depending on the length of the growing season and the temperature within the growing season. A belt in the southern area from the Swedish border to the Trondheimfjord area, and a tiny belt along the coast from here to Lofoten had the largest GDD within the growing season, between than 700-1200 °C. Only a zone at the eastern and western coast of the Oslofjord, had a larger GDD estimate, more than 1200 °C. In the mountain area in the south and northern Norway, the GDD estimate was less than 700 °C.

The change in the growing degree-days, GDD, in the scenario period (2021-2050) compared to the normal period, is supposed to be more than 100 % in the high mountain area in the southwestern and northern Norway. The large percentage is mostly because the growing season in this area in the normal period was short, and rather moderate changes in the growing season will affect the growing season and the GDD percentage estimate. The rest of the mountain area in the southern Norway, and the northern Norway, is supposed to have a change in the GDD between 30 – 100%. The change in the GDD in the southeastern Norway and the area around the Trondheimsfjord will be less than 30 %.

References

[1] Hanssen-Bauer. I, O.E. Tveito and E.J. Førland (2000) Temperature scenarios for Norway: Empirical Downscaling from the ECHAM/OPYC3 GSDIO intergration, DNMI report No 24/00 Klima

[2] Press, W.H., S.A Teukolsky, W.T. Vetterling and B.P. Flannery, 1992, Numerical Recipes in Fortran, Cambridge University Press.

[3] Skaugen, T.E. and O.E. Tveito, 2002, Heatng degree-days – Present conditions and scenario for the period 2021-2050. met.no report No 01/02 Klima

[4] Skaugen, T.E. and O.E. Tveito, 2002, Growing degree-days – Present conditions and scenario for the period 2021-2050. met.no report No 02/02 Klima (in prep.)

[5] Tveito, O.E., E.J. Førland, R. Heino, I. Hanssen-Bauer, H. Alexandersson, B. Dahlstrøm, A. Drebs, C. Kern-Hansen, T. Jònsson, E. Vaarby Laursen & Y. Westman, Nordic, 2000, Temperature maps, DNMI report no 09/00 Klima.

Evaluation of local climate scenarios in terms of cubic-fit to downscaled time series

by

R.E. Benestad

The Norwegian Meteorological Institute, Norway.

Two major objectives of the RegClim programme have been to produce local climate scenarios consistent with an anthropogenic global warming, and to assess the associated uncertainties. There are two important methods for deriving scenarios for the local climate, dynamical and empirical downscaling, and both are based on output from global coupled ocean-atmosphere general circulation models (AOGCMs). Scenarios produced through empirical downscaling at the Norwegian Meteorological Institute are described in Hanssen-Bauer *et al.* (2000, 2001), Hanssen-Bauer (2002), Hanssen-Bauer and Førland (2001b, 2001c), Benestad (2000, 2001a, 2002a, 2002b), Benestad and Førland (2001), and Benestad *et al.* (2002a).

The empirical downscaling at the Norwegian Meteorological Institute has employed two different methodologies that have been tested and documented in Hanssen-Bauer (2000a), Hanssen-Bauer and Førland (2001b), and Benestad (2000, 2001b). The downscaling models describe the relationship between large and small scales realistically (Benestad, 2000, 2001b; Hanssen-Bauer and Førland, 2000a), but the linear approximations and simplifications employed in the downscaling also introduce some uncertainties. Furthermore, the global climate scenarios produced by AOGCMs may also suffer from shortcomings (Benestad *et al.*, 2002b). Hence, both the AOGCMs and the downscaling contribute to the uncertainties in the local climate scenarios, and in order to assess the overall uncertainty, the downscaled scenarios must be evaluated against the observations. Local climate scenarios are suitable for evaluation studies since they can be compared directly with observations.

An evaluation of the climate scenarios must reflect their use, which often is the projection of future climatic trends[1] with a time-horizon of 30-50 years. There is little point of computing correlation scores or root-mean-square-errors (rmse) if it is the trends that are important[2]. On the other hand, the climatic trends can be derived from the climate model simulations for the past and compared directly with the observed trends. If the observed past trends cannot be reproduced by the models, then little confidence should be attached to the future trends, because

[1]The trend information can be used to derive temperature or precipitation changes.

[2]The correlation between two straight lines with non-zero slope (long-term trends) is ±1. However, for series with short-term variations superimposed onto weak trends, the correlation coefficients are dominated by the variations. Hence, a correlation score says little about the long-term trends. Similarly, the rmse is sensitive to the short-term variations if they are more prominent than the long-term trend.

there is no reason for the models to do a better job of describing the future than the past[3].

A long-term trend has traditionally been defined as a best-fit linear change with time. An inspection of the past temperatures in northern Europe, however, shows that a linear trend does not describe the accelerated warming in the early 20th century and the rapid warming since 1980. A linear best-fit over a 100-year period does not describe the trends over a 30-to-50-year time-horizon, and a linear fit to a 20-to-50-year-long time-series is strongly affected by (natural) interannual and decadal fluctuations. Hence, a linear-fit does not provide a suitable description of climatic trends over 30-50-year periods.

A regression fit of a cubic equation[4] in terms of time (x) to the temperature series (y) may give a better description of the trends on the 30-50-year timescale (Figure 1a). A cubic-fit can be found using a multiple regression that solves for four coefficients c_0 to c_3:

$$y = c_0 + c_1 x + c_2x^2 + c_3x^3 \quad (1)$$

Once the coefficients are known, it is simple to derive the rate of change (trend) from the first derivative:

$$dy/dx = c_1 + c_2x + c_3x^2 \quad (2)$$

The trends derived from the cubic-fits have the form of parabolas where the rate of change by definition (unless c_2 and c_3 are zero) tends to be highest in the beginning and the end of the record. This information has been imposed *a priory* when a cubic equation was chosen over a linear fit, but this also gives a better description of the actual past evolution of the temperature in northern Europe than a linear fit. Figure 1a shows the time evolution of the observed 30°N-75°N/30°W-40°E-mean temperature record (black) together with corresponding reproductions from an ensemble of different AOGCMs (grey). The best cubic-fits based on equation (1) are superimposed and shown in blue for the observations and red for the AOGCMs. The prominent interannual variations complicates the definition of the cubic trends, however, a visual inspection suggests that the cubic-fits give a reasonable description of the long-term temperature evolution. Figure 1b shows the trends derived using equation (2), with the observed trend shown in blue and simulations in red. Most scenarios suggest similar time evolution, but one AOGCM (HadCM3) describes an unrealistic cooling in the Oslo climate[5]. The blue curve lies within the range of model solutions (red curves), suggesting that the modeled trend values of the 30°N-75°N/30°W-40°E spatial mean temperature span the corresponding observed values. The same analysis for downscaled January temperature in Oslo is shown in Figure 2.

The interannual variations are more prominent for the downscaled values than for area mean values, in some cases making the trends difficult to define (Figure 3a,c). Large variations near the end points of the series will affect the

[3]Both the AOGCM output for the past and the future are independent to the observations, and the empirical downscaling models are the same for both.
[4]Which is mathematically only a less severely truncated Tailor series than the linear fit.
[5]This case needs further investigation.

solutions to the cubic-fit, but this problem may to some degree be solved by applying a low-pass filter to the series prior to the cubic-fit. Tests of the robustness of the cubic-fit trend analysis are shown in Figures 3c and 3d, and the long-term trends may not be well-defined in situations where the interannual variability is prominent compared to any long-term trend. Prominent interannual variations also represent a problem for the traditional linear trend approach. The evaluation of the downscaled scenarios has so far focused on the realism of the downscaled results - albeit with uncertainties, but the interpretation of this evaluation must take into account the difficulties in defining long-term trends[6]. Justifications for adopting the cubic-fit trend analysis are: (i) exactly the same procedure is done for each of the models and the observations[7]; (ii) that the cubic-fit trend-analysis can be applied in the same way to the downscaled scenarios for the future; and (iii) we know *a priori* that a linear trend does not give a good description of the climatic evolution for northern Europe.

A comparison between the observed trend and the past trends derived from the AOGCMs (Figure 2b) shows that the observed trend lies in the upper range of the AOGCM ensemble, suggesting that most of the models do not capture the most recent accelerated warming. It is more remarkable, however, that none of the AOGCMs capture the pronounced warming in the period at the turn of the 20th century[8] ('the early 20th century warming'). Figure 4 shows the trend-analysis for Oslo in April (a) and July (b), and for Tromsø in January (c) and July (d). The observed April-trend falls well within the multi-model ensemble, and in July, the observations are close to the AOGCM values[9]. In Tromsø, the observed early 20th century warming is much stronger in the observations than in the downscaled results in both January and July, but the most recent warming is within the model spread.

The mismatch in the early 20th century warming shown in Figures 2 and 4 brings up the question of whether the local climate scenarios really give a good description of the real world. On the one hand, these results show that there may be differences between the actual trends and those derived from the models, and the question whether these differences are significant or within the uncertainties in the trend-analysis must be considered[10]. On the other hand, it has been argued that the early 20th century warming is not a result of increased greenhouse gas concentrations in the atmosphere, and since the climate scenarios only account for a climate response to an enhanced greenhouse gas effect and internal variability, there is no reason for the climate models to reproduce the 20th century warming if it was due to other factors not taken into account (e.g. volcanism, landscape changes, solar activity). It is possible that the AOGCMs do not give a sufficiently good description of the internal variability or that the 14-member ensemble is too small to give a statistical representation of decadal-timesccale internal variations. Alternatively, the evaluation of the climate models may suggest that the

[6]A multi-model ensemble of 14 members is still too small to obtain a good sample of the uncertainties due to internal variations. Prominent interannual variability will also make it hard to define future climate trends or estimate significant future climate changes.
[7]The multiple regression in equation (1) is applied to time intervals of equal length for all cases.
[8]Several AOGCMs do in fact describe a cooling over the same time.
[9]The AOGCMs slightly overestimate the warming rate between 1920 and 1975.
[10]Can be tested through a Monte-Carlo approach.

downscaled scenarios are realistic in terms of a response to increased greenhouse gas concentrations, but they are not able to account for all of the climatic variations. These results highlight the need of improving our understanding of the natural variability and for identifying other possible forcing mechanisms that may be of importance for the climate, and for implementing them in the model scenarios.

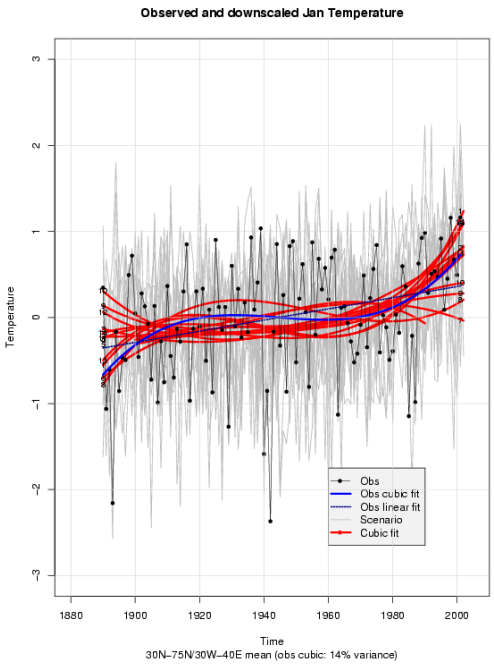

Figure 1a

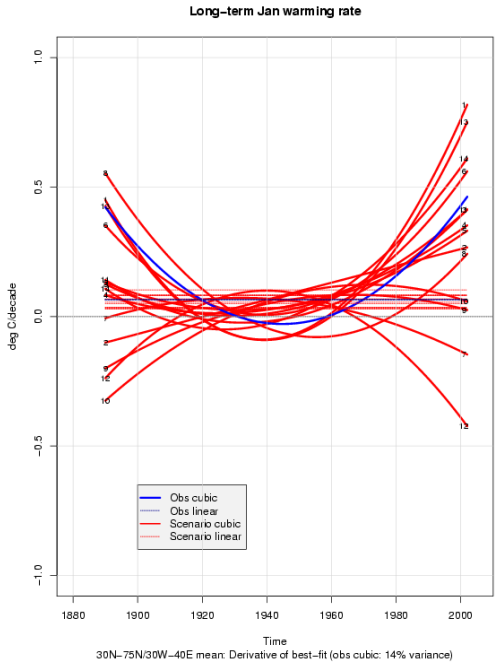

Figure 1b

Figure 1. (a) The evolution of the spatial mean temperature over 30 ºN-75 ºN/30 ºW-40 ºE. The observed values (temperatures from Univ. E. Anglia, Clim. Res. Unit (CRU): combined Hadley Centre SST and CRU T(2m) data:"hadcrut) are shown in black and the scenarios in grey. (b) The trend-analysis. The numbers refer to the various AOGCMs: 1=ECHAM4/OPYC3 GSDIO; 2=GFDL-19 GSA; 3-5=CCCma GSA; 6-7= ECHAM3 GSA; 8=HadCM3 GSA; 9-12=HadCM2 GSA; 13=CSIRO GSA; 14=ECHAM4/OPYC3 GSA. Linear trend fits are also shown for comparison.

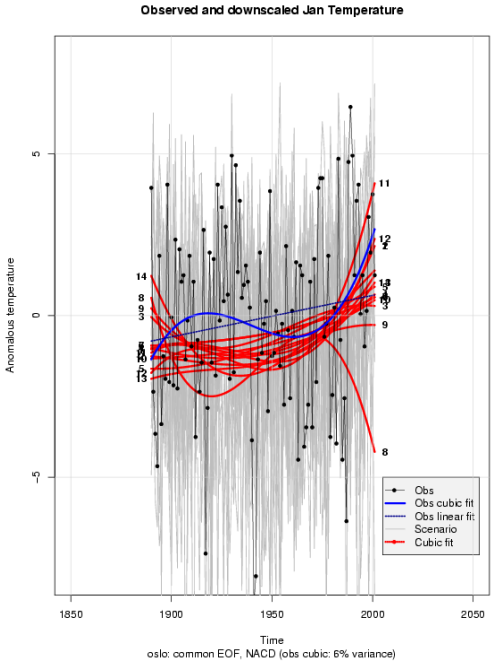

Figure 2a

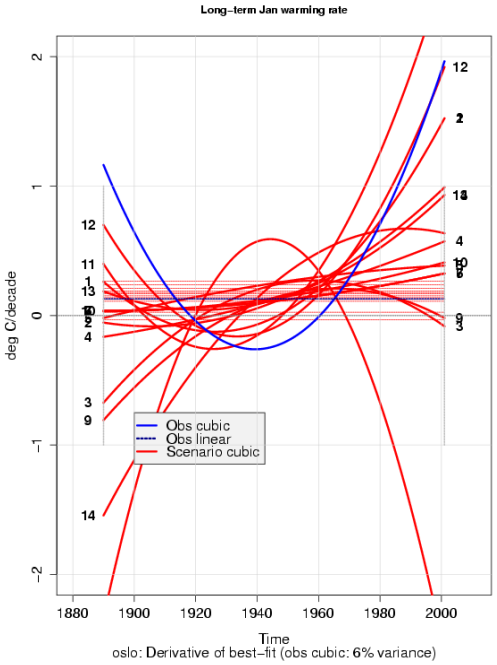

Figure 2b

Figure 2. The same analysis as in Figure 1, but for downscaled values for Oslo.

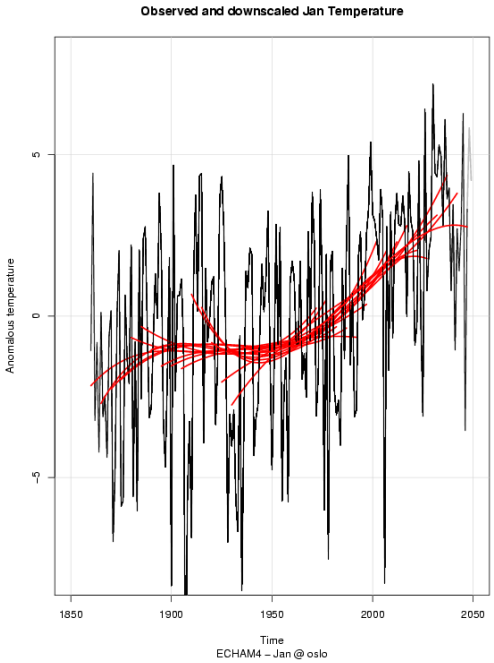

Figure 3a

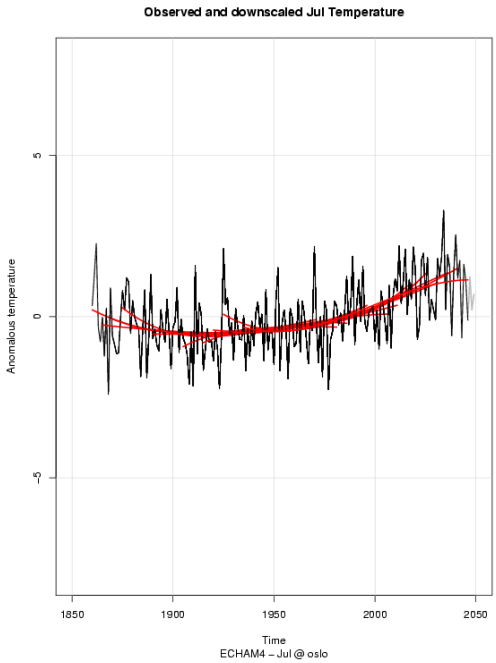

Figure 3b

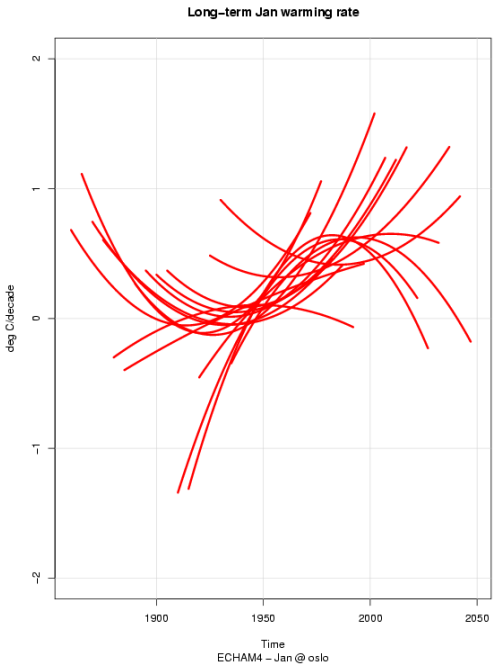

Figure 3c

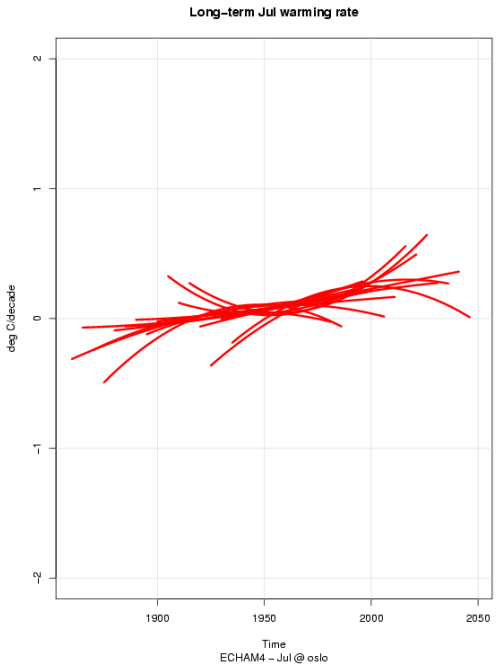

Figure 3d

Figure 3. Test of the cubic-fit trend-analysis. The cubic-fit and trend estimate has been repeated for the same series, but for different partially overlapping intervals.

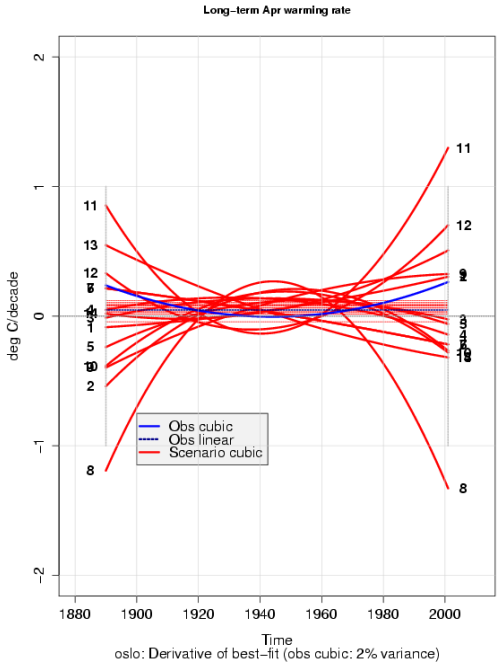

Figure 4a

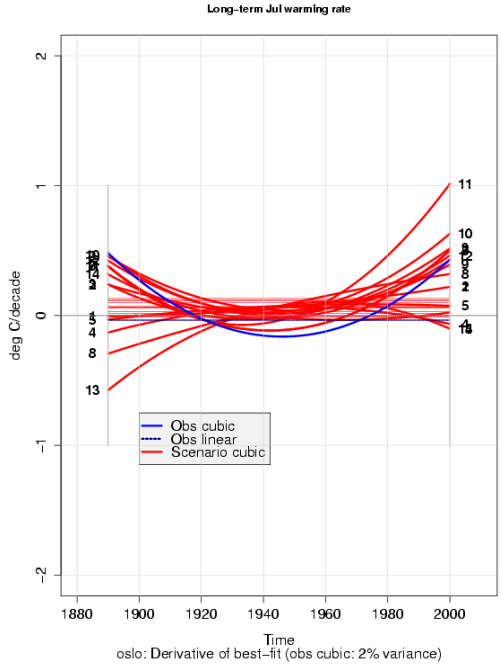

Figure 4b

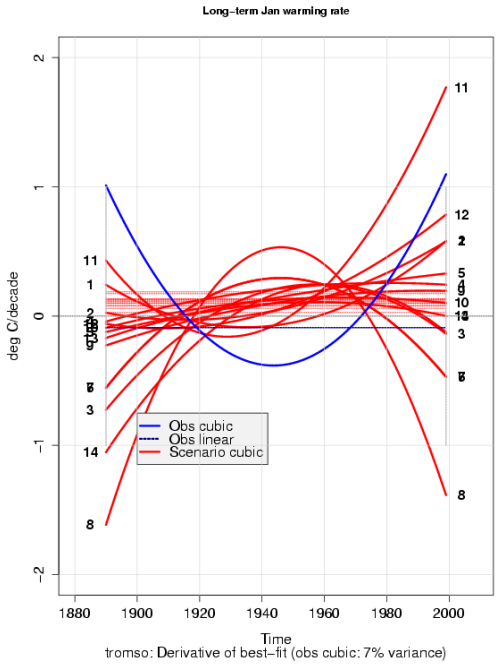

Figure 4c

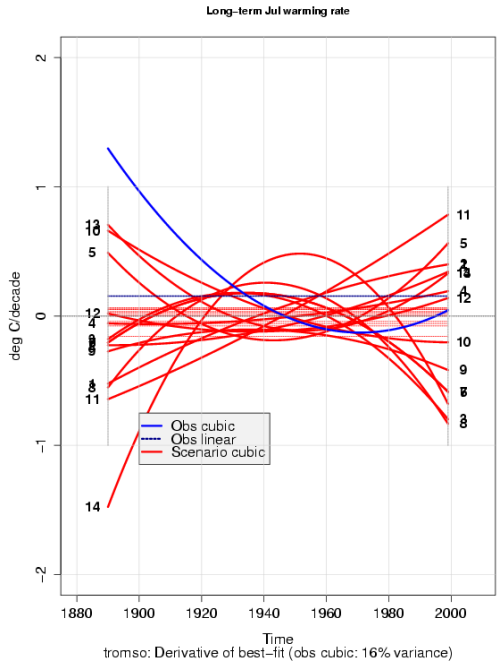

Figure 4d

Figure 4. Trend-analysis for downscaled Oslo temperature for April (a), July (b); Tromsø temperature for January (c) and July (d).

References

Benestad, R.E. (2000), Future Climate Scenarios for Norway based on empirical Downscaling and inferred directly from AOGCM results, DNMI Klima, 23/00, pp.127.

Benestad, R.E. (2001a), The cause of warming over Norway in the ECHAM4/OPYC3 GHG integration, *Int. J. Clim.,* **21,** 371-387.

Benestad, R.E. (2001b), A comparison between two empirical downscaling strategies, *Int. J. Clim.*, **21**, 1645-1668.

Benestad, R.E. and E.J. Førland (2001), pp. 471 - 481, in Brunet India, M. and López Bonillo, D. (Eds.): Detecting and Modelling Regional Climate Change, Springer-Verlag, Berlin Heidelberg Paris New York, 672 pp, 257.

Benestad, R.E. (2002a), Empirically downscaled temperature scenarios for northern Europe based on a multi-model ensemble, *Clim. Res*., in press. (C396)

Benestad, R.E. (2002b), Empirically downscaled multi-model ensemble temperature and precipitation scenarios for Norway, *accepted by Journal of Climate*.

Benestad, R.E., E.J. Førland and I. Hanssen-Bauer (2002), Empirically downscaled temperature scenarios for Svalbard, *Atmospheric Science Letters*, in press.

Benestad, R.E., I. Hanssen-Bauer, T.E. Skaugen and E.J. Førland (2002), Associations between the sea-ice and the local climate on Svalbard, **met.no** Klima, 07/02.

Hanssen-Bauer, I, O.E. Tveito and E.J. Førland (2000), Temperature scenarios for Norway. Empirical downscaling from ECHAM4/OPYC3. DNMI-KLIMA Report 24/00, 53 pp.

Hanssen-Bauer, I. and E.J. Førland (2000a), Temperature and precipitation variations in Norway 1900-1994 and their links to atmospheric circulation. *Int. J of Climatology*, **20**, No 14, 1693-1708.

Hanssen-Bauer, I. and E.J. Førland (2001b), Verification and analysis of a climate simulation of temperature and pressure fields over Norway and Svalbard. *Climate Research,* **16***, 225-235*.

Hanssen-Bauer, I. and E.J. Førland (2001c), Temperature- and SLP-fields over Norway and Svalbard deduced from a global coupled climate model: Are they realistic? *Int. Scientific meeting on detection and prediction of contemporary climate change and their effect in a regional scale*, Springer-Verlag, Berlin Heidelberg Paris New York, 672 pp.

Hanssen-Bauer, I, O.E. Tveito and E.J. Førland (2001), Precipitation scenarios for Norway. Empirical downscaling from ECHAM4/OPYC3. DNMI-KLIMA Report 10/01, 39 pp.

Hanssen-Bauer, I. (2002), Temperature and precipitation at Svalbard 1900 - 2050: Measurements and scenarios. Accepted by *Polar Record.*

Appendix A

Workshop Programme

RegClim – *Spring Seminar*

Olavsgård Hotel, Kjeller, 6. - 7. May 2002

Programme

Monday 6th May

Internal meeting

10:00 – 10:30 **Roar Skålin**, NorSerc and NOTUR
Norsk tungregning nå og frem til 2008: Maskinressurser og støttetjenester

10:30 – 11:00 **Terje Mørland**, Klimaprog
Rammer for ny søknad og annet nytt fra Klimaprog

End of internal meeting

11:00 – 11:30 COFFEE / TEA

SESSION I	11:30 – 13:00
Chair:	Eivind Martinsen, met.no

11:30 – 11:40 **Trond Iversen,** Project Leader
Welcome

11:40 – 12:10 **Göran Broström**, University of Göteborg
The sensitivity of the thermohaline circulation to equator-to-pole density forcing.

12:10 – 12:30 **Harald Loeng**, NOClim
A brief overview of NOClim including some recent results on ocean climate variability

12:30 – 12:50 **Mats Bentsen**, Helge Drange, Tore Furevik, Tianjun Zhou, NERSC
Simulated natural variability of the Atlantic Termohaline Circulation

13:00 – 14:00 LUNCH

SESSION II	14:00 – 15:30
Chair:	Trond Iversen, Igf-UiO

14:00 – 14:20 **Odd Helge Otteraa**, Helge Drange, NERSC
A possible coupling between the Arctic fresh water, the Arctic sea ice cover and the North Atlantic Drift. A case study

14:20 – 14:40 **Nils Gunnar Kvamstø**, Gfi-UiB
Simulated atmospheric sensitivity to a changed seasonal sea ice cycle in the Arctic.

14:40 – 15:20 **Nils Gunnar Kvamstø**, Gfi-UiB
Regional aspects in a CMIP experiment with BCM.
Part I and II

15:30 – 15:45 COFFEE / TEA

SESSION III	15:45 – 17:25
Chair:	Sigbjørn Grønås, Gfi-UiB

15:45 – 16:15 **Ulrich Cubasch**, DKRZ/MPI Hamburg
Modelling the late Maunder Minimum with a 3-dimensional OAGCM

16:15 – 16:35 **Tore F. Berglen**, IfG-UiO
Interactive global modelling of regional SO_2 and sulphate trends until 1996.

16:35– 16:55 **Gunnar Myhre**, IfG-UiO
Radiative forcing from sulphate with uncertainty estimates.

17:05 – 17:20 COFFEE / TEA and FRUIT

SESSION IV	17:20 – 18:30
Chair:	Eirik J. Førland, met.no

17:20 – 17:40 **Alf Kirkevåg**, IfG-UiO
How large is the direct effect of black carbon and sulphate aerosols?
Results from sensitivity experiments and response simulations

17:40 – 18:00 **Øyvind Seland**, IfG-UiO
Simulations of sulphate and black carbon aerosols: Sensitivity to the treatment of aerosol-cloud-chemistry interactions

18:00 – 18:20 **Jon Egill Kristjansson**, IfG-UiO
Simulations of aerosol indirect effect: Sensitivity to parameterisation assumptions and early results from 50-year response experiments

20:00 DINNER

Tuesday 7th May

SESSION V	09:00 – 10:30
Chair:	Nils Gunnar Kvamstø, Gfi-Uib

09:00 – 09:30 **Ole Bøssing Christensen**, Jens H Christensen, DMI
Latest results from experiments with the HIRHAM RCM over Europe

09:30 – 10:00 **Phil Graham**, Rossby Centre
Update on SWECLIM activities and Nordic climate cooperation

10:10 – 10:25 COFFEE / TEA

SESSION VI	10:25 – 11:35
Chair:	Lars Petter Røed, met.no

10:25 – 10:45 **Rasmus Benestad,** met.no
Evaluation of local climate scenarios

10:45 – 11:05 **Viel Ødegaard**, mat.no
Empirical Orthogonal Function analysis applied to MSLP from regional climate simulations

11:05 – 11:35 **Tim Stockdale**, ECMWF
Coupled modelling for seasonal forecasts

11:45 – 12:00 COFFEE / TEA

SESSION VII	12:00 – 13:00
Chair:	Helge Drange, NERSC

12:00 – 12:20 **Jens Debernard**, Øyvind Sætra and Lars Petter Røed, met.no
An update on the future wind, wave and surge climate using the dynamical downscaling of the global MPI GSDIO scenario as forcing.

12:20 – 12:40 **Jens Debernard** and Lars Petter Røed, met.no
Recent advances at met.no in the coupling of a sea-ice and an ocean model.

12:40 – 13:00 **Torill E. Skaugen,** met.no
Scenario for heating and growing season in Norway

13:00 – 14:00 LUNCH

14:00 – 17:00 INTERNAL MEETING

Appendix B

List of Participants

Participants at the RegClim Workshop and Internal Meeting

Olavsgård Hotel, Kjeller, 6 - 7 May 2002

Rasmus Benestad
Norwegian Meteorological Institute
P.O. Box 43 Blindern
NO-0313 OSLO
E-mail: rasmus.benestad@dnmi.no

Mats Bentsen
Nansen Environmental and
Remote Sensing Center
Edv. Griegsv. 3a
NO-5059 SOLHEIMSVIKEN
E-mail: mats@nrsc.no

Dag Bjørge
Norwegian Meteorological Institute
P.O. Box 43 Blindern
NO-0313 OSLO
E-mail: dag.bjorge@dnmi.no

Göran Broström
University of Göteborg
Sweden
E-mail: gobr@oce.gu.se

Ole Bøssing Christensen
Danish Meteorological Institute
Denmark
E-mail: obc@dmi.dk

Ulrich Cubach
Max-Planck-Institute for Meteorology
Model & Data Group
Hamburg, Germany
E-mail: Cubach@dkrz.de

Jens Debernard
Norwegian Meteorological Institute
P.O. Box 43 Blindern
NO-0313 OSLO
E-mail: jens.debernard@dnmi.no

Helge Drange
Nansen Environmental and
Remote Sensing Center
Edv. Griegsv. 3a
NO-5059 SOLHEIMSVIKEN
E-mail: helge.drange@nrsc.no

Siri Eriksen
CICERO
P.O. Box 1129 Blindern
NO-0317 OSLO
E-mail: siri.eriksen@cicero.uio.no

Tore Furevik Berglen
University of Oslo
Dept. of Geophysics
P.O. Box 1022 Blindern
NO-0315 OSLO
E-mail: t.f.berglen@geofysikk.uio.no

Eirik Førland
Norwegian Meteorological Institute
P.O. Box 43 Blindern
NO-0313 OSLO
E-mail: e.forland@dnmi.no

Phil Graham
Swedish Meteorological and Hydrological Institute
Rossby Centre
Sweden
E-mail: Phil.Graham@smhi.se

Sigbjørn Grønås
University of Bergen
Geophysical Department
Alleg. 70
NO-5007 BERGEN
E-mail: sigbjorn@gfi.uib.no

Inger Hanssen-Bauer
Norwegian Meteorological Institute
P.O. Box 43 Blindern
NO-0313 OSLO
E-mail: inger.hanssen-bauer@dnmi.no

Jan Erik Haugen
Norwegian Meteorological Institute
P.O. Box 43 Blindern
NO-0313 OSLO
E-mail: j.e.haugen@dnmi.no

Knut A. Iden
Norwegian Meteorological Institute
P.O. Box 43 Blindern
NO-0313 OSLO
E-mail: knut.a.iden@dnmi.no

Trond Iversen
University of Oslo
Dept. of Geophysics
P.O. Box 1022 Blindern
NO-0315 OSLO
E-mail: trond.iversen@geofysikk.uio.no

Alf Kirkevåg
University of Oslo
Dept. of Geophysics
P.O. Box 1022 Blindern
NO-0315 OSLO
E-mail: alf.kirkevag@geofysikk.uio.no

Jón Egill Kristjánsson
University of Oslo
Dept. of Geophysics
P.O. Box 1022 Blindern
NO-0315 OSLO
E-mail: j.e.kristjansson@geofysikk.uio.no

Nils Gunnar Kvamstø
University of Bergen
Geophysical Institute
Alleg. 70
NO-5007 BERGEN
E-mail: nilsg@gfi.uib.no

Harald Loeng
The Norwegian Institute of Marine Research
P.O. Box 1870 Nordnes
NO-5817 BERGEN
E-mail: harald.loeng@imr.no

Chris Lunder
Norwegian Institute for Air Research
P.O. Box 100
NO-2027 KJELLER
E-mail: crl@nilu.no

Eivind Martinsen
Norwegian Meteorological Institute
P.O. Box 43 Blindern
NO-0313 OSLO
E-mail: e.a.martinsen@dnmi.no

Gunnar Myhre
University of Oslo
Dept. of Geophysics
P.O. Box 1022 Blindern
NO-0315 OSLO
E-mail: gunnar.myhre@geofysikk.uio.no

Terje Mørland
The Research Council of Norway
P.O. Box 2700 St. Hanshaugen
N-0131 OSLO
E-mail: tmo@forskningsradet.no

Thor Erik Nordeng
Norwegian Meteorological Institute
P.O. Box 43 Blindern
NO-0313 OSLO
E-mail: t.e.nordeng@dnmi.no

Odd Helge Otteraa
Nansen Environmental and
Remote Sensing Center
Edv. Griegsv. 3a
NO-5059 SOLHEIMSVIKEN
E-mail: oddho@nrsc.no

Bård Romstad
CICERO
P.O. Box 1129 Blindern
NO-0317 OSLO
E-mail: baard.romstad@cicero.uio.no

Lars Petter Røed
Norwegian Meteorological Institute
P.O. Box 43 Blindern
NO-0313 OSLO
E-mail: larspetter.roed@dnmi.no

Øyvind Seland
University of Oslo
Dept. of Geophysics
P.O. Box 1022 Blindern
NO-0315 OSLO
E-mail: oyvind.seland@geofysikk.uio.no

Torill E. Skaugen
Norwegian Meteorological Institute
P.O. Box 43 Blindern
NO-0313 OSLO
E-mail: t.e.skaugen@dnmi.no

Jostein K. Sundet
University of Oslo
Dept. of Geophysics
P.O. Box 1022 Blindern
NO-0315 OSLO
E-mail: jostein.sundet@geofysikk.uio.no

Viel Ødegaard
Norwegian Meteorological Institute
P.O. Box 43 Blindern
NO-0313 OSLO
E-mail: viel.odegaard@dnmi.no

Roar Skålin
Norwegian Meteorological Institute
P.O. Box 43 Blindern
NO-0313 OSLO
E-mail: Roar.skalin@dnmi.no

Viel Ødegaard
Norwegian Meteorological Institute
P.O. Box 43 Blindern
NO-0313 OSLO
E-mail: viel.odegaard@dnmi.no